GC/MS/MS ON THE QUADRUPOLE ION TRAP MASS SPECTROMETER SOFTWARE DEVELOPMENT AND THE EXAMINATION OF THE EFFECTS OF ION POPULATION

By

TIMOTHY P. GRIFFIN

A DISSERTATION PRESENTED TO THE GRADUATE SCHOOL
OF THE UNIVERSITY OF FLORIDA IN PARTIAL FULFILLMENT
OF THE REQUIREMENTS FOR THE DEGREE OF
DOCTOR OF PHILOSOPHY

UNIVERSITY OF FLORIDA

1995

UNIVERSITY OF FLORIDA LIBRARIES

ACKNOWLEDGMENTS

There have been many people in my life who have made this possible. First, I would like to thank my family, in particular my mom and dad, for their encouragement and support throughout the time that I have spent here. If people would listen to us, the world would be a perfect place, i.e., a whole lot cleaner. A special thank you goes to Sara Griffin. We have had our problems and we are just now getting on with our lives, but I couldn't have gone this far without her belief in me.

I also would like to thank the many people that I have met over the years that have helped me to grow and develop into the great and humble person that I am today. In particular I would like to thank Linda Doubenmeir for her support during the times at Floyd Brown and Associates. It is surprising to me to this day that we made it through without losing too much of our minds. Thanks also goes to Floyd Brown for believing in a young punk right out of school. He offered me a chance to turn into a man and see the world from a different point of view.

I would especially like to thank Rick Yost. He gave me the freedom and support not only to develop into a true scientist but also a more self-confident person. Thanks to the Gate crew, which has been made up of many people

over the years, I lift my 32oz Coke to them all. Imagine grad school without caffeine and sugar--I don't think it could be done.

I am very indebted to Nate Yates who not only got me started on the software but also has been a true and caring friend during the these last four years. The canoe trips were a blast. All of the canoeing, swimming, camping and of course drinking made for a great stress relief. Life in Gainesville would be hard to imagine without the BBQs and dinners at Jim (Nerd Boy) and Tracy Stephenson's house. What a great way to relieve stress and the frustrations of scrapings and leavings.

I will never forget the afternoons sitting and watching the sights walk by with Don Eades and Brad Coopersmith; they were truly some awesome sights. I also would like to thank Shannan (I spelled it correctly) Carlson for her friendship over the past months, even if she didn't acknowledge me on her poster. We have had a lot of fun, and spent a lot of money; I'll never forget the Abby. It was great meeting another misunderstood person in the world. I would also like to acknowledge Matt Booth for all the discussions and help along the way. I also have enjoyed seeing how much Coke he could drink in a day.

A very special and heartfelt thank you goes to Emily Carter. During the time that I have known her I have truly felt alive. These last months would have been unbearable had it not been for her caring and understanding. From the moonlight on the beach to cards in the mail I will always cherish this time.

TABLE OF CONTENTS

ACKNOWLEDGMENTS ii

LIST OF TABLES vii

LIST OF FIGURES viii

ABSTRACT xvi

CHAPTERS

1 INTRODUCTION 1
- Background 1
- Specific Aims 3
- Function/Description of the Ion Trap 5
- Theory of Operation 13
  - Fundamental Parameters 13
  - Stability Diagram 14
- Tandem Mass Spectrometry 18
- RF/DC Isolation 21
- Overview of Dissertation 24

2 SOFTWARE DESCRIPTION 26
- Introduction 26
- Overview of Software 27
  - Pull Down Menu 30
  - Spectrum Display 35
  - Parameter Buttons 38
- Scan Editor 38
  - Clipboard Editor 39
  - SAP Table Editor 39
  - Scan Table Editor 44
- Custom Calibration 47
  - RF Calibration 47
  - DC Calibration 52
- Automatic Gain Control Editor 52
- Auxiliary Board 57

Auxiliary Board Description 58
Auxiliary Board Editor 68
GC Acquisition 71
Procedure Language 76
Procedure Words 76
Example Procedure Programs 78
Summary 85

3 RAMPED DC VOLTAGE 86
Experimental 88
Instrumentation 88
Automated Acquisition Procedure 89
Results and Discussion 92
Stability Boundary 95
Figures of Merit for Isolation 103
Isolation Efficiencies 106
Summary 112

4 MASS-SELECTIVE AUTOMATIC GAIN CONTROL 113
Introduction 113
Set Ionization Time 114
Variable Ionization Time (AGC) 117
Mass-selective Automatic Gain Control 125
Experimental 128
Instrumentation 128
Timing Diagram 128
Compounds 129
Results and Discussion 129
Summary 136

5 STABILITY DIAGRAM BOUNDARIES 138
Introduction 138
Background 138
Objectives 144
Experimental 144
Instrumentation 145
Scan Function 145
Mapping of Entire Stability Diagram 149
Detailed Examination of Boundaries 149
Isolation Efficiencies 152
Results and Discussion 152
Mapping Entire Stability Diagram 152
Detailed Study 164
Isolation Efficiency 169
Summary 176

6 EFFECTS OF ION POPULATION ON SECULAR FREQUENCY 178
  Introduction 178
  Background 179
  Objectives 183
  Experimental 184
    Scan Function 184
    Acquisition of Frequency Profile 189
    Ion Populations 189
    Compounds 191
  Results and Discussion 191
    Frequency Comparisons 191
    Changes in a_z Values 203
    Changes in q_z Values 203
  Summary 210

7 CONCLUSIONS AND FUTURE WORK 220
  Conclusions 220
    Gatorware 220
    Fundamental Studies 221
  Future Work 222
    Gatorware 222
    Fundamental Studies 224

REFERENCE LIST 225

BIOGRAPHICAL SKETCH 229

LIST OF TABLES

Table page

2-1 Auxiliary board memory map 63

2-2 List of control words (Assembly Language) 66

2-3 Scan Table flags for procedure 79

2-4 Scan Table values for procedure 80

2-5 SAP Table values for procedure 81

5-1 Experimental setup of previous studies 143

5-2 Experimental overview 146

6-1 Experimental parameters to obtain a frequency profile 190

LIST OF FIGURES

Figure page

1-1. Cross sectional view of the quadrupole ion trap mass spectrometer. The ion trap is composed of one ring and two endcap electrodes. The RF and DC voltages are applied to the ring electrode while the auxiliary frequency is applied to the endcap electrodes. The filament creates electrons to form ions within the ion trap while the detector is used to detect ions to acquire a mass spectrum. 7

1-2. Block diagram depicting the communication between the ITS-40 and personal computer. The communications can be seen as being composed of two parts. The first part is the acquisition and storage of the mass spectrum by the scan and acquisition processor (SAP) board while the second is the display and processing of the data by the personal computer (PC). Very limited real-time control of the ion trap is allowed the user. 9

1-3. Typical scan function for a QITMS. The mass spectrum is acquired as the RF trapping voltage is ramped to larger values and the ions become unstable and are ejected from the QITMS. Also note that the ions are ejected in order of increasing m/z. . 12

1-4. Graphical representation of the stability region of the QITMS. The overlap of the z and r stable regions (cross hatched) depicts the region of stability. The solid dots denote ions of different m/z. 16

1-5. Scan functions depicting the tandem mass spectrometry on a QITMS. Notice that the scan function uses two-step isolation to store a single m/z. In addition, the MS/MS stage is performed by collision-induced dissociation (CID). 20

1-6. Graphical representation of two-step isolation. Notice that the ejection of the low m/z and high m/z are performed at different positions in the stability diagram. The m/z of interest also must be placed in close proximity to the stability boundaries. 23

2-1. Main screen of the ITS-40 software and Gatorware. The exec page is the central location to reach all sub routines of the software. To reach the ITS-Scan < ^ G> is typed from this page followed by ITS-SCAN. 29

2-2. The main screen of Gatorware called ITS-Scan. This is the primary screen for controlling the QITMS. It includes a real-time display of the mass spectrum and nine of the most commonly adjusted parameters. 32

2-3. The options pull down menu. The menu allows the user to control the automatic calculation and downloading of the scan function to the SAP. In addition, the display and real-time acquisition can be set up through this menu. 34

2-4. Menu control to download the firmware to the SAP. The menu also enables the user to send the scan function to the QITMS to control the operation of the trap. 37

2-5. The scan table clipboard allows the user to control the order of the tables in the scan function. Tables also can be added and deleted from the scan function. 41

2-6. The SAP table editor allows the user to directly control the lines that the microprocessor uses to operate. This editor allows the most flexibility; however, thorough knowledge of the QITMS electronics is necessary. 43

2-7. The scan table editor is a simplified editor. The editor requires the user to know the fundamental parameters of the QITMS; however, no knowledge of the electronic is necessary. 46

2-8. The tools pull down menu enables the user to calibrate the instrument. The calibration includes the RF and DC voltages along with the auxiliary board. 49

2-9. The mass calibration is the calibration of the RF voltage. The calibration can be performed with either the standard calibration compound (PFTBA) or the user can input the masses to use. In addition, the user can use the custom scan functions to calibrate the QITMS. 51

2-10. Calibration editor for the DC voltage. The calibration is performed by attaching a voltmeter to J3 of the power board. The response of the DC voltage supply to the set DAC is then determined. The slope and offset are then entered into the editor. 54

2-11. Automatic gain control editor allows the user to use custom scan functions for AGC. The parameters that are used in the AGC calculations can be altered in this editor. See Chapter 4 for further details and an example using the editor. 56

2-12. Block diagram of the auxiliary board used with Gatorware. The board communicates directly with the microprocessor on the SAP which allows different frequencies to be used during a scan function. 60

2-13. Block diagram depicting the communication of the 80186 microprocessor with memory and external devices. The 80186 uses PCS lines to control which device is being communicated with. The auxiliary board uses the PCS 2 line. 62

2-14. The auxiliary board editor lets the user control the frequency to apply to the endcap electrodes. The frequency can be changed during any table in a scan function. 70

2-15. The acquisition editor lets the user have the ability to acquire data during a GC run. The autosampler and GC along with the QITMS editors can be reached from this screen. 73

2-16. The QITMS editor controls the acquisition of the data during a GC run. All data acquired through this method are centroid. Scan functions made in ITS-Scan can be used during a GC run; set the background mass to 11 and type in the SE Filename. . 75

3-1. Oscilloscope traces of ramped RF and DC voltages. The upper trace is proportional to the RF voltage measured at the DAC out (197mV/div corresponding to $32V_{0p}$ actual RF) on the Analog Board. The lower trace is the DC voltage (50 V/div) measured at J3 of the Power Board. The time scale is 0.1 ms/div. 91

3-2. Scan function depicting the q_z, a_z values used for the experiments. The a_z value for high mass ejection (Table 2) was first examined, followed by that for low mass ejection (Table 3). 94

3-3. Experimental determination of the stability boundary at q_z=0.71 for single-step and ramped DC voltages. The theoretical stability diagram boundary is depicted by the solid line. 97

3-4. The approach to the stability diagram boundary of ions at a range in m/z: (a) Theoretical approach and (b) approach with overshoot of the DC voltage. 99

3-5. Oscilloscope traces for changing the DC voltage on an ITS-40 from 0 to 130V. The desired voltage is reached by one large voltage change. The overshoot can be as large as 15% of the desired value. 102

3-6. Simulation showing the trajectories for m/z 100 at q_z=0.710 while (a) a_z=0.00 and (b) a_z=-0.235. Notice the larger z excursion near the β_z=1 boundary. 105

3-7. Plot of the efficiencies for isolation of m/z 56 and ejection of (a) m/z 57 and (b) m/z 55 of 1-octene using ramped and single-step DC voltage methods. 108

3-8. Oscilloscope traces for changing the DC voltage on an ITMS from 0 to 130 V. The desired voltage is reached by (a) one large voltage change and (b) two steps of voltage change with an initial change of 90 V. 111

4-1. The response of the ion trap mass spectrometer for set ionization times. The space charge region is placed in an arbitrary location. 116

4-2. The response of the ion trap mass spectrometer with AGC. Notice that the ionization time decreases to keep the number of ions out of the space charge region. 119

4-3. AGC scan function depicting the RF voltage and ion intensity detected. Notice the two sections of the scan function: prescan and analytical scan. 121

4-4. Chromatogram showing the effect of AGC. Furan was bled into the ion trap vacuum manifold at a constant rate (manifold pressure = $4x10^{-7}$torr) during the entire run. Dimethyl disulfide was injected onto the GC column in the splitless mode. Notice the complete loss of the furan ion signal as dimethyl disulfide elutes due to a large decrease in the ionization time. 124

4-5. MSAGC scan function depicting the RF voltage and ion intensity detected. Two-step isolation is used during the prescan to store and detect only the ion of interest. 127

4-6. Structure of the compound (molecular weight M+4) used for the experiments on co-eluting peaks. The asterisks (*) denote the sites for additional isotopic labeling in the internal standard (M+8). 131

4-7. Calibration curves for m/z 199 (internal standard) for (a) AGC and (b) MSAGC. Point A coresponds to 525 ng of the compound and its internal standard. Point B corresponds to 525 ng of the compound and 4 ng of the internal standard. Average of triplicate injections are shown, with error bars corresponding to ±1 standard deviation. 133

4-8. Mass spectra of 525 ng of compound with 4.0 ng of the co-eluting internal standard. The mass spectra are for (a) AGC and (b) MSAGC. 135

5-1. Experimentally determined stability diagram[32]. The diagram shown by the dashed line is the theoretical diagram. The experimental diagram was determined using Ne^+ ionized for the different times shown. 142

5-2. Scan function used for determining the stability boundaries. The only changes during the experiments occur during table 3. 148

5-3. Diagram depicting the slices of the stability diagram examined. The smaller dashed lines indicate the region where high resolution experiments also were performed. 151

5-4. Experimentally determined stability diagram for Ar^+ with no helium. The solid line denotes the theoretical stability boundaries. 154

5-5. Blown-up sections (a) upper apex (b)bottom left of Figure 5-4. The solid line denotes the theoretical boundary. 156

5-6. Single slice of the stability diagram for Ar^+ q_z=0.70 without helium. The slice shown is depicted in the inset. The major non-linear resonances are indicated. 159

5-7. Topographical map showing the entire stability diagram for Ar^+ without helium. The map is for 0.2 ms ionization time. The solid line is the theoretical location of the stability boundaries. 161

5-8. Topographical map showing the entire stability diagram for Ar^+ without helium. The map is for 10ms ionization time. The solid line is the theoretical location of the stability boundaries. 163

5-9. Location of the stability boundary for different mass-to-charges at q_z=0.700. The dotted line denotes the theoretical position of the boundary. 166

5-10. Change in the a_z value for different ionization times (q_z=0.700). The changes are measured with respect to 0.5 ms ionization times. The dotted line denotes the step size that was used for these experiments. 168

5-11. Location of the stability boundary for different mass-to-charges at q_z=0.850. The dotted line denotes the theoretical position of the boundary. 171

5-12. Change in the a_z value for different ionization times (q_z=0.850). The changes are measured with respect to 0.5 ms ionization times. The dotted lines denotes the step size used for these experiments. 173

5-13. Isolation efficiencies for different ion populations and mass-to-charges. Isolation efficiency is defined in equation 3-1. 175

6-1. Three ion profiles for different ion populations. The ion probe used was the $C_4H_4O^+$ ion of furan (m/z 68) at q_z=0.85 and a_z=0.00. The auxiliary freuqency was 0.100 mV_{0p} with the starting phase equal to zero. 181

6-2. The method used to determine the secular frequency. The frequency profile shown is for the $C_4H_8^+$ fragment ion from butanol (m/z 56) at q_z=0.205 and a_z=0.00. The middle point corresponding to 20% above the minimum value was said to be the secular frequency. 186

6-3. Scan function used to obtain the frequency profiles. The only section that was changed during the experiments was the resonant excitation section. 188

6-4. Frequency dependence of the butanol ion (m/z 56) without helium buffer gas. The solid line denotes the theoretical values. 194

6-5. Frequency dependence of the furan ion (m/z 68) without helium buffer gas. The solid line denotes the theoretical values. . . . 196

6-6. Frequency dependence of the thiophene ion (m/z 84) without helium buffer gas. The solid line denotes the theoretical values. 198

6-7. The effect of ion population on the secular frequency. The secular frequencies for (a) q_z=0.30 and (b) q_z=0.70 are depicted for a range of ion populations. 200

6-8. The change of frequency versus set q_z values. The ion probes are (a) $C_4H_8^+$, (b) $C_4H_4O^+$, and (c) $C_4H_4S^+$ for ion populations of 30,000 counts. 202

6-9. The effect of different storage parameters, i.e., q_z values, on the a_z values for $C_4H_8^+$ from butanol (m/z 56) without helium. The Δa_z was determined by the secular frequency [equation 6-4]. . 205

6-10. The effect of different storage parameters, i.e., q_z values, on the a_z values for $C_4H_4O^+$ from furan (m/z 68) without helium. The Δa_z was determined by the secular frequency [equation 6-4]. . 207

6-11. The effect of different storage parameters, i.e., q_z values, on the a_z values for $C_4H_4S^+$ from thiophene (m/z 84) without helium. The Δa_z was determined by the secular frequency [equation 6-4]. 209

6-12. The deviation of the experimentally determined q_z value from theory for the butanol ion (m/z 56) without helium. The solid line denotes the theoretical response which was calculated using the iterative approach. 212

6-13. The deviation of the experimentally determined q_z value from theory for the furan ion (m/z 68) without helium. The solid line denotes the theoretical response which was calculated using the iterative approach. 214

6-14. The deviation of the experimentally determined q_z value from theory for the thiophene ion (m/z 84) without helium. The solid line denotes the theoretical response which was calculated using the iterative approach. 216

6-15. The change in q_z versus the set q_z. The ion probes are (a) $C_4H_8^+$, (b) $C_4H_4O^+$, and (c) $C_4H_4S^+$ for ion populations of 30,000 counts. 218

GC/MS/MS ON THE QUADRUPOLE ION TRAP MASS SPECTROMETER: SOFTWARE DEVELOPMENT AND THE EXAMINATION OF THE EFFECTS OF ION POPULATION

By

TIMOTHY P. GRIFFIN

December 1995

Chairman: Dr. Richard A. Yost
Major Department: Chemistry

Since tandem mass spectrometry (MS/MS) was first developed as an analytical technique, it has become the method of choice to solve many analytical problems. Currently, tandem mass spectrometry is performed primarily on triple quadrupole mass spectrometers. However, the quadrupole ion trap mass spectrometer promises to be the next generation mass spectrometer. The high sensitivity of the ion trap makes it ideal for multiple stages of tandem mass spectrometry (MS^n).

Tandem mass spectrometry is performed in the ion trap by applying an external frequency to the endcap electrodes. When the external frequency equals the frequency of ion motion, the ions absorb energy and their orbits increase. This increase causes the ions to undergo energetic collisions with the buffer gas and fragment. Theoretically, ion frequency can be calculated; however, the actual ion frequencies change with changing ion population.

This change of ion frequency makes it difficult to automate the process of MS/MS on the quadrupole ion trap. This dissertation presents studies of the effect of ion population upon the trapping parameters to help to predict accurately the ion frequency. In addition to the frequency studies, a method has been developed to automatically control the number of ions of a given mass-to-charge ratio in the ion trap, called mass-selective automatic gain control, to help alleviate the frequency shifts; this should make it easier to predict the ion frequency for MS/MS.

Ion traps that are currently commercially available are designed to be routine analytical instruments; therefore, user control of the trapping parameters is not available. The operation of the ion trap, as opposed to other mass spectrometers, is software-intensive, meaning that most changes in operation of the ion trap can be performed by software changes. To perform fundamental studies on the ion trap, software was written to allow complete control of the trapping parameters. In addition, a digital frequency synthesizer along with its control software was developed which allows the study of ion frequency.

CHAPTER 1
INTRODUCTION

Background

Currently, tandem mass spectrometry (MS/MS) is performed most commonly on triple quadrupole mass spectrometers[1]. The high sensitivity and high MS/MS efficiency of the quadrupole ion trap mass spectrometer (QITMS) [2] make it ideal for multiple stages of tandem mass spectrometry (MS^n). In addition, the QITMS is software-intensive (rather than hardware-intensive) which allows the user to change its operation quickly and easily. The QITMS is still in the early stages of development and many fundamental questions still need to be answered, though its inherent capabilities show this instrument to hold promise as the next generation tandem mass spectrometer.

Recent capabilities of the QITMS include mass range extension[3], high resolution[4], and ion injection[5]. These features of the ion trap show that it is a highly versatile instrument. However, many of the above-mentioned features are only available on research grade instruments, designed to allow flexibility which enables the researcher to develop techniques that use the ion trap to its fullest potential (limited by the hardware). To take full advantage of this flexibility, the user must know and understand the complex fundamental properties of the ion trap. Most commercially available ion trap mass spectrometers, on the other hand, were designed for routine analysis which limits flexibility of the instrument, but makes their operation easy and relatively straightforward. For example, most commercial ion trap mass spectrometers are designed for routine gas chromatography mass spectrometry (GC/MS); however, only research grade ion trap mass spectrometers perform MS/MS experiments. Within the past few months, a new generation of commercial instruments have been introduced which promise routine GC/MS/MS on the QITMS. The manufacturers use different techniques to implement GC/MS/MS and there is not yet consensus by the scientific community as to which method or methods give the best results.

The compact size of the QITMS makes it ideal for a benchtop instrument. In addition, the ion trap has a higher sensitivity then beam instruments (e.g., triple quadrupole) [2], due in part to high storage efficiency. Ions can be trapped and detected for seconds or even minutes in the ion trap with higher transmission rates than on the triple quadrupole mass spectrometer. There are limitations, however, to the number of ions that can be stored in the ion trap as columbic interactions between stored ions in the confined space become significant. These columbic interactions, often referred to as "space charge," cause degradation of performance (e.g., loss of mass resolution).

The effects of space charge upon parameters important to tandem mass spectrometry (e.g., ion secular frequency) makes GC/MS/MS in an ion trap a challenge. During a chromatographic run, the number of ions that are formed and stored can vary by orders of magnitude as compounds elute from the column. The efficiency of MS/MS is dependent on the number of ions in the ion trap. Thus, it is impossible to determine a single set of operating parameters to use during an entire GC/MS/MS run. Techniques to overcome these limitations previously have been performed in this laboratory [6]. The aim of this work was to design methods to adjust automatically the MS/MS parameters during a GC run to make GC/MS/MS in the QITMS a routine analytical method.

Specific Aims

To develop techniques to automate GC/MS/MS in an ion trap mass spectrometer, it was necessary to write new instrument control software, as well as to implement several hardware modifications. This software enables the researcher to control all of the functions of the ion trap including some not previously available even with research grade ion trap mass spectrometers. It was with this software that the effects of ion population upon the operation of the ion trap were examined, as well as the new methods for GC/MS/MS automation.

The need to develop a more powerful research grade instrument was based on the fact that the commercially available research grade ion trap mass spectrometer (Finnigan MAT ITMS) was developed in the mid-1980's and does not allow sufficient control of the ion trap. The ITMS uses an imbedded 8086 microprocessor coupled with an 80286 PC to control the operation of the QITMS. The 8086 and the 80286 PC have limited memory; therefore, the design severely limits the usefulness of the ion trap. In addition, the software can be very difficult to use and does not always function as expected, in part because there is not enough memory to permit easy-to-use software to be written. A more advanced version of the ITMS software called Ion Catcher Mass Spectrometer (ICMS) software was written in this lab by Nathan A. Yates[7]. Although ICMS was a marked improvement over the original ITMS software, it was still limited.

We have developed a new research grade instrument based upon a commercially available second generation GC/MS instrument (Finnigan MAT ITS-40). The ITS-40 software is designed for routine GC/MS and allows very limited control of the ion trap. The modifications which were made were designed to allow the user full control of the instrument. The source code that allowed the modifications to be made to the ITS-40 was furnished by Finnigan MAT. Although most modifications to the ITS-40 were software, some hardware changes were necessary. The new control software for the ITS-40 is called Gatorware.

Procedures to automate MS/MS on the ion trap were developed in Gatorware. These include the ability to change the DC voltage smoothly, which helps to improve RF/DC isolation. A method to adjust automatically the ion formation time was also developed based upon automatic gain control (AGC) first developed by Finnigan MAT[8]. The improvement in mass isolation is necessary to perform efficient MS/MS, while varying the ion formation time controls the number of ions produced and stored in the ion trap. The effects of the numbers of ions stored during operation of the ion trap were investigated in detail.

Function/Description of the Ion Trap

A cross sectional view of the ion trap is shown in Figure 1-1. The ion trap consists of two endcap electrodes and a ring electrode. The inner surfaces of all electrodes are machined to a hyperbolic shape. A radio frequency (RF) voltage and a direct current (DC) voltage are applied to the ring electrode. The two voltages coupled with the hyperbolic shape of the electrodes create a quadrupolar trapping field which allows ions to be stored within the ion trap. In addition to the RF and DC voltages an auxiliary frequency can be applied to the endcap electrodes which enables the examination of the ion frequencies as well as ion excitation for MS/MS. The filament provides electrons to form ions from electron ionization (EI) of neutral compounds within the QITMS, while the detector is an electron multiplier used to detect the ions as they are ejected from the ion trap.

A diagram showing the communication link between the ITS-40 and a personal computer (PC) is shown in Figure 1-2. The voltages that are applied

Figure 1-1. Cross sectional view of the quadrupole ion trap mass spectrometer. The ion trap is composed of one ring and two endcap electrodes. The RF and DC voltages are applied to the ring electrode while the auxiliary frequency is applied to the endcap electrodes. The filament creates electrons to form ions within the ion trap while the detector is used to detect ions to acquire a mass spectrum.

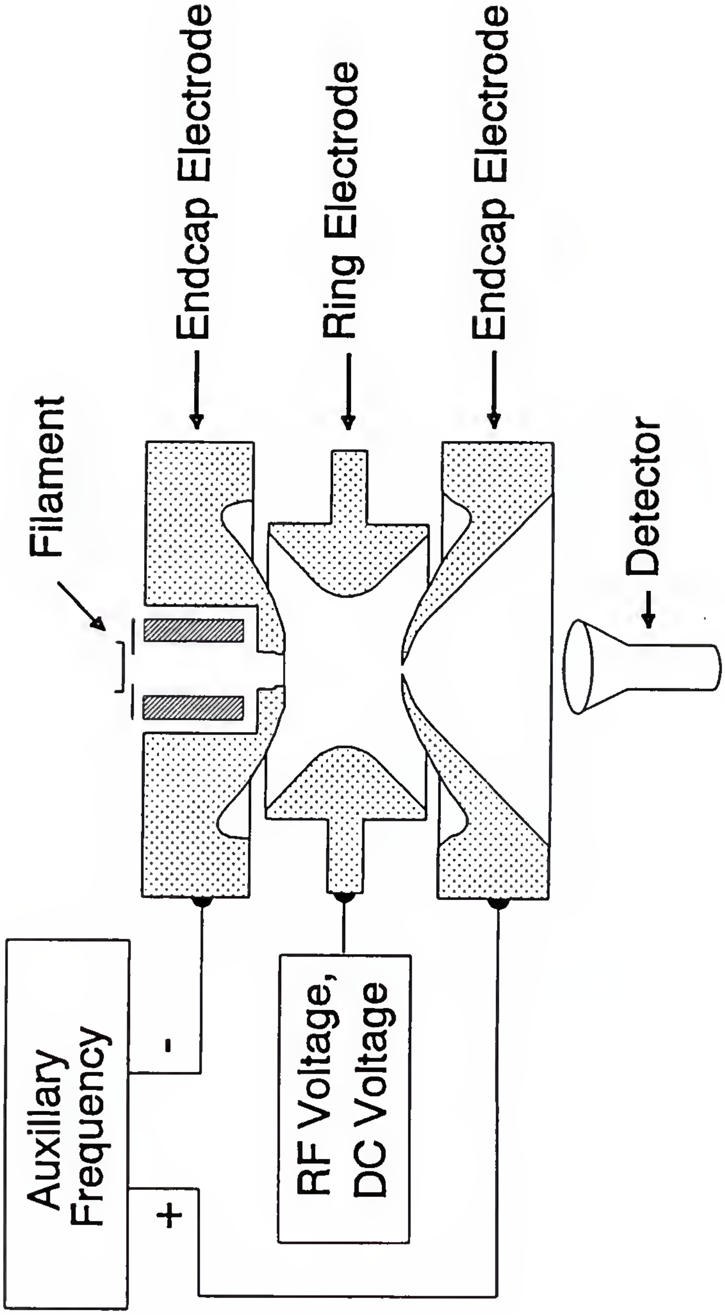
Filament
Endcap Electrode
Ring Electrode
Endcap Electrode
Detector
Auxillary Frequency
-
+
RF Voltage, DC Voltage

Figure 1-2. Block diagram depicting the communication between the ITS-40 and personal computer. The communications can be seen as being composed of two parts. The first part is the acquisition and storage of the mass spectrum by the scan and acquisition processor (SAP) board while the second is the display and processing of the data by the personal computer (PC). Very limited real-time control of the ion trap is allowed the user.

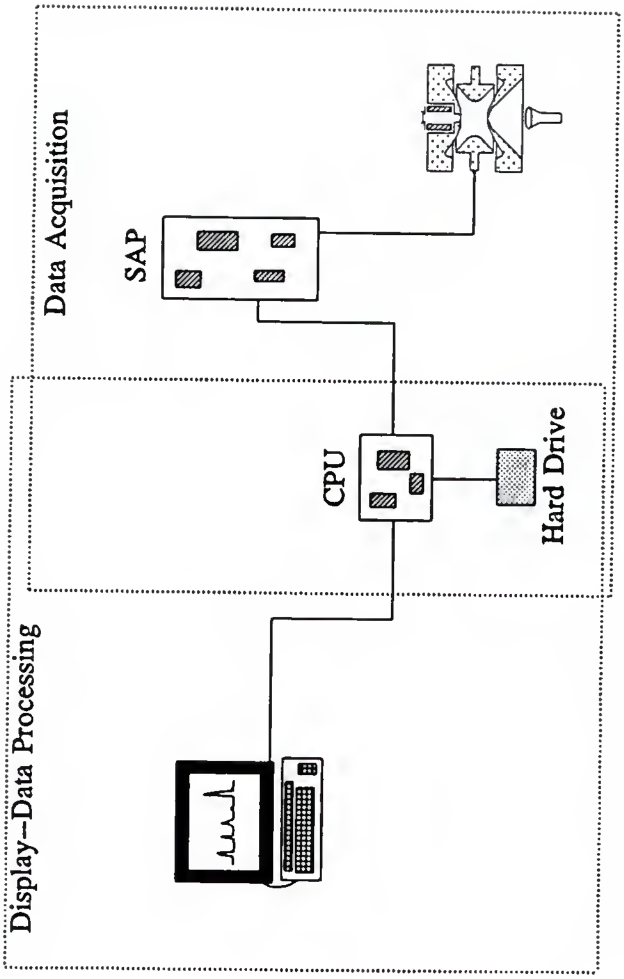
Data Acquisition
SAP
CPU
Hard Drive
Display–Data Processing

to the ion trap are controlled by a 80186 microprocessor, on the ITS-40, which is located on the scan and acquisition processor (SAP) board. In addition to controlling the voltages applied to the ion trap, the SAP also processes the data acquired from the detector. The data can then be sent to the PC and downloaded to the hard drive or displayed on the screen. All post-acquisition routines are performed on the PC. The SAP controls the voltages by sequentially stepping through a list of instructions or tables known as scan tables. The entire list of tables is called a scan list (or scan function).

A diagram of a typical EI scan function is shown in Figure 1-3. The top trace is the amplitude of the RF trapping voltage applied to the ring electrode while the bottom trace is the detected ion signal. In table 1 (Figure 1-3) the SAP sets the RF voltage to zero for a set time. In table 2, the SAP applies the correct RF value to the ring electrode and the electrons are gated into the ion trap to form ions. Table 3 requires the ramping of the RF voltage. During the table, the electron multiplier, located behind an endcap electrode, is enabled. This is accomplished by raising the voltage applied to the detector to give a gain of 10^5; voltages typically run at -1100 to -1600 V. When the detector is not active the voltage is lowered to a value less then the operating voltage to conserve the life of the detector. Ions are then ejected from the ion trap in order of increasing m/z and detected by the electron multiplier. A mass spectrum is thus produced. Finally, the SAP causes the RF voltage to drop to zero during Table 4 to "empty" the ion trap of any remaining ions.

Figure 1-3. Typical scan function for a QITMS. The mass spectrum is acquired as the RF trapping voltage is ramped to larger values and the ions become unstable and are ejected from the QITMS. Also note that the ions are ejected in order of increasing m/z.

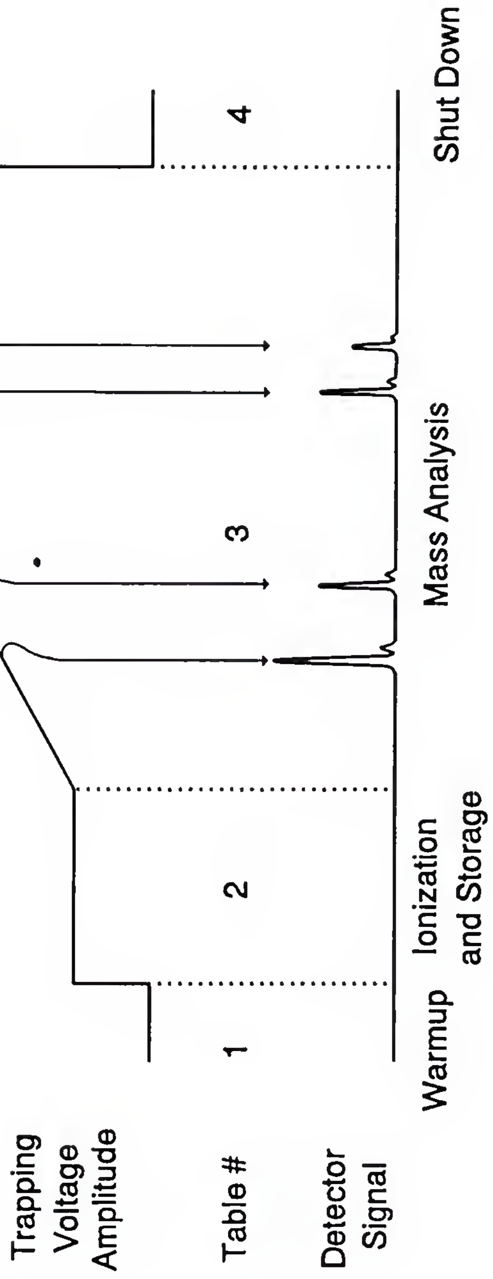
Trapping Voltage Amplitude
Table #
Detector Signal
1
2
3
4
Warmup
Ionization and Storage
Mass Analysis
Shut Down

Theory of Operation

Fundamental Parameters

Three fundamental parameters of the quadrupole ion trap are important to understanding how the ion trap operates. The fundamental parameters are q_z, a_z, and β_z and are discussed in length in Quadrupole Storage Mass Spectrometry [9]. The parameter q_z is related to the RF voltage by

$$q_z = \frac{4eV}{m(r_o^2+2z_o^2)\Omega^2} \tag{1-1}$$

Where V is equal to the RF voltage (0-peak), e is the charge on an electron (1.60219×10^{-19}C), m is the mass of the ion ((u)$\times 10^{-3}$kg mol^{-1})(6.02205×10^{23} mol^{-1})$^{-1}$, z_o is the distance (m) from center of trap to the endcap electrode, r_o is the distance (m) from the center of the trap to the ring electrode, and Ω is $2\pi f$ where f is the frequency of the RF voltage (in Hz). The a_z parameter is related to the DC voltage (U) by

$$a_z = \frac{-8eU}{m(r_o^2+2z_o^2)\Omega^2} \tag{1-2}$$

In addition, if the a_z and q_z are known β_z, which will be related to the ion frequency later, can be calculated from the equation

$$\beta_z = \left[a_z + \cfrac{q_z^2}{(2+\beta_z)^2 - a_z - \cfrac{q_z^2}{(4+\beta_z)^2 - a_z - \cfrac{q_z^2}{(6+\beta_z)^2 - a_z - \ldots\text{etc}}}} + \cfrac{q_z^2}{(\beta_z-2)^2 - a_z - \cfrac{q_z^2}{(\beta_z-4)^2 - a_z - \cfrac{q_z^2}{(\beta_z-6)^2 - a_z - \ldots\text{etc}}}} \right]^{\frac{1}{2}} \tag{1-3}$$

Which can be simplified (for $q_z<0.80$) to

$$\beta_z = \left[a_z - \frac{(a_z-1)q_z^2}{2(a_z-1)^2 - q_z^2} - \frac{(5a_z+7)q_z^4}{32(a_z-1)^3(a_z-4)} - \frac{(9a_z^2+58a_z+29)q_z^6}{64(a_z-1)^5(a_z-4)(a_z-9)} \right]^{\frac{1}{2}} \tag{1-4}$$

Stability Diagram

Different combinations of a_z and q_z cause ions of particular mass-to-charge (m/z) ratios to be stored within the ion trap. A plot of the regions of ion stability vs. values of a_z,q_z, called a stability diagram, is shown in Figure 1-4. The plot shows regions of stability in the z direction, between the endcaps, and in the r direction, within the ring electrode. To be stored ions must stay within the boundaries of the three electrodes. Ions, therefore, are only stored

Figure 1-4. Graphical representation of the stability region of the QITMS. The overlap of the z and r stable regions (cross hatched) depicts the region of stability. The solid dots denote ions of different m/z.

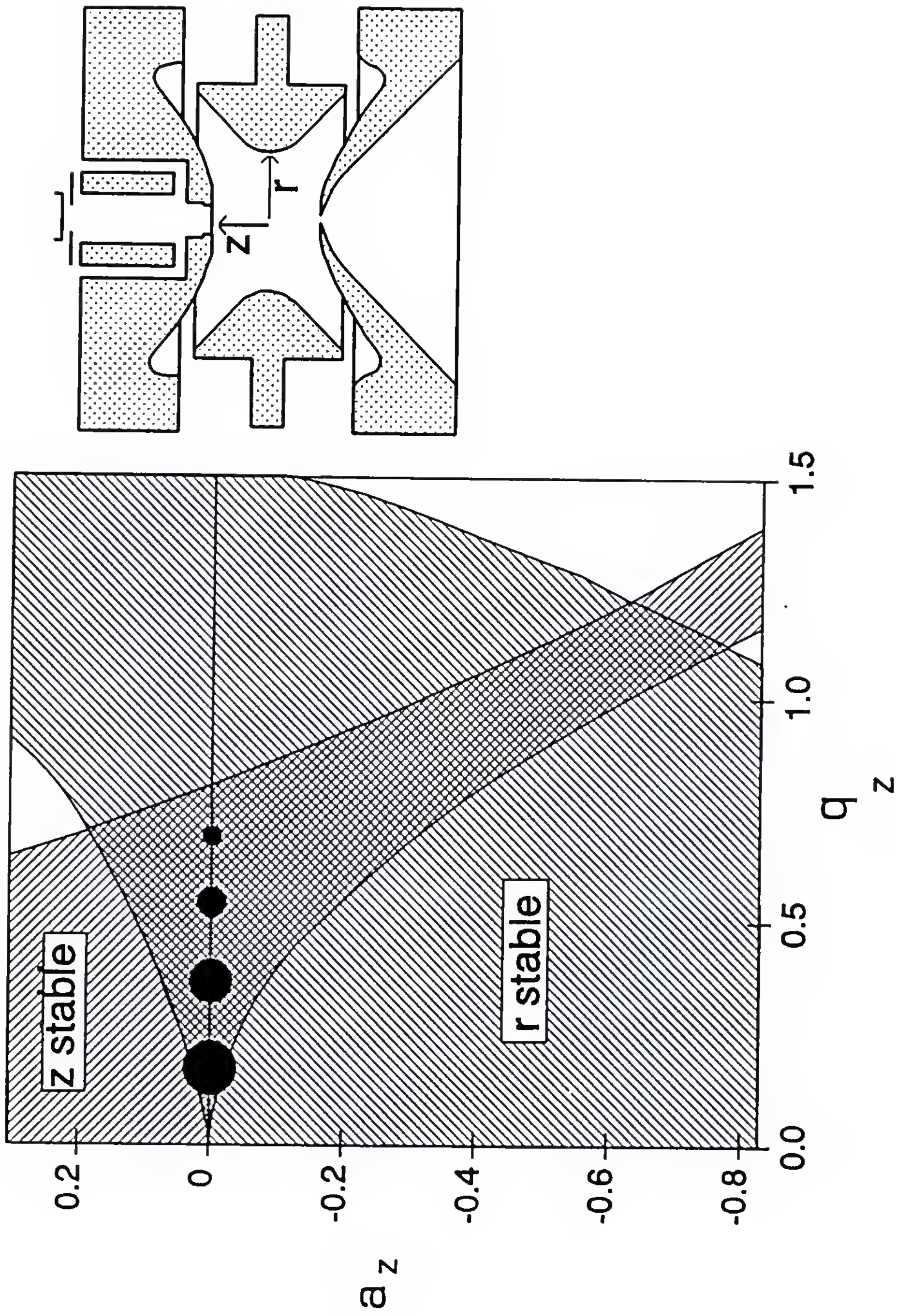
z stable
r stable
a_z
q_z
0.2
0
-0.2
-0.4
-0.6
-0.8
0.0
0.5
1.0
1.5
z
r

in the ion trap where z stable and r stable regions overlap (shown in Figure 1-4 by the cross-hatched region). In other words, ions are stable and can be stored within the ion trap when combinations of RF and DC voltages correspond to a_z, q_z points that lie within the cross hatched region.

Ions that are stored within the ion trap move with a particular frequency of motion, the secular frequency, which is a function of the ions m/z, as well as the a_z and q_z values. The frequency that the ions move within the ion trap is related to β_z by the equation

$$\omega_z = \frac{\beta_z \Omega}{2} \tag{1-5}$$

Where ω_z is the ion secular frequency (Hz) of motion in the z direction and Ω is the frequency (Hz) of the RF voltage applied to the ring electrode.

Notice in equation 1 that q_z is inversely proportional to the m/z of the ion. For a given RF voltage, ions with lower m/z values are at higher q_z values. This is shown graphically by the circles in Figure 1-4; the relative size of the dots denotes the relative m/z of the ions. A mass spectrum is acquired in the mass-selective instability scan [10] mode when the RF voltage is ramped while the DC voltage is held at zero; the ions become unstable, and thus are ejected from the ion trap in order of increasing m/z.

Tandem Mass Spectrometry

The method most commonly used for fragmenting ions to perform tandem mass spectrometry is collision-induced dissociation (CID). On the ion trap, MS/MS includes five steps (warmup, ionization, isolation, CID, and detection), a seen in the scan function shown in Figure 1-5.

The warmup step (table 1, Figure 1-5) gives the SAP time to reset and warmup the electronics. The ionization step (table 2, Figure 1-5) is the same as for the normal EI scan function (Figure 1-3). During the ionization step electrons are gated into the ion trap. The electrons collide with the sample eluting from the GC causing ions to be formed. The RF voltage then traps and stores ions that fall within the stability region in Figure 1-4. To fragment only the ion of interest it is necessary to store ions of a single m/z in the ion trap (called isolation) before fragmentation can be done. The isolation step (table 3, Figure 1-5) ejects all but ions of the m/z of interest from the ion trap.

As is shown in table 4 (Figure 1-5), after ions of a single m/z are stored within the ion trap an auxiliary frequency is applied to the endcap electrodes. When the auxiliary frequency corresponds to the secular frequency of the isolated ions they absorb energy and the size of their orbits increase. This increase causes the ions to undergo energetic collisions with the constant pressure of helium buffer gas that is in the ion trap. As the ions collide with the helium, energy is deposited into the ions and fragmentation occurs. The resulting fragment ions are trapped and stored. Finally, the ions are

Figure 1-5. Scan functions depicting the tandem mass spectrometry on a QITMS. Notice that the scan function uses two-step isolation to store a single m/z. In addition, the MS/MS stage is performed by collision-induced dissociation (CID).

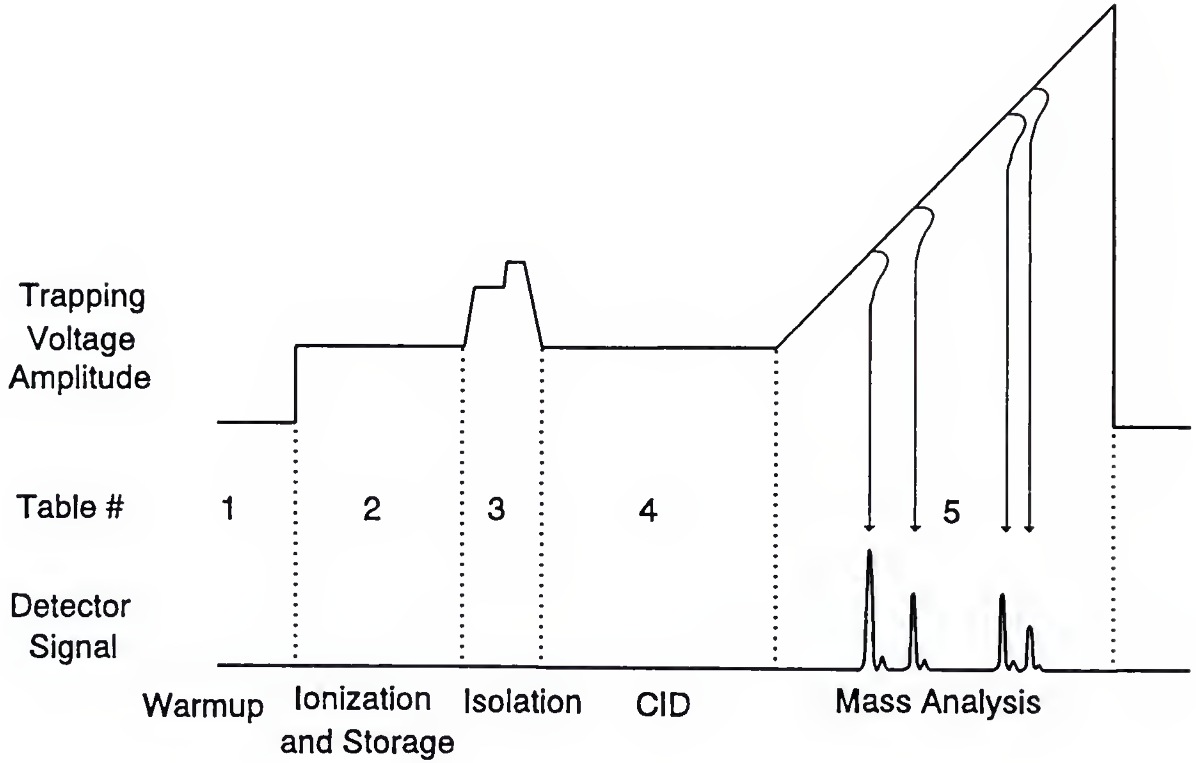
Trapping Voltage Amplitude
Table #
Detector Signal
1
2
3
4
5
Warmup
Ionization and Storage
Isolation
CID
Mass Analysis

sequentially ejected from the ion trap, using the mass selective instability scan to acquire a mass spectrum (table 5, Figure 1-5).

RF/DC Isolation

To distinguish which of the detected ions are fragment ions formed by CID from those ions which were formed during ionization, it is imperative to isolate a single m/z in the ion trap before CID occurs. Isolation is performed in a number of ways including apex [11], two-step[12,13], white noise[14], broad band[15], , SWIFT[16], filtered noise field[17], and forward-reverse scans[18]. All of the methods except two-step and apex use auxiliary frequencies applied to the endcap electrodes. The use of frequencies can make the techniques difficult and problematic to use when sample concentration varies (see Effect of Ion Population, below). Therefore, two-step isolation was used primarily for the work presented in this dissertation.

Two-step isolation is shown graphically in Figure 1-6. The ions are first formed and stored at a low q_z and $a_z = 0$ (point A). The RF and DC voltages are then set so that the ion of interest lies just within the stability diagram at point B. At point B the higher m/z are no longer stable within the ion trap and are ejected. After the high masses are ejected from the ion trap the RF and DC voltages are changed until the ion of interest lies within the stability diagram at point C. While the ion of interest is at point C, ions of lower m/z are no longer stable within the ion trap and are ejected. The RF and DC

Figure 1-6. Graphical representation of two-step isolation. Notice that the ejection of the low m/z and high m/z are performed at different positions in the stability diagram. The m/z of interest also must be placed in close proximity to the stability boundaries.

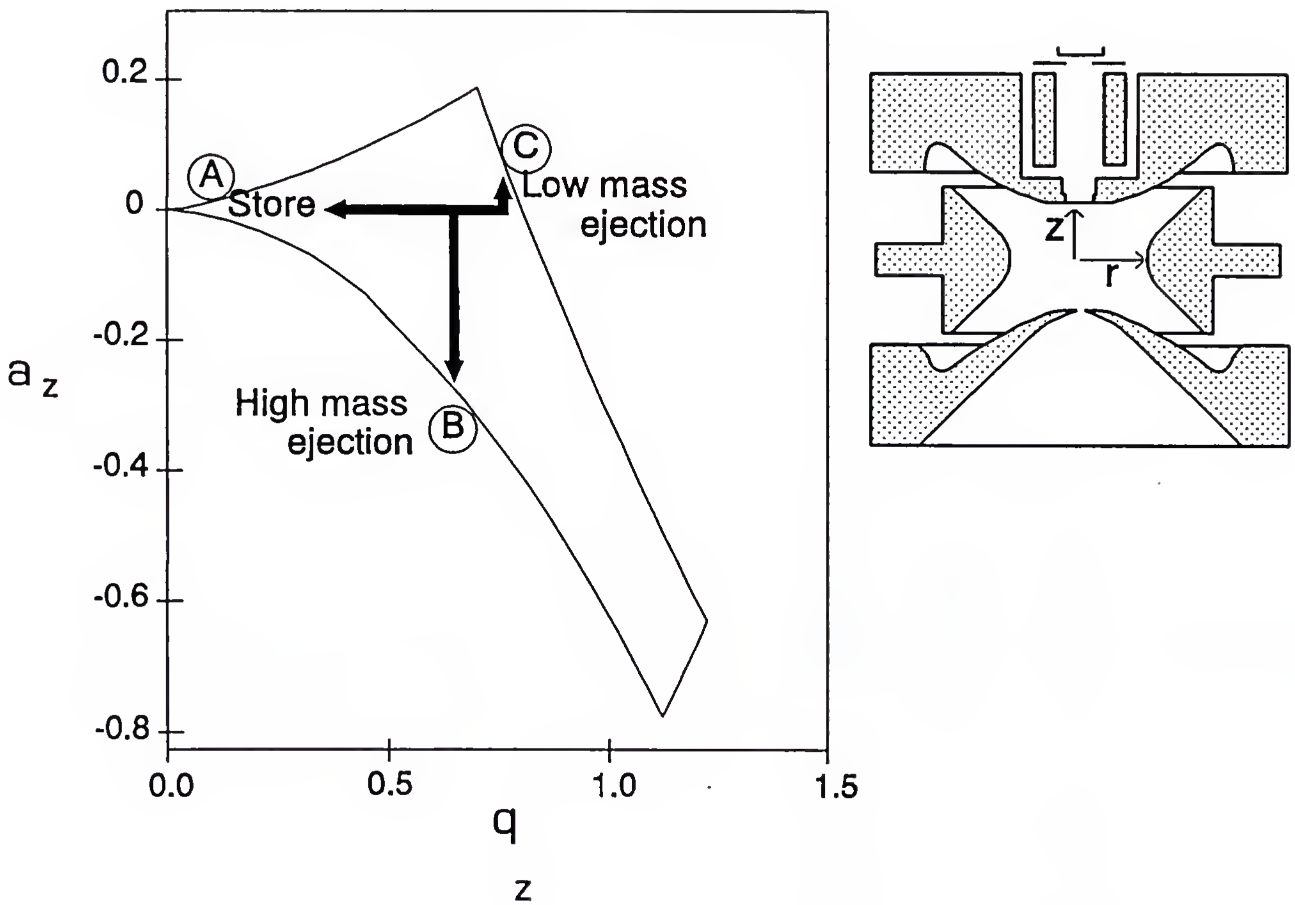
0.2
0
-0.2
-0.4
-0.6
-0.8
a z
0.0
0.5
1.0
1.5
q
z
Ⓐ
Store
Ⓒ
Low mass ejection
High mass ejection
Ⓑ
z
r

voltages are then lowered to correspond to point A in Figure 1-6. Further experiments including CID can then be performed on the single m/z ions stored within the ion trap.

Two-step isolation requires exact knowledge of the location of the stability diagram boundaries to use the correct RF and DC voltages. Any movement of the stability diagram boundaries can affect the efficiency of isolation. In addition, the efficiency of isolation might vary depending upon the compound. The reason for the variations are not understood. These problems demonstrate the need to improve the isolation techniques.

Overview of Dissertation

This dissertation focuses on two areas. The first is the development of the software to control the ion trap mass spectrometer (Chapter 2). The second is the use of the software to examine ways of automating GC/MS/MS in an ion trap mass spectrometer (Chapters 3-6).

Chapter 2 provides an overview of the software that was written to control the ITS-40 ion trap mass spectrometer. This dissertation includes a detailed description of the control software and the functions that are made available by the software. A description of the automatic acquisition routine, along with examples, is also included in this chapter.

Chapter 3 describes a method of changing the DC voltage in a smooth manner. The method helps to alleviate overshoot of the DC voltage. A detailed examination of the effect of the method upon isolation efficiencies is also examined.

Chapter 4 discusses a method to continually adjust the ion formation time to control the number of ions of a particular m/z that are created and stored. The method is used to determine the linear dynamic range of a co-eluting drug and its isotopically labeled internal standard.

Chapter 5 examines the effect that stored ion population has upon the operation of the ion trap. The position of the stability diagram boundaries for different stored ion populations is examined. The effect of different mass-to-charges also is examined.

Chapter 6 examines the effect that the stored ion population has upon the effective a_z,q_z parameters. The frequency of the ions at different q_z values is examined for different ion populations. The effect of mass-to-charge upon secular frequencies is also studied in close detail.

Chapter 7 presents the conclusions and suggestions for future work. The chapter is a summary of the work presented in this dissertation. Possibilities for future studies also are suggested.

CHAPTER 2
SOFTWARE DESCRIPTION

Introduction

The quadrupole ion trap mass spectrometer (QITMS) is a very versatile instrument, primarily due to its software-intensive nature. Properly designed software enables the function of the QITMS to be varied by a simple command. This has allowed many facets of the QITMS to be investigated and operating techniques to be developed. This dissertation will describe software and hardware, named Gatorware, that was developed to control a commercially available QITMS (ITS-40 by Finnigan MAT).

The ITS-40 was designed as a routine GC/MS instrument and as such the user has very limited control of its function. Gatorware was designed to allow the user complete control of the ITS-40's operation. In this way a research grade instrument was developed from one designed for routine use. The goal of Gatorware was to make an instrument to allow the development of techniques which make GC/MS/MS on an QITMS a routine analytical tool. While Gatorware was designed for ease of use, understanding of the fundamentals of the QITMS is necessary. An option also was included that allows direct control of the SAP; this option requires the user to know basic electronics and in particular how the ITS-40 operates. Gatorware is, in many ways, based on the Ion Catcher software (ICMS) [16] developed in our laboratory by Nathan A. Yates. ICMS, however, is for use with the ITMS (see Chapter 1) and thus does not provide the versatility that is available with Gatorware. The source code for the ITS-40 which enabled the development of Gatorware was furnished by Finnigan MAT.

This chapter of the dissertation gives a detailed look at Gatorware. Included is a walk through of all the features that are incorporated in the software. A simple explanation of how the microprocessor that controls the ITS-40 operates also is included. New procedure words which permit automation of the experiments are explained and examples given.

Overview of Software

Gatorware is a DOS-based system which can be entered by typing <DS> at the DOS prompt (in the correct directory). The first screen seen upon entering the software is the Exec Page (Figure 2-1). The Exec Page is the primary screen of the software and allows access to lower level routines. For example, the screen in Figure 2-1 shows a listing of the user programs that are available. The primary routine of Gatorware is called ITS-Scan. This dissertation only describes those functions not available on the unmodified ITS-40, unless otherwise noted.

Figure 2-1. Main screen of the ITS-40 software and Gatorware. The exec page is the central location to reach all sub routines of the software. To reach the ITS-Scan <^G> is typed from this page followed by ITS-SCAN.

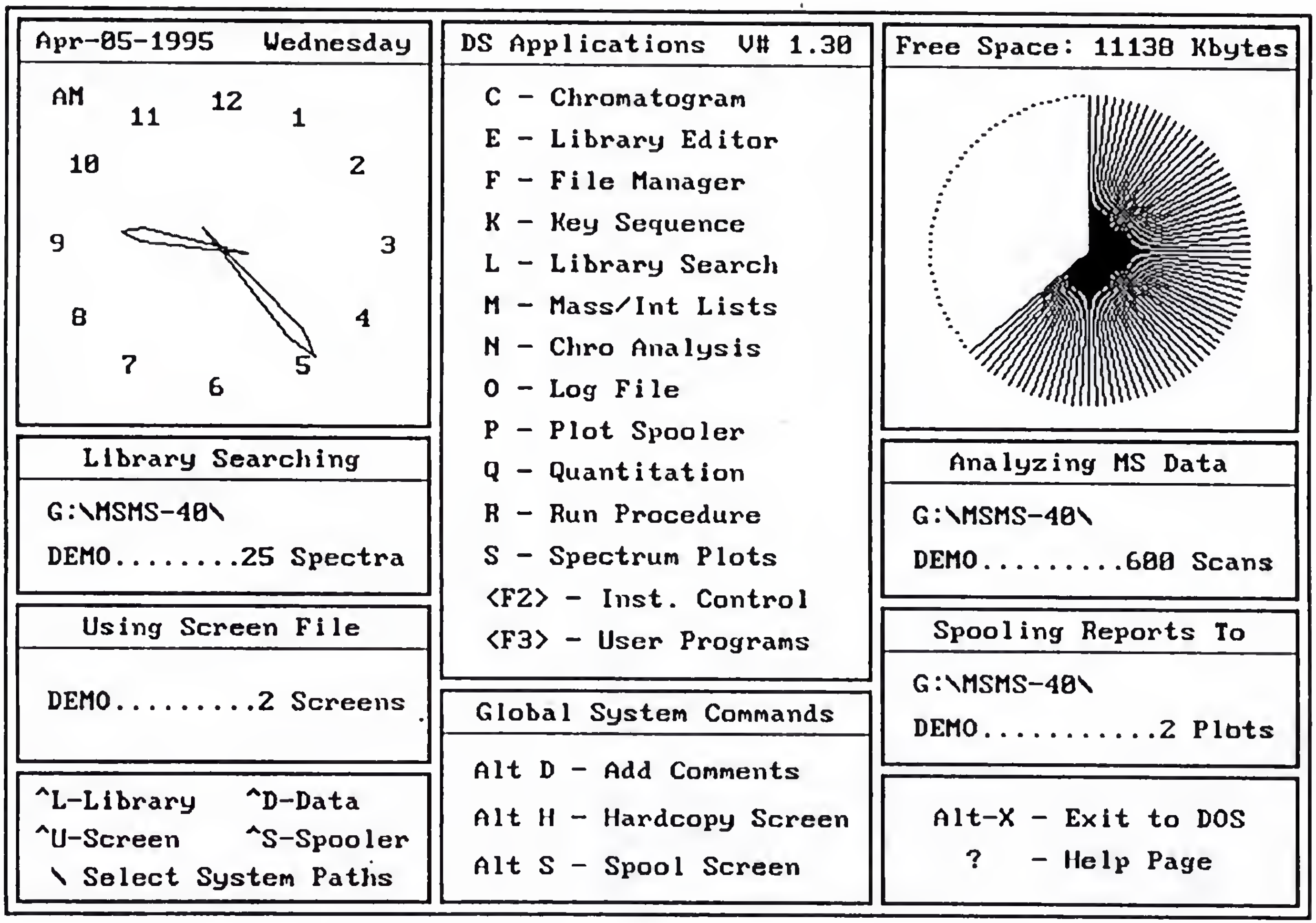

```
Apr-05-1995    Wednesday

Library Searching
G:\MSMS-40\
DEMO........25 Spectra

Using Screen File
DEMO.........2 Screens

^L-Library    ^D-Data
^U-Screen     ^S-Spooler
 \ Select System Paths

DS Applications   V# 1.30
  C - Chromatogram
  E - Library Editor
  F - File Manager
  K - Key Sequence
  L - Library Search
  M - Mass/Int Lists
  N - Chro Analysis
  O - Log File
  P - Plot Spooler
  Q - Quantitation
  R - Run Procedure
  S - Spectrum Plots
  <F2> - Inst. Control
  <F3> - User Programs

Global System Commands
 Alt D - Add Comments
 Alt H - Hardcopy Screen
 Alt S - Spool Screen

Free Space: 11138 Kbytes

Analyzing MS Data
G:\MSMS-40\
DEMO.........600 Scans

Spooling Reports To
G:\MSMS-40\
DEMO..........2 Plots

Alt-X - Exit to DOS
  ?   - Help Page
```

The major display of ITS-Scan (Figure 2-2) allows the user to adjust the SAP and thus, the function of the QITMS. The software is mouse driven, although textual strings can be entered through the keyboard, which facilities the use of the software. The primary screen (Figure 2-2) consists of three major areas: the pull down menu, the mass spectrum, and inputs for nine major parameters. In addition, the multiplier, filament, and RF voltages can be enabled by a click of the mouse button. The ability to adjust the trapping parameters and see, in real-time, how the mass spectrum is affected enables the user to smoothly and quickly fine tune the operation of the QITMS.

Pull Down Menu

The pull down menu allows the user to the set up the instrument and software before acquiring a mass spectrum. For example, under options (Figure 2-3) the user can decide if the data will be displayed in profile or centroid mode. Profile shows all of the data points that correspond to the RF DAC steps and thus, values between integer mass units (u) are seen. Centroid converts the profile data to integer u values so that lines corresponding only to integer u are in the spectrum. Acquiring in centroid mode is limiting and can cause experimental errors. For example, if the peak corresponding to a m/z of interest does not lie in the correct location the centroid routines can split the peak into two different integer u values. This splitting can cause erroneous interpretation of the data. The ITS-40 normally acquires only centroid data.

Figure 2-2. The main screen of Gatorware called ITS-Scan. This is the primary screen for controlling the QITMS. It includes a real-time display of the mass spectrum and nine of the most commonly adjusted parameters.

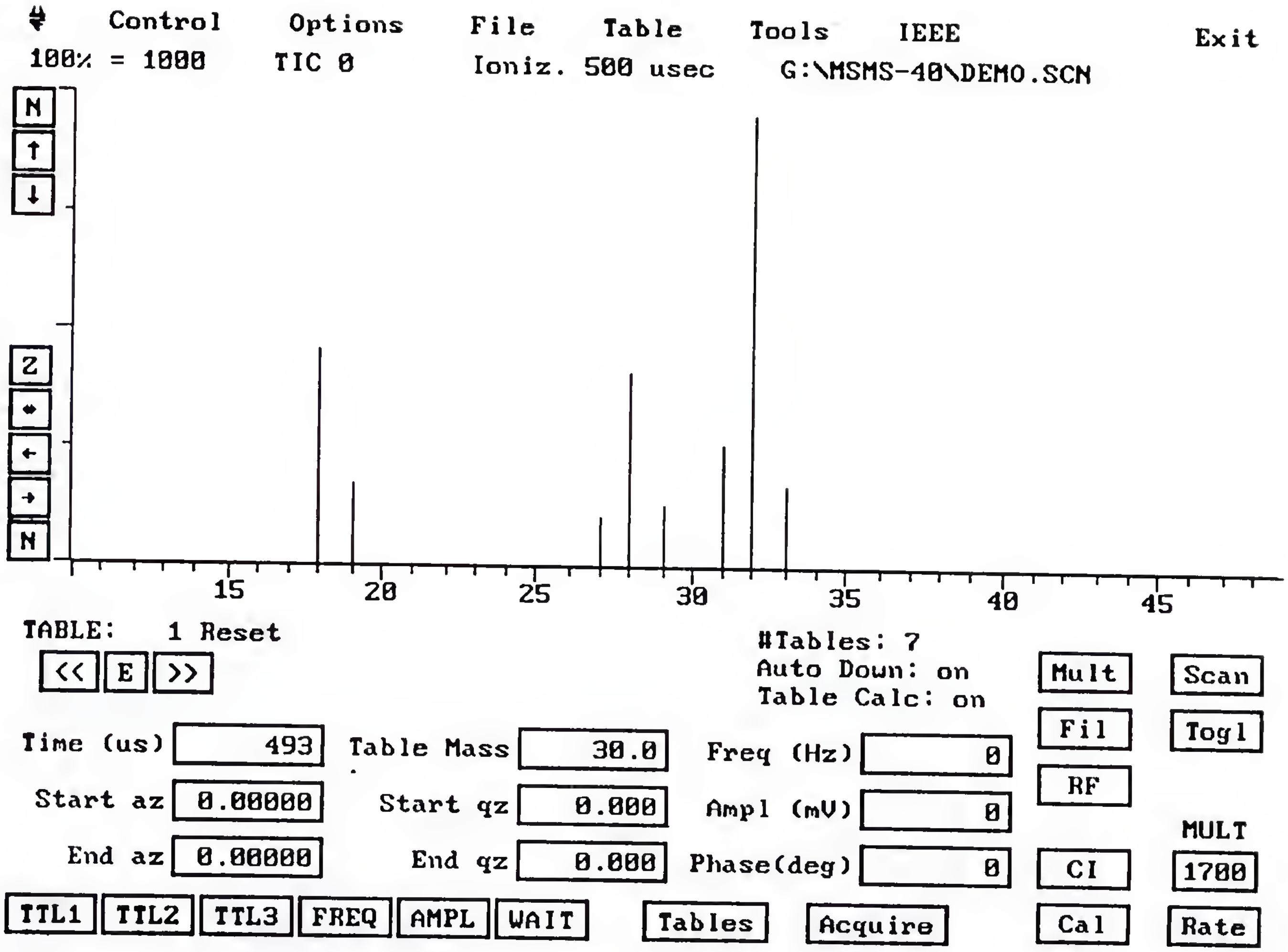

100% = 1000   TIC 0   Ioniz. 500 usec   G:\MSMS-40\DEMO.SCN

TABLE: 1 Reset

#Tables: 7
Auto Down: on
Table Calc: on

Time (us) 493
Start az 0.00000
End az 0.00000
Table Mass 30.0
Start qz 0.000
End qz 0.000
Freq (Hz) 0
Ampl (mV) 0
Phase(deg) 0
MULT 1700

Figure 2-3. The options pull down menu. The menu allows the user to control the automatic calculation and downloading of the scan function to the SAP. In addition, the display and real-time acquisition can be set up through this menu.

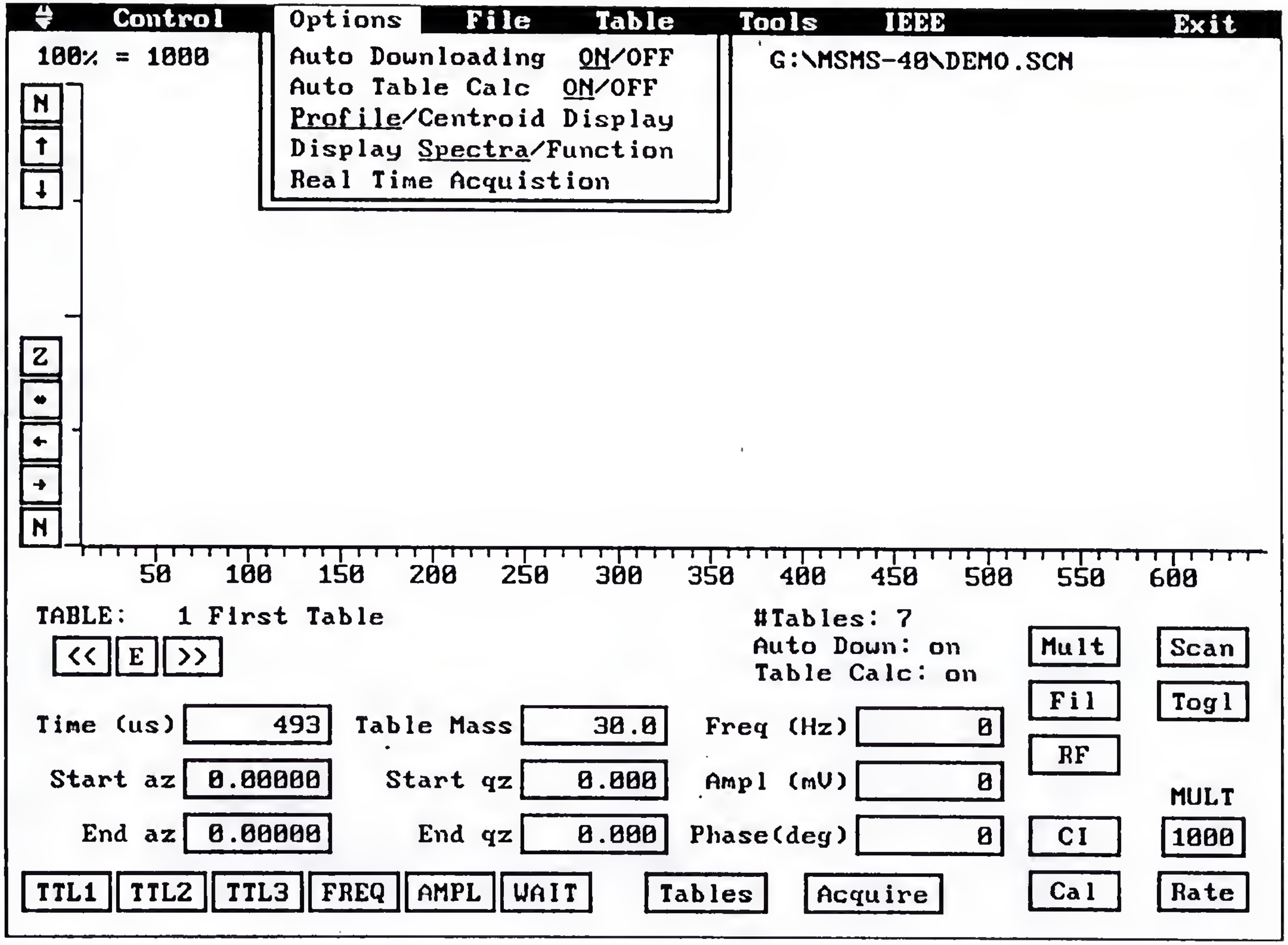

100% = 1000

G:\MSMS-40\DEMO.SCN

TABLE: 1 First Table

#Tables: 7
Auto Down: on
Table Calc: on

Time (us) 493
Start az 0.00000
End az 0.00000

Table Mass 30.0
Start qz 0.000
End qz 0.000

Freq (Hz) 0
Ampl (mV) 0
Phase(deg) 0

MULT 1000

Therefore, routines were written to acquire both profile and centroid data to ASCII files. To set up the acquisition file, "Options|Real Time Acquisition" is selected in the menu. This option allows the user to select centroid or profile data, enter the mass range, and the name of the file to write. After the file is set up by the menu option, the Acquire button at the bottom center of the main screen can be highlighted. This button tells the software to write the data to the disk after every mass spectrum is taken. The data that are collected in this manner can be manipulated in any spreadsheet program that accepts ASCII files. A program, Gatorwork, also was written to manipulate the ASCII data files acquired in Gatorware.

Many of the functions that are made available in Gatorware required extensive changes to the microprocessor control software on the SAP. The modified software is called GATORware, as opposed to Gatorware. Before ITS-Scan can be used, GATORware must be downloaded, it is automatically downloaded upon entrance of Gatorware. It is often necessary, however, to download GATORware while in ITS-Scan; to do so "Control|Load GATORware" is selected from the menu (Figure 2-4).

Spectrum Display

The middle section of the ITS-Scan main screen shows the currently acquired mass spectrum (Figure 2-2). The y-axis can be scaled manually, by clicking on the arrows on the upper left of the y-axis. An automatic scaling

Figure 2-4. Menu control to download the firmware to the SAP. The menu also enables the user to send the scan function to the QITMS to control the operation of the trap.

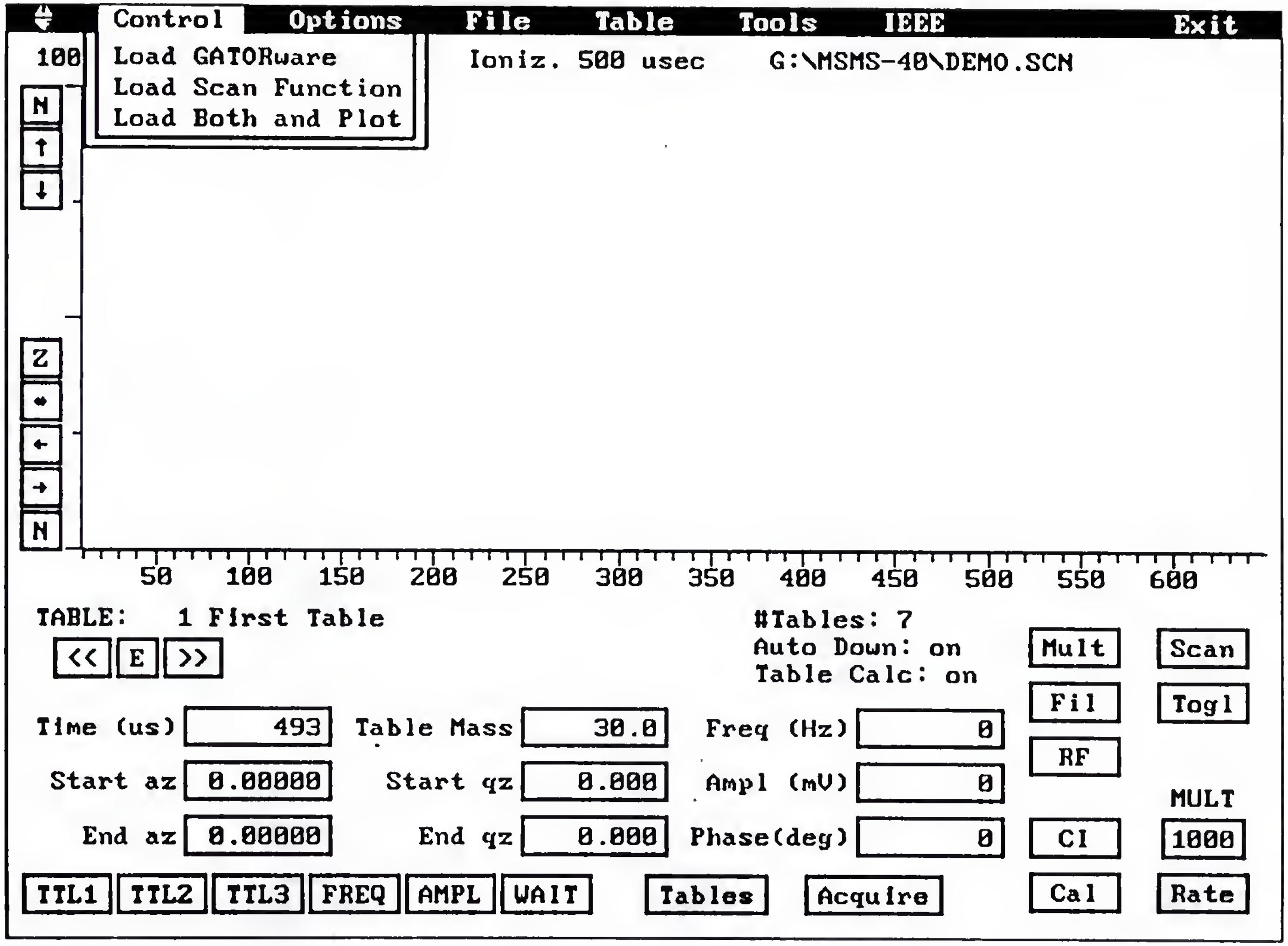

Ioniz. 500 usec G:\MSMS-40\DEMO.SCN

TABLE: 1 First Table

#Tables: 7
Auto Down: on
Table Calc: on

Time (us) 493
Start az 0.00000
End az 0.00000
Table Mass 30.0
Start qz 0.000
End qz 0.000
Freq (Hz) 0
Ampl (mV) 0
Phase(deg) 0
MULT 1000

feature also is available by clicking on the normalize button (N). The values for 100% of the displayed scale along with the total ion intensity (TIC or RIC) are shown at the top of the display. The ionization time and currently used scan function also are shown. In addition, the x-axis scale can be adjusted by using the buttons located to the bottom left of the spectrum or the mass range can be selected by dragging the mouse over the required range on the x-axis.

Parameter Buttons

Located below the mass spectrum display are inputs for nine of the most frequently adjusted parameters. The values that are used for the current table are shown and can be adjusted to see, in real-time, the effect that the parameter changes have upon the mass spectrum. In addition, six of the table flags can be toggled from this display. The currently active table number also is displayed along with arrows to change the active table. Any table can be jumped to by clicking on the table number. Clicking on the <E> displays the Scan Table Editor to allow control of all of the QITMS's operations (see Scan Table Editor below).

Scan Editor

The operation of the QITMS can be altered by changing the scan function that is currently being used. For example, to change from EI to chemical ionization (CI) the scan function must be modified to include a reaction time. In order for the operator to have complete control of the operation of the QITMS a Scan Editor was designed. The editor consists of three major parts. The first is the Clipboard Editor which enables the modification of the entire scan function. The second is the SAP Table Editor which modifies the SAP control lines. The Scan Table Editor is the third section. This editor is a simplified method for controlling the SAP control lines.

Clipboard Editor

A listing of the scan function that is being edited can be shown by selecting "Table|Scan Clip". The Scan Table Clipboard (Figure 2-5) shows a listing of the tables that compose the scan function, a simple EI scan function in this case (Figure 2-5). In addition, the tables can be erased, inserted, or their order changed. These abilities by themselves are useful; however, the flexibility of the software is further enhanced by the addition of table editors that allow each table to be individually modified.

SAP Table Editor

The SAP table editor (Figure 2-6) allows the user complete control of the SAP. The editor can be entered by clicking on the SAP Table box in the Scan Table Editor. The editor enables the user to enter the values that the SAP uses to determine its operation. For example, Start RF DAC, Number Steps of No Data, and Number Wait Loops are values that the user must enter to

Figure 2-5. The scan table clipboard allows the user to control the order of the tables in the scan function. Tables also can be added and deleted from the scan function.

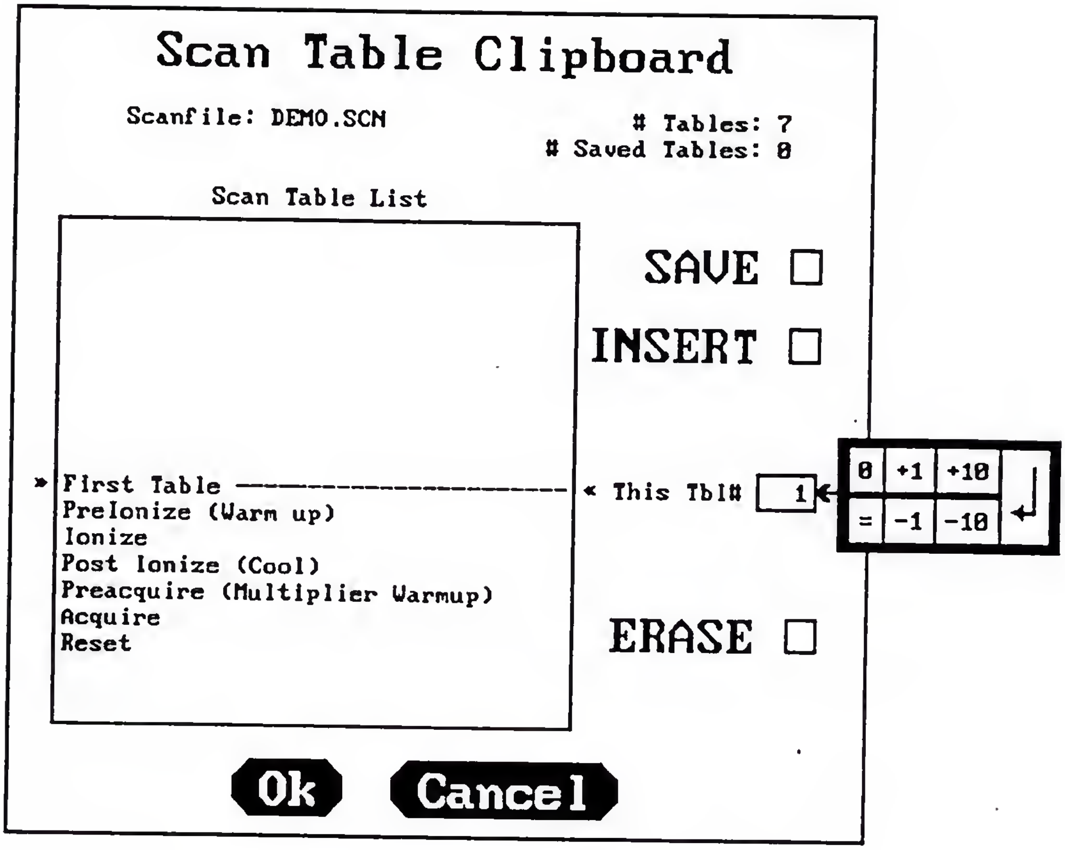

Scan Table Clipboard

Scanfile: DEMO.SCN

Tables: 7
Saved Tables: 0

Scan Table List

» First Table
PreIonize (Warm up)
Ionize
Post Ionize (Cool)
Preacquire (Multiplier Warmup)
Acquire
Reset

« This Tbl# 1

Figure 2-6. The SAP table editor allows the user to directly control the lines that the microprocessor uses to operate. This editor allows the most flexibility; however, thorough knowledge of the QITMS electronics is necessary.

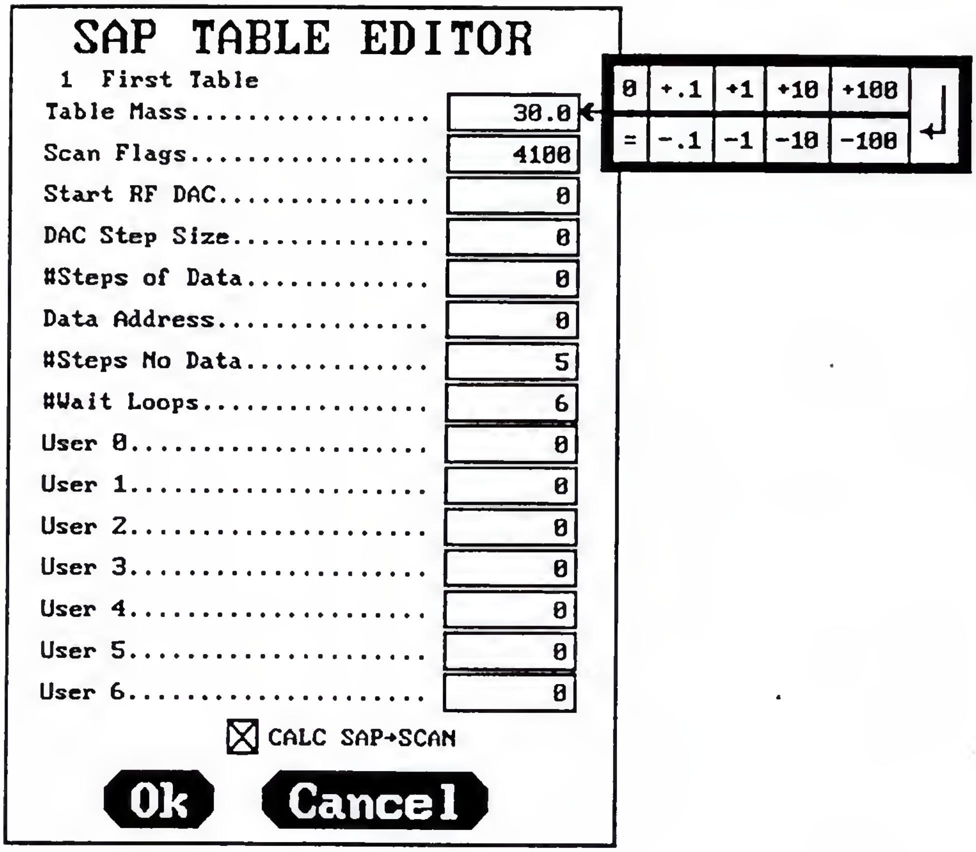

SAP TABLE EDITOR

1 First Table

Table Mass.................	30.0
Scan Flags.................	4100
Start RF DAC...............	0
DAC Step Size..............	0
#Steps of Data.............	0
Data Address...............	0
#Steps No Data.............	5
#Wait Loops................	6
User 0.....................	0
User 1.....................	0
User 2.....................	0
User 3.....................	0
User 4.....................	0
User 5.....................	0
User 6.....................	0

☒ CALC SAP→SCAN

control the RF voltage to apply to the ring electrode. While this allows the most flexibility in the operation of the QITMS, it requires that the user have a thorough knowledge of how the electronics operate, making the editor difficult and time-consuming for most experiments. To help facilitate the use of Gatorware, the Scan Table Editor was written.

Scan Table Editor

The Scan Table Editor (Figure 2-7) has inputs for fundamental trap parameters such as a_z and q_z, and automatically calculates the SAP control values. The editor can be entered by clicking on the "E" located on the bottom left of the main screen of ITS-Scan. Inputs for table time, start and end q_z, and table mass also are available. In addition, the user can select table types, e.g., acquisition, ionization, or AGC. The table mass and q_z or a_z values are used to calculate the RF or DC voltage (equation 1 and 2, Chapter 1) to apply to the ring electrode, after which the correct digital-to-analog converter (DAC) values are calculated and sent to the SAP. In this way, the user can use the same scan function for examining ions of different m/z; the only change that is necessary is to the table mass. The scan table editor facilitates the use of the instrument while retaining the versatility that is necessary for many experiments. To use this editor, knowledge of the fundamental trap parameters is required. No knowledge of electronics, however, is needed to use this editor.

Figure 2-7. The scan table editor is a simplified editor. The editor requires the user to know the fundamental parameters of the QITMS; however, no knowledge of the electronic is necessary.

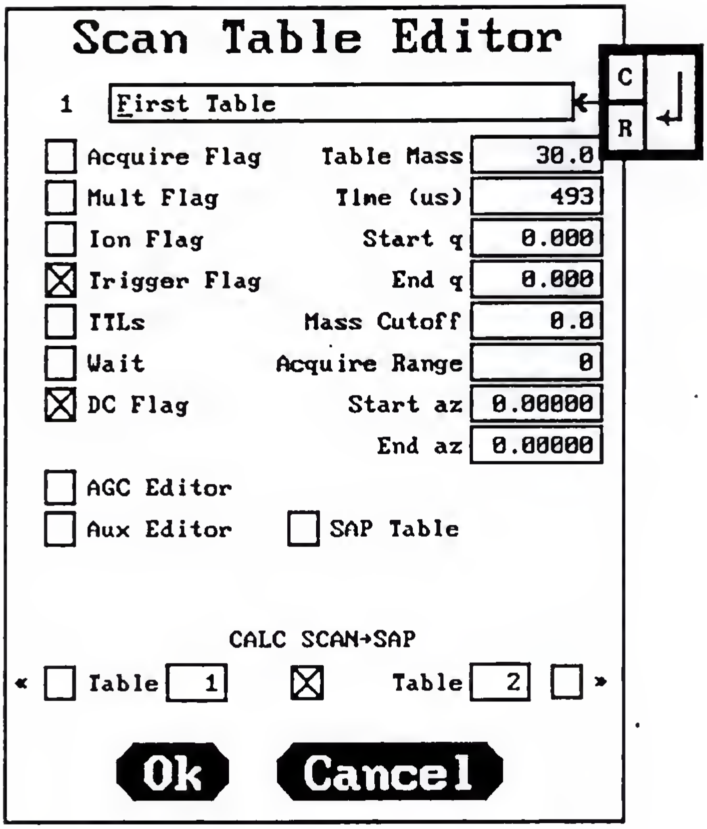

Scan Table Editor

1 First Table

☐ Acquire Flag — Table Mass: 30.0
☐ Mult Flag — Time (us): 493
☐ Ion Flag — Start q: 0.000
☒ Trigger Flag — End q: 0.000
☐ TTLs — Mass Cutoff: 0.0
☐ Wait — Acquire Range: 0
☒ DC Flag — Start az: 0.00000
End az: 0.00000

☐ AGC Editor
☐ Aux Editor — ☐ SAP Table

CALC SCAN→SAP
« ☐ Table 1 — ☒ — Table 2 ☐ »

Custom Calibration

In order for the correct RF and DC voltages to be applied to the ring electrode, the voltages must be calibrated. The ITS-40 only allows for very limited methods for calibration of the RF voltage; no means are available to calibrate the DC voltage. The RF calibration was modified to enable the user more control of the calibration. In addition, DC calibration was added to Gatorware to ensure the correct values are applied to the ring electrode.

RF Calibration

The QITMS calibration routines were modified to allow the user to select the scan function to use for calibration. The ITS-40 only allows calibration using perfluortributylamine (PFTBA) with a normal EI or CI scan function. For this reason custom calibration routines were written for Gatorware. These routines are selected by the "Tools|Mass Calibration" pull down menu (Figure 2-8). The Mass Calibration Box (Figure 2-9) has options that can be selected using the mouse and includes user masses and the ability to use a custom scan function. The user masses option furnishes the user with the ability to calibrate with compounds other than PFTBA. The ability to use custom scan functions enables different techniques, other then GC, to be used for the introduction of samples into the QITMS. This function is very helpful for experiments that require mass range extension or high resolution.

Figure 2-8. The tools pull down menu enables the user to calibrate the instrument. The calibration includes the RF and DC voltages along with the auxiliary board.

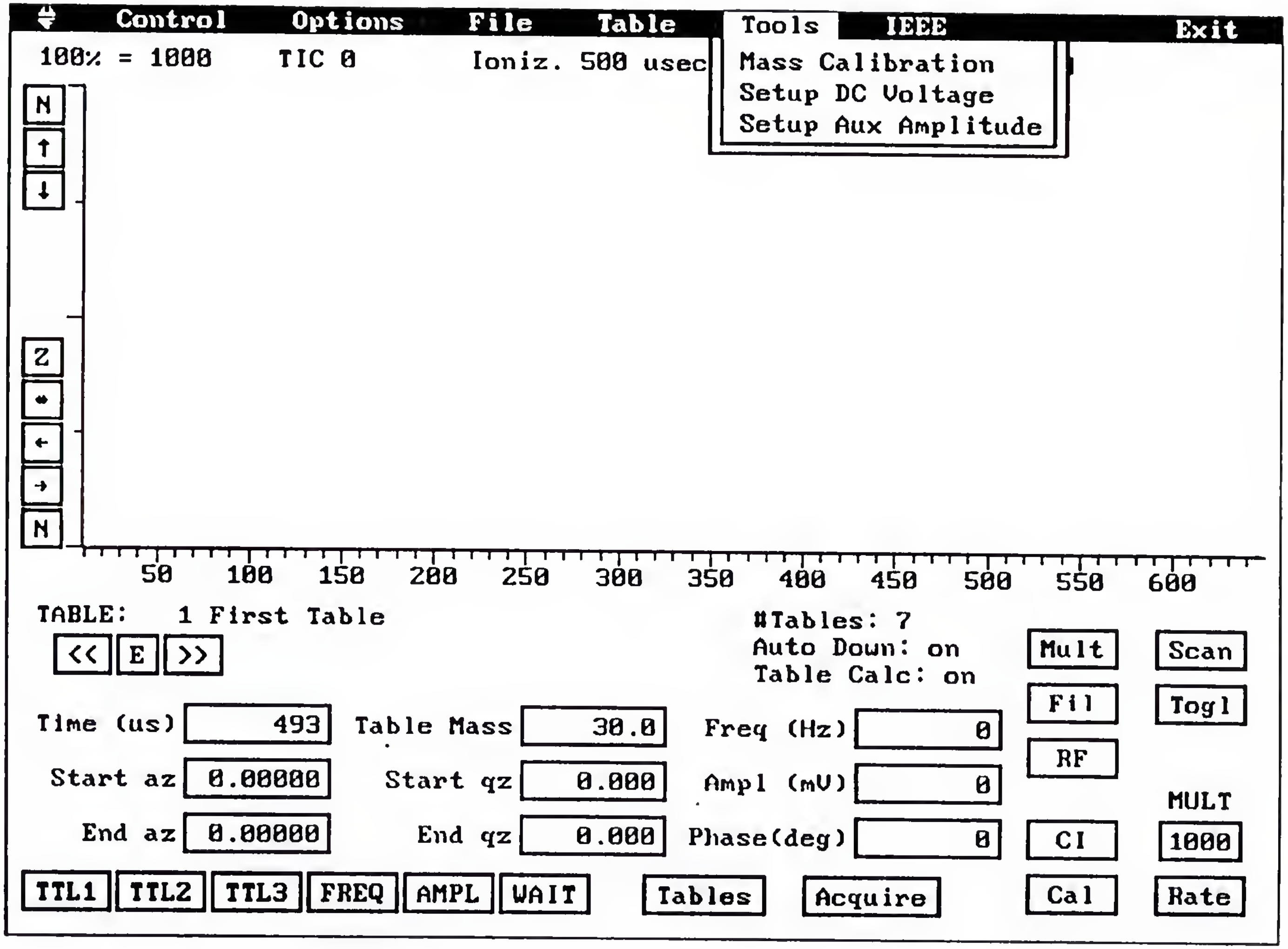

100% = 1000 TIC 0 Ioniz. 500 usec

TABLE: 1 First Table

#Tables: 7
Auto Down: on
Table Calc: on

Time (us) 493
Start az 0.00000
End az 0.00000
Table Mass 30.0
Start qz 0.000
End qz 0.000
Freq (Hz) 0
Ampl (mV) 0
Phase(deg) 0
MULT 1000

Figure 2-9. The mass calibration is the calibration of the RF voltage. The calibration can be performed with either the standard calibration compound (PFTBA) or the user can input the masses to use. In addition, the user can use the custom scan functions to calibrate the QITMS.

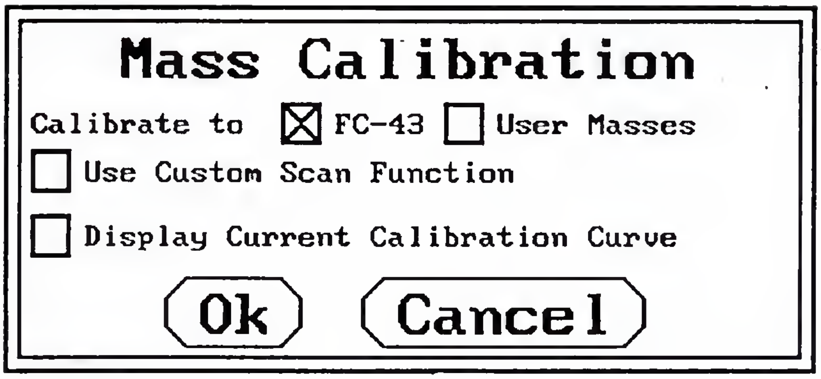

Mass Calibration

Calibrate to ☒ FC-43 ☐ User Masses

☐ Use Custom Scan Function

☐ Display Current Calibration Curve

DC Calibration

In order to apply the DC voltage to the ring electrode, the value to enter into the DC DAC must be calculated. The calibration of the DC voltage is performed by selecting "Tools|Setup DC Voltage" in the pull down menu (Figure 2-8). A voltmeter is then attached to J3 on the power board of the ITS-40. The calibration slope and intercept of the DC DAC value versus the measured DC voltage output is determined. The slope and intercept are then entered into the software (Figure 2-10).

Automatic Gain Control Editor

Automatic gain control (AGC) and automatic reaction control (ARC), developed by Finnigan MAT, [6] are methods to control the ion population formed and stored in the QITMS. AGC for EI, and ARC for CI, are methods to automatically adjust the ionization time to keep the number of stored ions out of the space charge region. A detailed description can be found in chapter 4 of this dissertation.

The Scan Table Editor has a sub-editor for AGC and ARC which is selected by clicking on the AGC Editor Box (Figure 2-7). The AGC Editor (Figure 2-11) allows new methods of AGC and ARC to be developed and optimized. See chapter 4 for experiments using the AGC Editor.

Figure 2-10. Calibration editor for the DC voltage. The calibration is performed by attaching a voltmeter to J3 of the power board. The response of the DC voltage supply to the set DAC is then determined. The slope and offset are then entered into the editor.

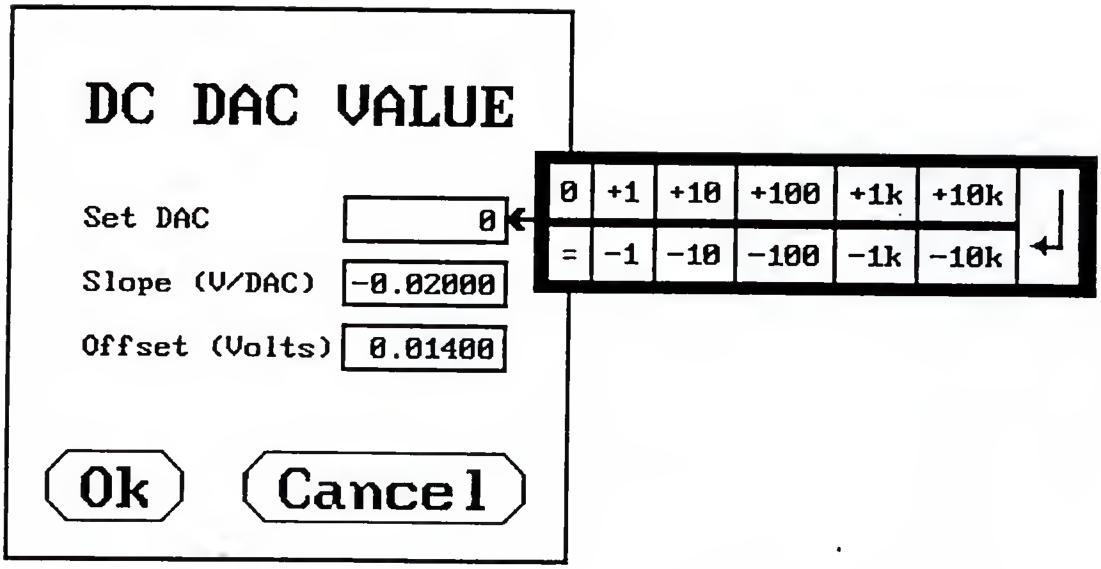

DC DAC VALUE

Set DAC 0

Slope (V/DAC) -0.02000

Offset (Volts) 0.01400

Figure 2-11. Automatic gain control editor allows the user to use custom scan functions for AGC. The parameters that are used in the AGC calculations can be altered in this editor. See Chapter 4 for further details and an example using the editor.

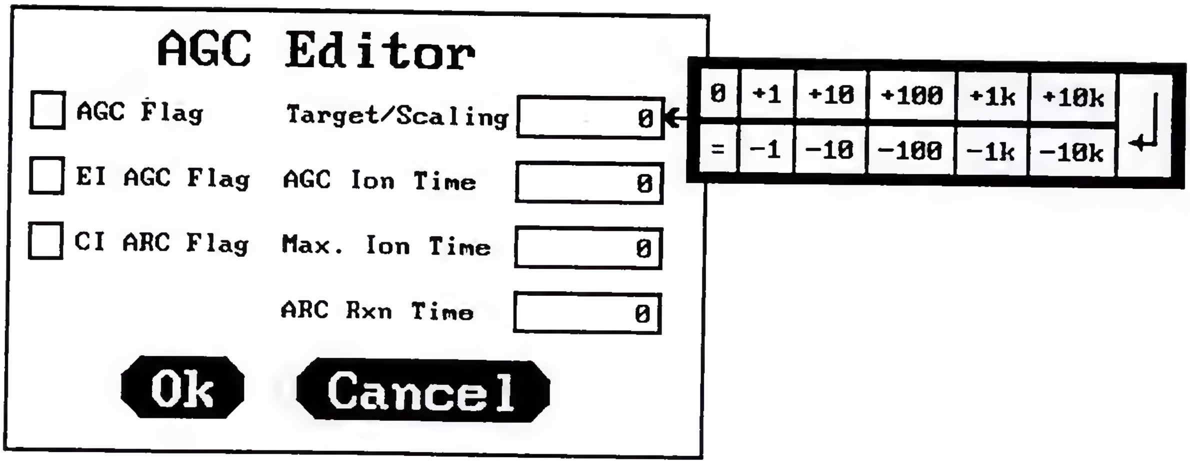

AGC Editor

☐ AGC Flag

☐ EI AGC Flag

☐ CI ARC Flag

Target/Scaling 0

AGC Ion Time 0

Max. Ion Time 0

ARC Rxn Time 0

Auxiliary Board

The ability to select the frequency and amplitude of the auxiliary frequency to apply to the endcap electrodes permits a frequency profile of the ions to be performed. The auxiliary board allows the auxiliary frequency to be set equal to the secular frequency of motion. When these two frequencies are equal, the orbits of the ions increase. The increased orbit can cause CID or ion ejection to occur. When the energy absorbed by the ion increases, the ion orbit within the boundaries of the electrodes, more energetic collisions with the helium buffer gas occur causing fragmentation. When the orbit of the ions increase beyond the boundaries of the electrodes ion ejection occurs. In both cases, CID and ejection, the ion intensity decreases when the auxiliary frequency equals to the secular frequency of the ions. It is important to be able to control the amplitude of the auxiliary frequency to effect CID. If the amplitude is too large, the orbits of the ions become so large that the ions strike an electrode. Therefore, the amplitude must be large enough to increase the orbits while small enough to prevent ion ejection. An auxiliary board (designed and built by Nathan Yates, Scott Quarmby, and myself) and control software (designed and written by Nathan Yates and myself) were designed to allow the user either to perform CID or the acquisition of frequency profiles.

Auxiliary Board Description

A diagram depicting the auxiliary board is shown in Figure 2-12. The board can be seen as being composed of three parts. The first is the decoding which allows the microprocessor on the SAP to communicate with the auxiliary board. The second is the frequency synthesizer that applies the frequency to the endcap electrodes. The third is the TTL In which lets external devices trigger the QITMS.

The communication of the frequency board to the microprocessor located on the SAP is performed as is shown in Figure 2-13. The 80186 microprocessor uses a 16 bit bus to communicate with memory and external devices. A detailed description of the operation of the 80186 microprocessor can be found in Microsystem Components Handbook--Microprocessors Volume 1, 1986[19]. The architecture of the microprocessor uses peripheral chip select (PCS) lines to let the external devices know if they should read the data on the bus. Up to seven peripheral devices can be controlled by the microprocessor (PCS 0 - 6). The PCS lines correspond to specific address blocks. For example, (with the base address equal to 8000h) when an address between 807Ch-81FFh is written to or read from, the PCS 2 line is activated. In this way the microprocessor can communicate with a specific device to perform an operation. The auxiliary board was designed to use the PCS 2 line. The memory map for the auxiliary board is shown in Table 2-1. There are seven spare addresses that are not used on the board. The

Figure 2-12. Block diagram of the auxiliary board used with Gatorware. The board communicates directly with the microprocessor on the SAP which allows different frequencies to be used during a scan function.

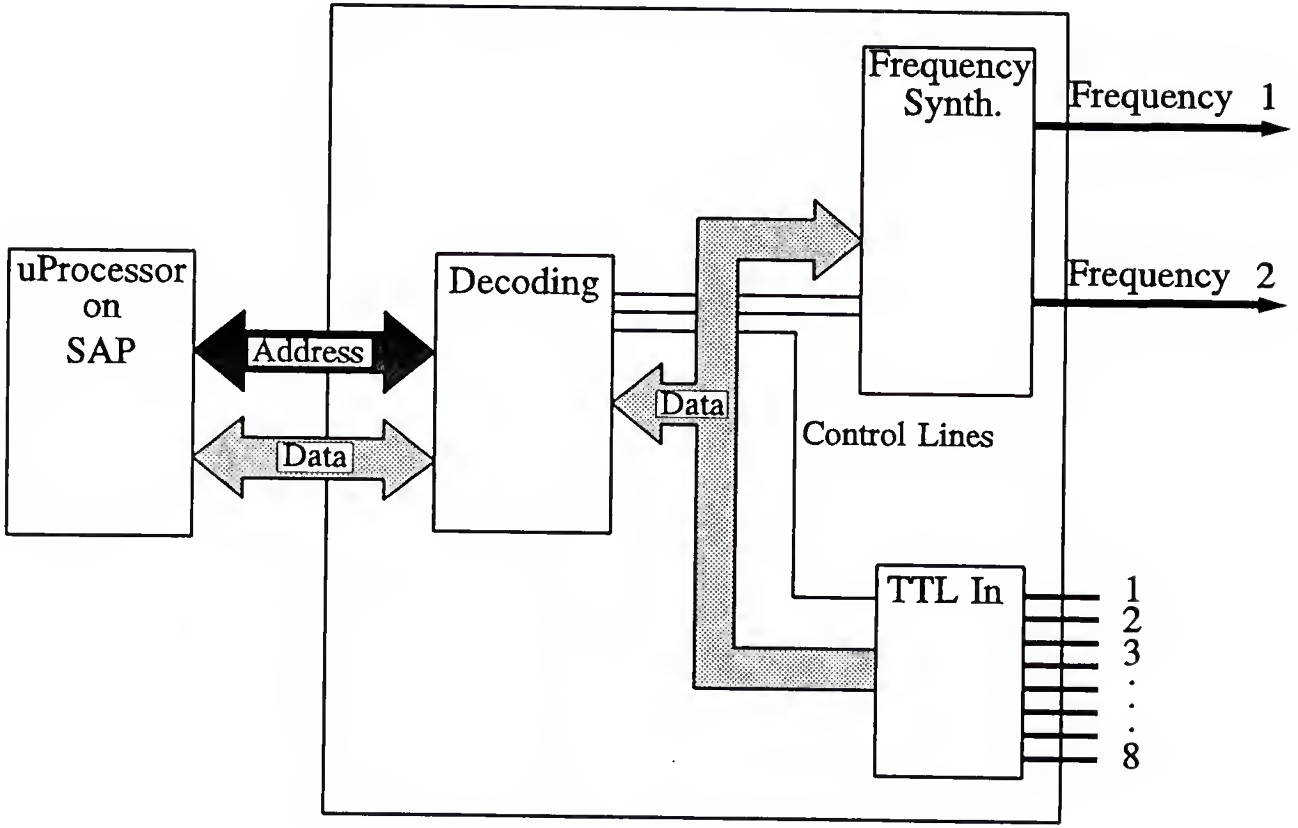
uProcessor
on
SAP
Address
Data
Decoding
Data
Frequency
Synth.
Frequency 1
Frequency 2
Control Lines
TTL In
1
2
3
. . .
8

Figure 2-13. Block diagram depicting the communication of the 80186 microprocessor with memory and external devices. The 80186 uses PCS lines to control which device is being communicated with. The auxiliary board uses the PCS 2 line.

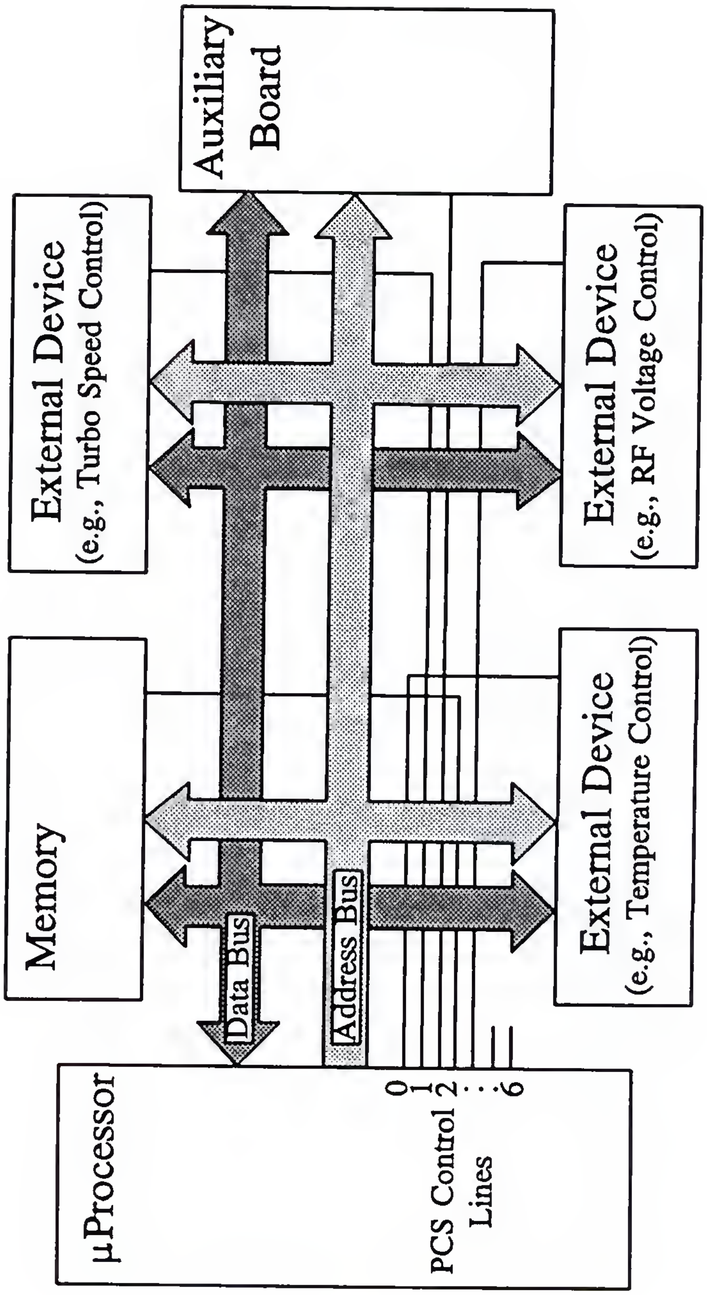
µProcessor
PCS Control Lines
0
1
2
6
Data Bus
Address Bus
Memory
External Device (e.g., Temperature Control)
External Device (e.g., Turbo Speed Control)
External Device (e.g., RF Voltage Control)
Auxiliary Board

Table 2-1. Auxiliary Board Memory Map.

Address (Hex)	Description
00	DDS1 Phase Increment A (PIRA) bits 0-7 (LSB)
02	DDS1 PIRA bits 8-15
04	DDS1 PIRA bits 16-23
06	DDS1 PIRA bits 24-31 (MSB)
08	DDS1 Phase Increment B (PIRA) bits 0-7 (LSB)
0A	DDS1 PIRB bits 8-15
0C	DDS1 PIRB bits 16-23
0E	DDS1 PIRB bits 24-31 (MSB)
10	DDS Synchronous Mode Control (SMC)
12	DDS1 Reserved
14	DDS1 Asynchronous Mode Control (AMC)
16	DDS1 Reserved
18	DDS1 Accumulator Reset Register (ARR)
1A	DDS Reserved
1C	DDS1 Asynchronous Hop Clock (AHC)
1E	DDS1 Reserved
20	DDS2 PIRA bits 0-7 (LSB)
22	DDS2 PIRA bits 8-15
24	DDS2 PIRA bits 16-23
26	DDS2 PIRA bits 24-31 (MSB)
28	DDS2 PIRB bits 0-7 (LSB)
2A	DDS2 PIRB bits 8-15
2C	DDS2 PIRB bits 16-23
2E	DDS2 PIRB bits 24-31 (MSB)
30	DDS2 SMC

Table 2-1 -- continued.

Address (Hex)	Description
32	DDS2 Reserved
34	DDS2 AMC
36	DDS2 Reserved
38	DDS2 ARR
3A	DDS2 Reserved
3C	DDS2 AHC
3E	DDS2 Reserved
40	DDS Control Port (16-bit register)
44	DDS1 & DDS2 HOPCLK (synchronous)
48	DDS1 & DDS2 PMCLK (synchronous)
4C	DDS1 & DDS2 EXTMUXCLK (synchronous)
50	Amplitude Control DACA
54	Amplitude Control DACB
58	Balun DACCS
5C	BALUN DACST
60	No Connection (N/C) Spare
64	N/C Spare
68	TTL Out Strobe
6C	N/C Spare
70	N/C Spare
74	N/C Spare
78	N/C Spare
7C	N/C Spare

assembly program that controls the microprocessor uses a structured variable list so that the control words correspond to the correct memory locations. A listing of the control words is shown in Table 2-2. It is important to note that the control words are written in the same order as the memory map and extra padding is used to line up the control words to the correct memory locations.

The Qualcomm Q2334 dual direct digital synthesizer was the chip used to synthesize the frequencies. The Q2334 has the ability to output two independent frequencies. The starting phase also can be selected for each frequency. A direct digital synthesizer (DDS) works on the basis that a sine wave can be generated by accumulating a predetermined phase increment. This phase increment value can be calculated based on the following equation.

$$F_G = \frac{F_S * \Delta\Phi}{2^N} \tag{2-1}$$

where F_G is the generated frequency, F_s is the clock frequency, $\Delta\Phi$ is the phase increment value, and N is the number of bits in the phase accumulator. A detailed description of the Q2334 can be found in the Technical Data Sheet available from Qualcomm[20]. The amplitude of the frequency is controlled by a multiplying digital-to-analog converter (DAC) that is controlled by the software. The frequency is coupled to the endcap electrodes by a balun circuit provided by Finnigan MAT.

The TTL In lines enable external devices to trigger the QITMS to start scanning. The values of the TTL In lines are compared against a value that the

Table 2-2. List of control word (Assembly Language).

Variable	Size
_PI_1_A_0	word
_PI_1_A_1	word
_PI_1_A_2	word
_PI_1_A_3	word
_PI_1_B_0	word
_PI_1_B_1	word
_PI_1_B_2	word
_PI_1_B_3	word
_SMC_1	word
_AMC_1	word
_ARR_1	word
_A_HOP_CLOCK1	word
_PI_2_A_0	word
_PI_2_A_1	word
_PI_2_A_2	word
_PI_2_A_3	word
_PI_2_B_0	word
_PI_2_B_1	word
_PI_2_B_2	word
_PI_2_B_3	word
_SMC_2	word
_AMC_2	word
_ARR_2	word
_A_HOP_CLOCK2	word
_CONTROL_PORT	word

Table 2-2 -- continued.

Variable	Size
_S_HOP_CLOCK	word
_PM_CLOCK	word
_EXTMUX_CLOCK	word
_DDS_AMPL_A	word
_DDS_AMPL_B	word
_BAL_DACCS	word
_BAL_DACST	word
_ADC_STROBE	word
_ADC_CHIP_SELECT	word
_TTL_OUT	word
_TTL_IN	word

user inputs; if the values are equal the QITMS operates as normal. If the two values are not equal the QITMS will hold at the current RF and DC voltages until they are equal. In this manner the QITMS will idle at the given RF and DC voltages until external devices tell it to start scanning. This can be used to synchronize the QITMS's operation with another device, e.g., a time-of-flight mass spectrometer. The software was written so that the TTL In is compared to the input values at the beginning of the scan tables, i.e., before any changes are made for that table.

Auxiliary Board Editor

The Auxiliary Board Editor is shown in Figure 2-14 and can be accessed by clicking on the Aux Editor button in the Scan Table Editor. The editor has inputs for controlling the frequency, amplitude, and starting phase for one auxiliary frequency. The frequency can be adjusted from approximately 50kHz to 1.1MHz. The limit for the frequency is primarily from the balun circuit that is used to couple the frequency synthesizer to the endcap electrodes. The synthesized frequency, however, cannot be more then half of the clock speed used to drive the Q2334 (4MHz clock speed in this case). The amplitude can be varied from 0 to 10 $V_{0\text{-}p}$. The starting phase can be adjusted by increments of 45°. These controls allow the maximum flexibility that could be designed into the hardware. Although the control software for the microprocessor was

Figure 2-14. The auxiliary board editor lets the user control the frequency to apply to the endcap electrodes. The frequency can be changed during any table in a scan function.

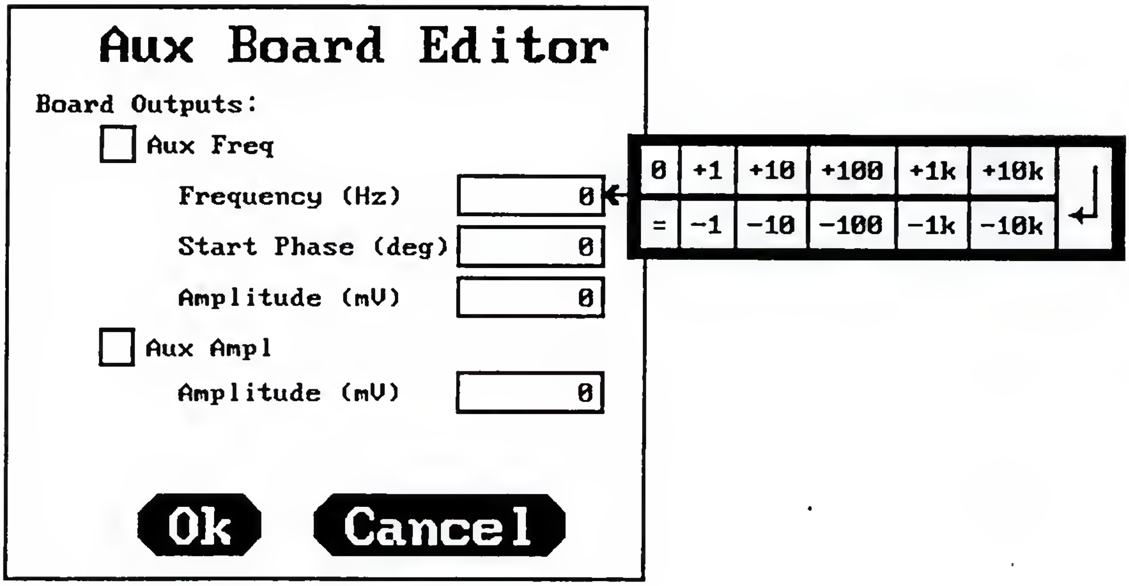

Aux Board Editor

Board Outputs:

☐ Aux Freq

Frequency (Hz) 0

Start Phase (deg) 0

Amplitude (mV) 0

☐ Aux Ampl

Amplitude (mV) 0

written to use both channels of the frequency synthesizer (see Table 2-1 and 2-2), memory limitations in ITS-Scan (i.e., 64kb for FORTH) permit the use of only one channel. An amplitude control, however, is available for a second device, such as an arbitrary waveform generator.

GC Acquisition

The acquisition control for the ITS-40 can be entered by typing <A> in the Exec Page. The acquisition editor is shown in Figure 2-15. The software lets the user name the file to which to write the data (DATA FILE). In addition, the user can set up the autosampler (AS METH), the gas chromatograph (GC METH), and the QITMS (ACQ METH). The editor for the QITMS is shown in Figure 2-16. The values that are normally able to be adjusted are shown on the left hand side of the editor. The software was modified to permit the use of scan functions built in ITS-Scan. The input SE filename is the name of the scan function that was built and saved to disk (in the same directory as the method file). When background mass is set to eleven (11), the microprocessor will use the custom scan function; all other times it will use the scan functions normally used on the ITS-40. In this manner, both types of scan functions can be used and a comparison of the custom scan function can be made those normally available. The control buttons to enable Auto ion control (AGC or ARC) and Cal gas are still active.

Figure 2-15. The acquisition editor lets the user have the ability to acquire data during a GC run. The autosampler and GC along with the QITMS editors can be reached from this screen.

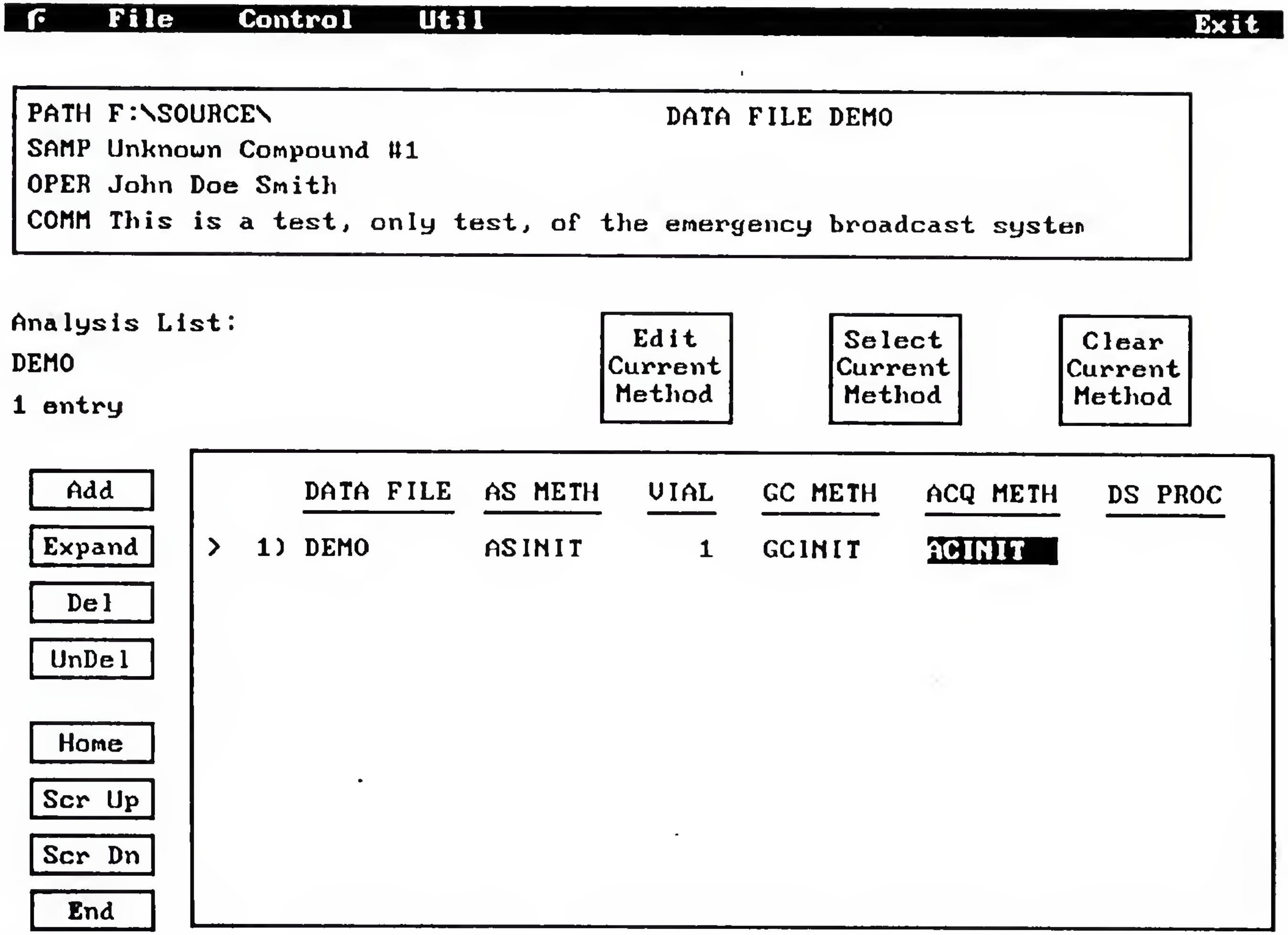

```
PATH F:\SOURCE\                          DATA FILE DEMO
SAMP Unknown Compound #1
OPER John Doe Smith
COMM This is a test, only test, of the emergency broadcast systen
```

```
Analysis List:
DEMO
1 entry
```

```
       DATA FILE   AS METH   VIAL   GC METH   ACQ METH   DS PROC
> 1) DEMO          ASINIT       1   GCINIT    ACINIT
```

Figure 2-16. The QITMS editor controls the acquisition of the data during a GC run. All data acquired through this method are centroid. Scan functions made in ITS-Scan can be used during a GC run; set the background mass to 11 and type in the SE Filename.

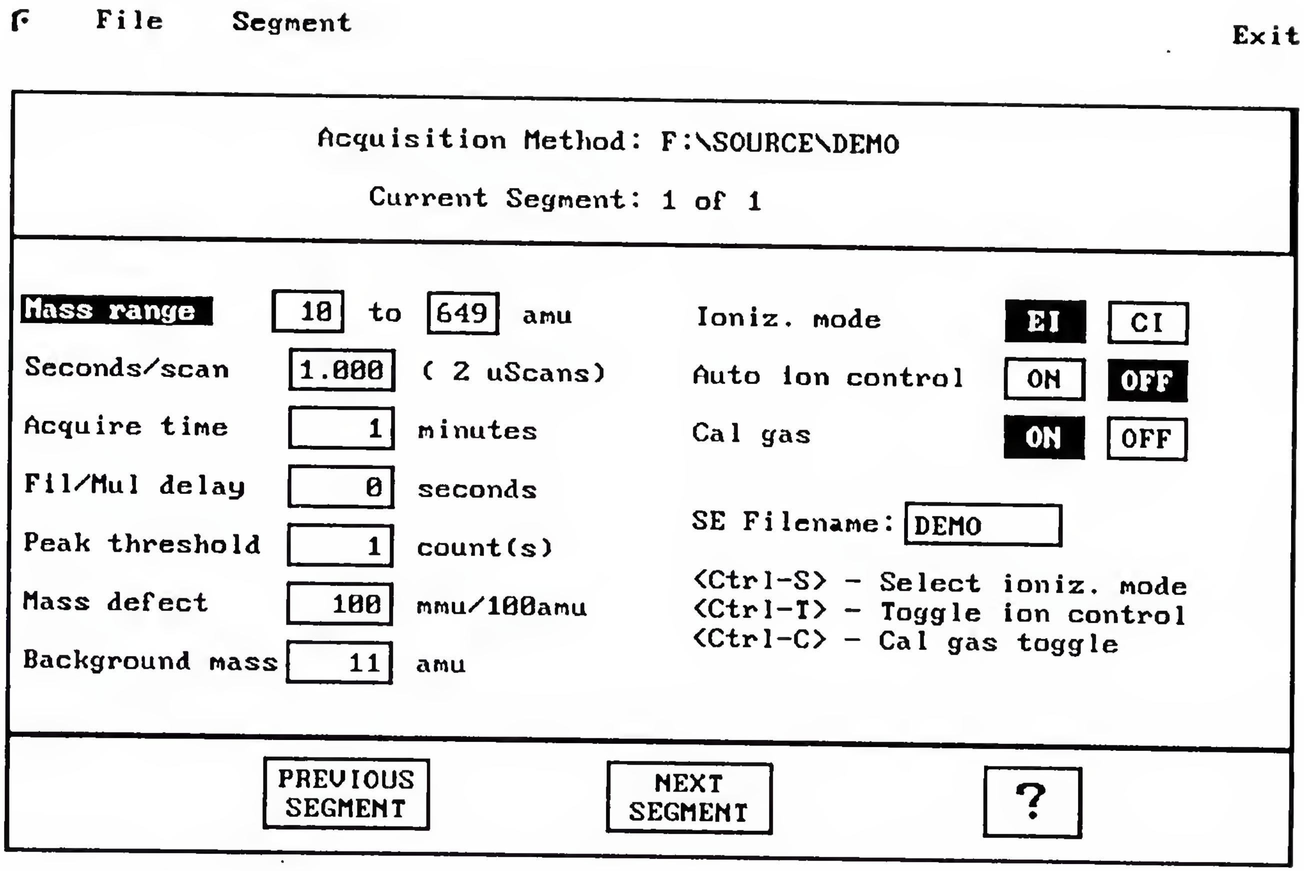

Acquisition Method: F:\SOURCE\DEMO

Current Segment: 1 of 1

Mass range 10 to 649 amu
Seconds/scan 1.000 (2 uScans)
Acquire time 1 minutes
Fil/Mul delay 0 seconds
Peak threshold 1 count(s)
Mass defect 100 mmu/100amu
Background mass 11 amu

Ioniz. mode [✓ EI] CI
Auto ion control ON [✓ OFF]
Cal gas [✓ ON] OFF

SE Filename: DEMO

<Ctrl-S> - Select ioniz. mode
<Ctrl-T> - Toggle ion control
<Ctrl-C> - Cal gas toggle

Procedure Language

Many experiments that are performed on the QITMS are not simple gas chromatographic runs. The experiments are used to determine the effect of a specific parameter upon the function of the QITMS (for example, the determination of the optimum q_z to use for ionization). The optimization employs a series of experiments that sequentially changes the q_z value and takes a mass spectrum after each change. In this manner, a plot of ion intensity vs. q_z can be used to determine the optimum q_z value. While the experiments can be performed by hand, the ability to automatically perform these experiments save time and enables a more detailed look at the parameter under investigation. The unmodified ITS-40 software does not have any method to obtain data other then centroid acquired during a GC run. Therefore, routines were added to the procedure language to permit acquisition of both profile and centroid data. In addition, methods to automate experiments also were incorporated. The procedure routines make available all of the routines that are incorporated in ITS-Scan. The scan functions are first made in ITS-Scan; the procedure routines are then run to automatically change specific values in the scan function and acquire the mass spectra.

Procedure Words

Following is a list of the procedure words, along with their definitions, that were written to facilitate automation of acquisition routines.

PIF

Start of a PIF-PTHEN or PIF-PELSE-PTHEN conditional structure.

Example: (if we make PEAK-INTENSITY an integer)

```
FORTH
PEAK-INTENSITY 2000 PROCEDURE PIF <
        FORTH
                INCREASE-IONIZATION-TIME
        PROCEDURE
PELSE
        FORTH
                GET-NEXT-SCAN
        PROCEDURE
PTHEN
```

Comment: If the statement is true (i.e., PEAK-INTENSITY < 2000) we increase the ionization time , otherwise we get the next scan. The PIF statement does not have to have the PELSE statement however, the PTHEN statement tells when the argument is over and must be present. Any compare functions (e.g., <, >, =) can be used.

PELSE

See PIF.

PTHEN

See PIF.

SCAN-ENTER

Enters the scan editor for the procedure language.

SCAN-EXIT

Turns off all control lines to the QITMS and exits the procedure.

<TIMES>

Starting position of a procedure loop operation.

Example: (SCN-COUNTER is the number of times left to loop)

```
        FORTH 10 PROCEDURE <TIMES>
FORTH
        SCN-COUNTER .
        PROCEDURE
        <LOOP>
```

Comment: The number of items that the loop is to run must be put onto the stack what the FORTH call. The <TIMES> and <LOOP> must be called in the PROCEDURE. <TIMES1> and <LOOP1> are also available for nested loops.

<LOOP>
See the example for <TIMES>.

In order to change the appropriate values in the scan function, the user must know the correct names of the table flags (Table 2-3), the table scan values (Table 2-4), and the table SAP values (Table 2-5). Any of these values can be modified during a procedure by using FORTH commands. In order to change the variable the value is put on the stack before the variable. It is subsequently stored by either D-> or -> for double or single precession numbers, respectively. It is important to note that FORTH uses only integer arithmetic and thus, no decimal points are used.

Example Procedure Programs

An example procedure program (with comments) is listed below. The example procedure is meant to show how to turn on the instrument and set up and load a custom scan function from the computer's hard drive. After the scan function is loaded from the disk the values can be changed as desired. The scan function can then be used for the subsequent acquisitions. Also included is an example of opening an ASCII acquisition file; up to three files can be opened at one time (numbered 0, 1, 2). GATORware also can be downloaded to the SAP to insure that the system is reset. Before ITS-Scan can be used in the procedure it must first be loaded into memory. This is accomplished by typing < ^ G> at the Exec Page, then <ITS-SCAN> and

Table 2-3. Scan Table Flags for Procedure.

ION-FLAG	Ionize during this table
PROTECT-FLAG	Turn multiplier on
DC-FLAG	DC voltage enable - not used for ramped DC voltage
TRIGGER-FLAG	Trigger enable
ACQUIRE-FLAG	Acquire during this table only
TTL1-FLAG	Spare TTL 1 pulse
TTL2-FLAG	Spare TTL 2 pulse
TTL3-FLAG	Spare TTL 3 pulse
CALC-AGC-FLAG	Calc AGC values - AGC scan table
EI-AGC-FLAG	AGC ionization table - variable time
SCAN-TBL-FLAG	Tells which editor to use (SAP or SCAN)
TABLE-CALC-FLAG	Enables calculations from Scan Table to SAP Table
EXT-FREQ-FLAG	Auxiliary frequency board enable
EXT-AMPL-FLAG	Auxiliary amplitude control enable
TTL-IN-FLAG	Turn on TTL inputs

Table 2-4. Scan Table Values for Procedure.

TABLE-MASS	Table mass in u * 10
TABLE-START-Q	Start q_z value
TABLE-END-Q	End q_z value
TABLE-START-AZ	Start a_z value
TABLE-END-AZ	End a_z value
TABLE-SCAN-RANGE	Range to acquire over
TABLE-MAX-AGC-TIME	Max time for AGC
TABLE-AGC-TIME	Time used in AGC prescan
TABLE-FREQUENCY	Auxiliary frequency
TABLE-AMPLITUDE	Auxiliary amplitude
TABLE-PHASE	Auxiliary phase
TABLE-AMPL1	Auxiliary amplitude control
TABLE-TTL-IN	TTL In value

Table 2-5. SAP Table Values for Procedure.

TABLE-SCAN-FLAGS	Value of the scan flags
TABLE-START-DAC	Start RF DAC value for table
TABLE-DATA-STEPS	Number RF DAC acquire steps
TABLE-NO-DATA-STEPS	Number RF DAC non acquire steps
TABLE-DAC-STEP-SIZE	Size of RF DAC steps
TABLE-DATA-ADDRESS	Memory address for acquisition (on SAP)
TABLE-WAIT-LOOPS	Padding to equal Table Time
TABLE-USER0	Used for multiple functions
TABLE-USER1	Used for multiple functions
TABLE-USER2	Used for multiple functions
TABLE-USER3	Used for multiple functions
TABLE-USER4	Used for multiple functions
TABLE-USER5	Used for multiple functions
TABLE-USER6	Used for multiple functions

return, exiting the screen, typing <R>, the name of the procedure, and the return key again.

In the following example the code is written between the solid lines, listed by screens. Comments within the code are denoted by the back slash (\), i.e., anything following the back slash is ignored when the procedure is run. Any text written between the lines can be entered into the software and the procedure will run as described. Preceding each screen listing further explanations of the code are given to explain the purpose of each command. The comments between each screen listing are not to be entered into the software, they only are included here to help further the understanding of the code.

The first screen is used to turn on the QITMS. The voltages and gases (e.g., for CI) are stabilized. When it is not necessary to turn on a particular item a back slash before the command will disable the function.

```
Screen 1
        SCAN-ENTER                  \ enter ITS-Scan
        FORTH
                TOGGLE-RF           \ turn on RF voltage
                TOGGLE-MULT         \ turn on multiplier
                TOGGLE-FIL          \ turn on filament
                TOGGLE-CG           \ open cal gas vial
                TOGGLE-CI           \ open CI gas line
                SELECT-CENT-MODE    \ display centroid data
                10000 MSEC-WAIT     \ let everything stabilize for 10 seconds
        PROCEDURE
```

The second screen shows examples of three new procedure functions. The first is the use of an if statement to control the flow of the program. To change the flow of the example program the two values being compared (1 and 2) must be altered. The commands, as written, will only perform the statements following the PIF without performing the commands following the PELSE statement. The second new function is the downloading of GATORware to the SAP. The scan function must first be created in ITS-Scan. The scan function can then be loaded into memory from the PC's hard drive with the third procedure function.

```
Screen 2
\ Example of if-else-then statement in the procedure language.
\ Example of loading the firmware and a scan function from disk.
     FORTH 1 2 PROCEDURE         \ put values to compare on stack
     PIF <                       \ compare values
          FORTH
               LOAD-FIRMWARE     \ if 1 < 2 load gator to SAP
          PROCEDURE
     PELSE                       \ otherwise do
          FORTH
               " DEMO"           \ name of scan function file
               LOAD-SCAN-FILE    \ read from disk and load to SAP
          PROCEDURE
     PTHEN
```

The third screen shows how to open an acquisition file. The file number, mass range, and acquire type must all be initialized. Three data files can be opened at one time, numbered 0 - 2. The mass range is set by storing the starting and ending values, in u * 10. For example, 750. is equal to 75.0 u. The type of data (i.e., profile or centroid) must also be set by putting a true flag into the appropriate location. In addition, a 30-space comment line and the name of the data file can be set. The command LOAD-RT-FILE opens the data file which was set up for acquisition.

```
Screen 3
\ Open the correct acquisition file
        FORTH
                0 -> FILE#                          \ data file number
                750. D-> PROF-LO-MASS               \ lowest mass to acquire
                800. D-> PROF-HI-MASS               \ highest mass to acquire
                FALSE -> PROF-ACQUIRE?              \ acquire profile data?
                TRUE  -> CENT-ACQUIRE?              \ or centroid data

                \ 123456789012345678901234567890 length of comment line
                " This is the comment line"
                SAVE-RT-COMMENT                     \ save comment in memory
                " DATA" LOAD-RT-FILE                \ open file with name in " "
        PROCEDURE
```

An example of changing one table of a scan function can be seen in screen 4. This example shows the q_z and a_z values being modified for table 3. The first command loads table three into editor memory, the next four commands modify the values. The scan table is then stored into memory and downloaded to the SAP, after which a mass spectrum is taken. This routine can be looped the correct number of times (using <LOOP>), and the values incremented by using the D+> command.

```
Screen 4
\ Initialize the variables in the table and take a scan
        FORTH
                3 SHOW-TABLE                        \ display correct table
                  700. D-> TABLE-START-Q            \ start q = 0.700
                  700. D-> TABLE-END-Q              \ end q = 0.700
                 00000. D-> TABLE-START-AZ          \ start a = 0.00000
                -75000. D-> TABLE-END-AZ            \ end a = -0.75000
                STORE-TABLE                         \ save table in memory
                LOAD-SCAN                           \ load scan function to SAP
                GET-NEXT-SCAN                       \ get data, display, and save
        PROCEDURE
```

The last screen of the procedure must include SCAN-EXIT. This command turns off all of the voltages and gases and in addition, closes all of the data files.

```
Screen 5
\ Exit ITS-Scan
        SCAN-EXIT                                \ close all files and turn all off
```

Summary

A research grade instrument was successfully developed from a commercial instrument designed for routine GC/MS analysis. The modifications were primarily software; however, some hardware modifications also were necessary. The software, called Gatorware, enables the user to have complete control of the operation of the ion trap mass spectrometer, including MS/MS. To enable MS/MS to be performed on the modified instrument, an auxiliary board was designed and built to allow computer-controlled frequencies to be applied to the endcap electrodes. With the software and hardware modifications, MS/MS can be performed along with other functions not previously available on the instrument. These functions include profile acquisition of mass spectra, the ability to modify AGC scan functions, and routines to automate experiments performed on the instrument. All of the experiments discussed in this dissertation were accomplished with the use of Gatorware. Additionally, Gatorware is being used by other researchers.

CHAPTER 3
RAMPED DC VOLTAGE

Introduction

To perform many experiments in the ion trap mass spectrometer, it is necessary to isolate ions of a single mass-to-charge (m/z). Ion-ion repulsions (space charge) limit the number of ions that can efficiently be stored and detected in the ion trap mass spectrometer. Isolation of a narrow m/z range will decrease the number of unwanted ions in the QITMS, thus reducing space charge and increasing the linear dynamic range [21-27]. Isolation of ions of a single m/z is also necessary to perform tandem mass spectrometry (MS/MS). The most common isolation methods (i.e., two-step[12, 13] and apex[11]) employ combinations of RF and DC voltages to approach the boundaries of the stability diagram.

Finnigan ion traps change the DC voltage in one step; thus, the rate of DC voltage change is the slew rate of the power supply (approximately 1.85V/μs). There are two problems associated with large, fast changes in the DC voltage, the expansion of the ion cloud and the inability of a power supply to change to a given voltage instantaneously.

Rapid changes in the DC voltage may cause the ion cloud to expand, which will be shown in more detail below. This possible expansion can cause the ions to become unstable and leave the QITMS, causing a loss of ion signal. The use of helium buffer gas helps to decrease the effects of this expansion. However, as the ions approach the stability boundary the orbits are inherently large, as shown below, which can enhance the effects of fast changes of the DC voltage.

An additional problem with large, fast changes of the DC voltage is the fact that power supplies are not able to change instantaneously from a set voltage to a different value. In designing a power supply which permits rapid changes in voltage, the time-constant is kept small. As a result, the output of the power supply may go past the wanted value for a short time before settling to the correct voltage. This phenomena is called overshoot. The overshoot can affect the performance of the QITMS, as evidenced by a decrease in the ion signal during isolation. This decrease is due, in part, to the a_z and q_z parameters being placed outside of the stability diagram for a short time. If the overshoot is too large and lasts too long, the ion signal can be totally lost.

In this chapter, a technique is examined for overcoming the problems associated with large, fast DC voltage changes. Instead of changing the DC in one large step, Gatorware permits the DC voltage to be altered in several small steps, in effect ramping the DC voltage. This ramp is analogous to the common practice of ramping the RF voltage. A marked improvement in isolation, along with a decrease in the time necessary for efficient isolation, has been observed.

Experimental

Experiments were performed to examine the effect of using ramped DC voltages on two-step mass isolation. The experiments were designed to enable a comparison of ramped versus single-step changes in DC voltage. The experiments consisted of examining the effect of the two isolation methods for ejection of both low and high mass ions.

Instrumentation

All data were collected using Gatorware on an ITS-40 (Finnigan MAT, San Jose, CA). See Chapter 2 of this dissertation for details on the software. Additional hardware modifications included the attachment of an ion gauge (model 27 gauge controller, Granville-Phillips, Boulder, CO) to the base of the ITS-40 ion trap manifold, and the replacement of the chemical ionization (CI) gas flow control valve with a Negretti flow control valve (Fareham, Hauts, England) to allow finer control of the sample pressure. For these experiments, 1-octene (Matheson Coleman & Bell Manufacturing Chemists, Norwood, OH) was introduced into the manifold via the CI gas inlet without further purification. The background subtracted sample pressure was 7×10^{-6} torr gauge reading. The ion trap was maintained at 220°C. Helium buffer gas was introduced via the gas chromatographic (GC) column into the ion trap to yield an indicated vacuum-chamber pressure of approximately $3x10^{-5}$torr[28].

As is shown in Figure 2-2, the scan editor allows the user to select the starting and ending values of a_z and q_z for each table in a scan function. The appropriate DC values for isolation are calculated using the table mass and the correct parameters in the Mathieu Equations (equations 1 and 2, Chapter 1) for the ITS-40 ion trap analyzer. Using the starting and ending values for a_z, table mass, and table time the software determines the correct values for the SAP. An example depicting ramping the DC voltage, along with a corresponding RF voltage ramp, is shown in Figure 3-1. The plots show a_z stepped from 0.00 to -0.20 (0 to 172VDC) with the q_z stepped from 0.00 to 0.400 (0 to $667V_{0\text{-}p}$); the table time equaled 1ms. Notice that each DC voltage step corresponds to an RF voltage step, thus allowing concurrent ramping of RF and DC voltages. This function is used extensively in experiments discussed in following chapters of this dissertation. The plots shown in Figures 3-1 and 3-7 were obtained by a digital storage oscilloscope (Model 9400--125 MHz, LeCroy, Switzerland).

Automated Acquisition Procedure

The experiment was performed in two parts. The first was the examination of ejection efficiencies for ions of m/z higher than the m/z to be isolated; the second examined the ejection efficiencies for ions of lower m/z.

Figure 3-1. Oscilloscope traces of ramped RF and DC voltages. The upper trace is proportional to the RF voltage measured at the DAC out (197 mV/div corresponding to $32V_{0p}$ actual RF) on the Analog Board. The lower trace is the DC voltage (50 V/div) measured at J3 of the Power Board. The time scale is 0.1 ms/div.

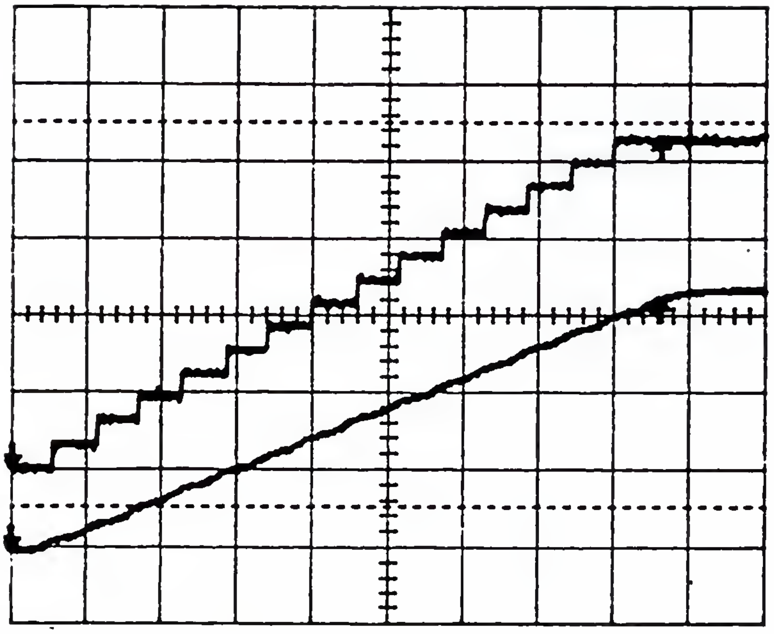

The scan function for two-step isolation used to examine the isolation efficiencies is shown in Figure 3-2. It is important to note that the q_z for the isolation steps were held constant throughout the experiment; q_z=0.710 for ejection of high m/z and q_z=0.85 for ejection of low m/z. To examine the efficiency for high mass ejection (Figure 3-2, Table 2) the a_z value was stepped from a_z=-0.200 to a_z=-0.450 with a step size of -0.001 (0.356VDC) at q_z=0.710. The efficiency for low mass ejection (Figure 3-2, Table 3) was examined by stepping the a_z value from a_z=0.000 to a_z=0.0750 with a step size of 0.001 (-0.356 VDC) at q_z=0.85.

The profile ion intensities for fragment ions in the range m/z 54-58 of 1-octene at each a_z value were saved to disk. The intensities for m/z 56 were then graphed vs. a_z. The resulting plot permitted a close examination of the stability boundaries. The effects on isolation of the different techniques for changing the voltage also were examined. The ion signal was determined by adding the total profile intensity for each DAC point that corresponded to the ion of interest. This was done to alleviate problems of using centroid data for certain experiments (see chapter 2).

Results and Discussion

The results of these studies can be broken into two separate sections. The first is the determination of the stability diagram boundaries. This is important to examine because two-step and apex isolation require the m/z of

Figure 3-2. Scan function depicting the q_z, a_z values used for the experiments. The a_z value for high mass ejection (Table 2) was first examined, followed by that for low mass ejection (Table 3).

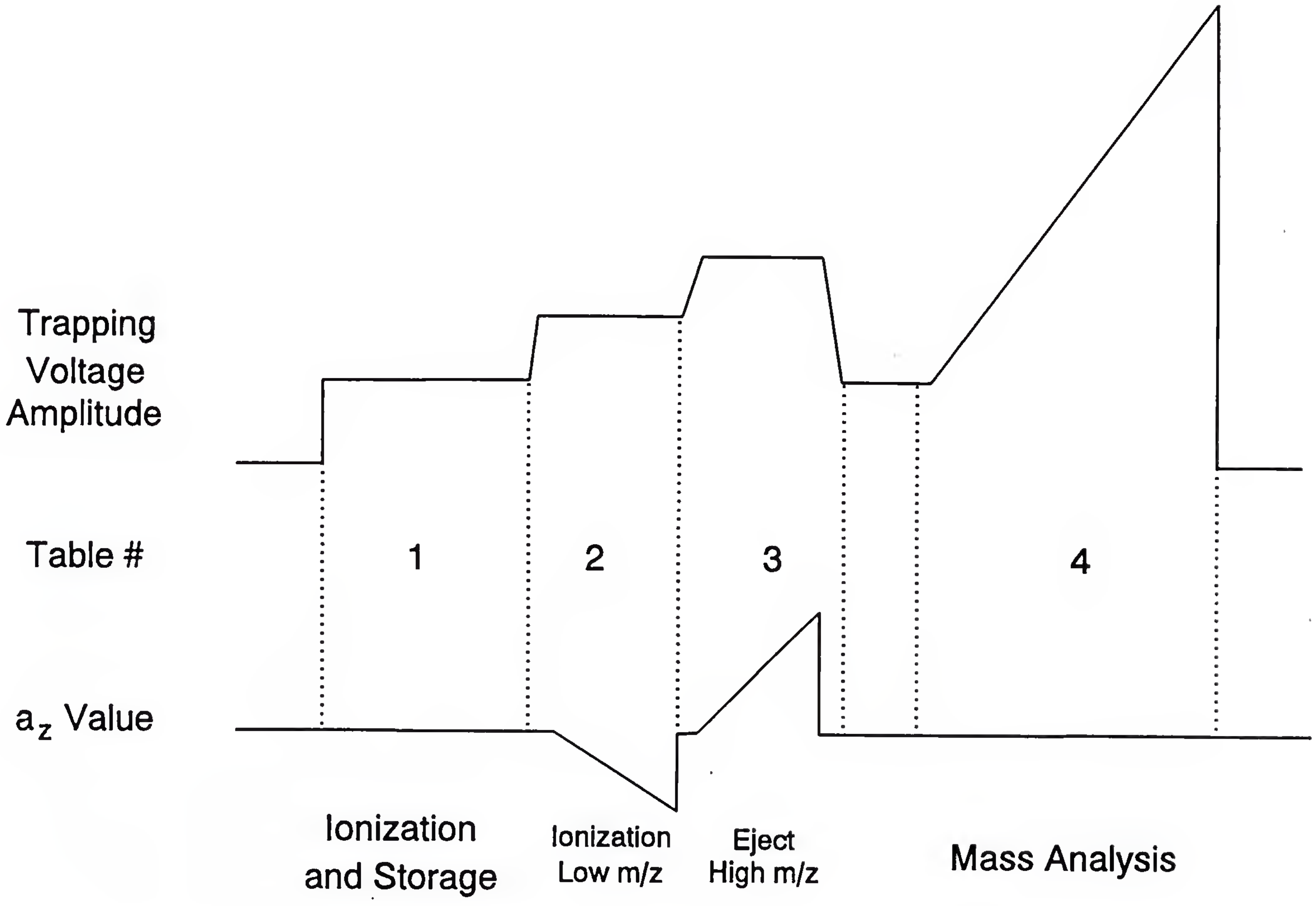
Trapping Voltage Amplitude
Table #
a_z Value
1
2
3
4
Ionization and Storage
Ionization Low m/z
Eject High m/z
Mass Analysis

interest to be placed in close proximity to the boundary. The second section examines the results of isolation. The major goal of this section is to determine any effect that the new technique has on isolation efficiencies.

Stability Boundary

By eliminating the overshoot, the use of a ramped DC voltage should enable ions of a particular m/z to be moved closer to the theoretical stability edge before loss of ion signal than should the use of a single-step DC voltage. The theoretical stability edge at $\beta_z=1$, which occurs at $q_z=0.710$ and $a_z=-0.239$, is used to eject ions with m/z higher than m/z 56 of 1-octene (see Chapter 1). The plot of the ion intensity at $q_z=0.710$ for each a_z (step increments = 0.001) can be seen in Figure 3-3; the theoretical stability boundary is depicted by the solid vertical line. The use of ramped DC voltage enabled the ions to approach the a_z,q_z values that correspond to the theoretical position of the stability boundary. Single-step DC, however, lost all ions approximately 0.01 a_z units prior to reaching the theoretical boundary. The boundary also was seen to be sharper, or better defined, for ramped DC voltage. These effects can be explained by two factors. The first is the stepped DC voltage overshooting the requested voltage. The second factor is fast expansion of the ion cloud.

A simple explanation of the overshoot of the DC voltage upon the position of the ions in the stability diagram can be seen in Figure 3-4. As

Figure 3-3. Experimental determination of the stability boundary at $q_z=0.71$ for single-step and ramped DC voltages. The theoretical stability diagram boundary is depicted by the solid line.

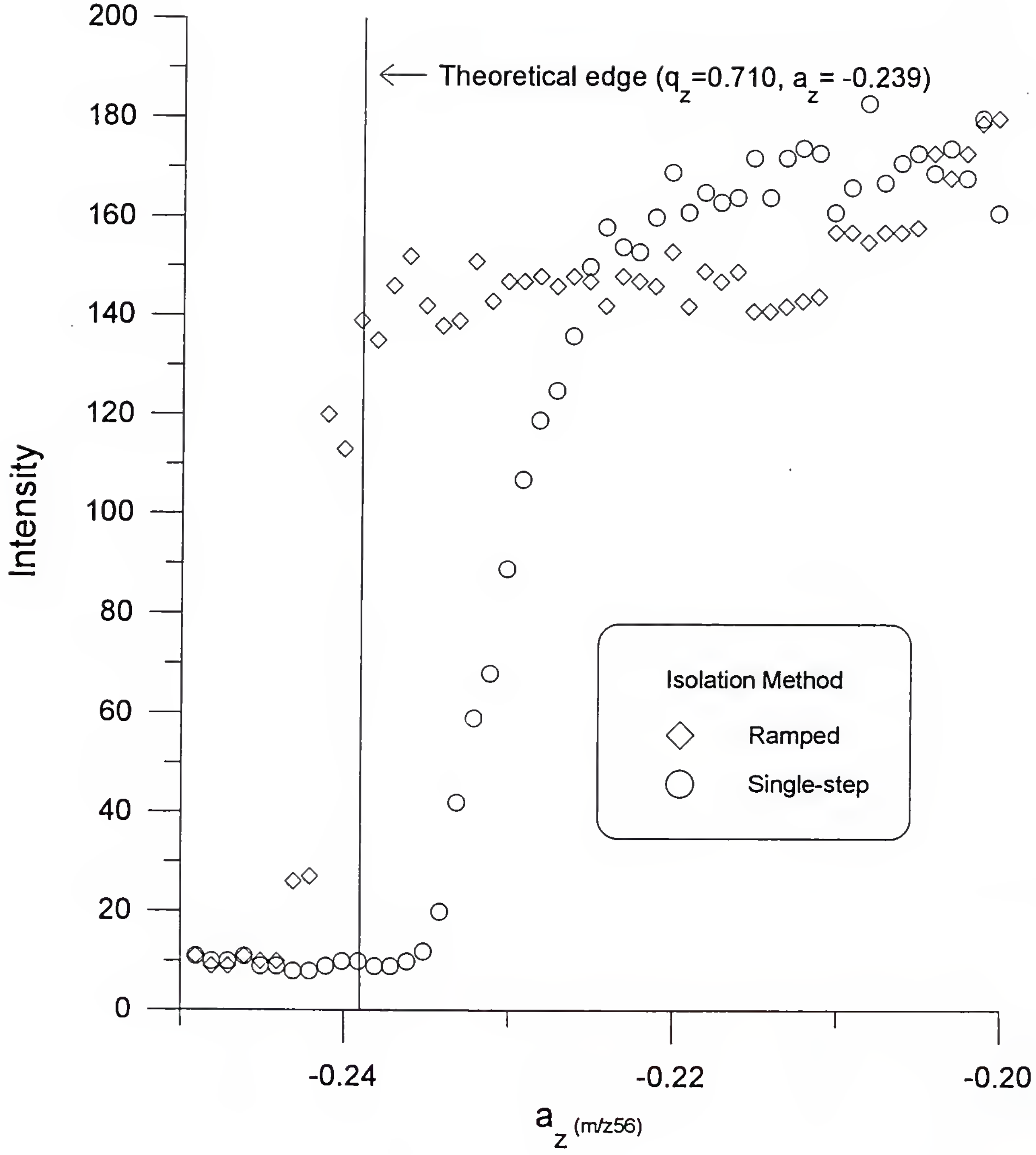
200
180
160
140
120
100
80
60
40
20
0
Intensity
Theoretical edge (q_z=0.710, a_z= -0.239)
-0.24
-0.22
-0.20
a_z (m/z56)
Isolation Method
◇ Ramped
○ Single-step

Figure 3-4. The approach to the stability diagram boundary of ions at a range in m/z: (a) Theoretical approach and (b) approach with overshoot of the DC voltage.

(a)

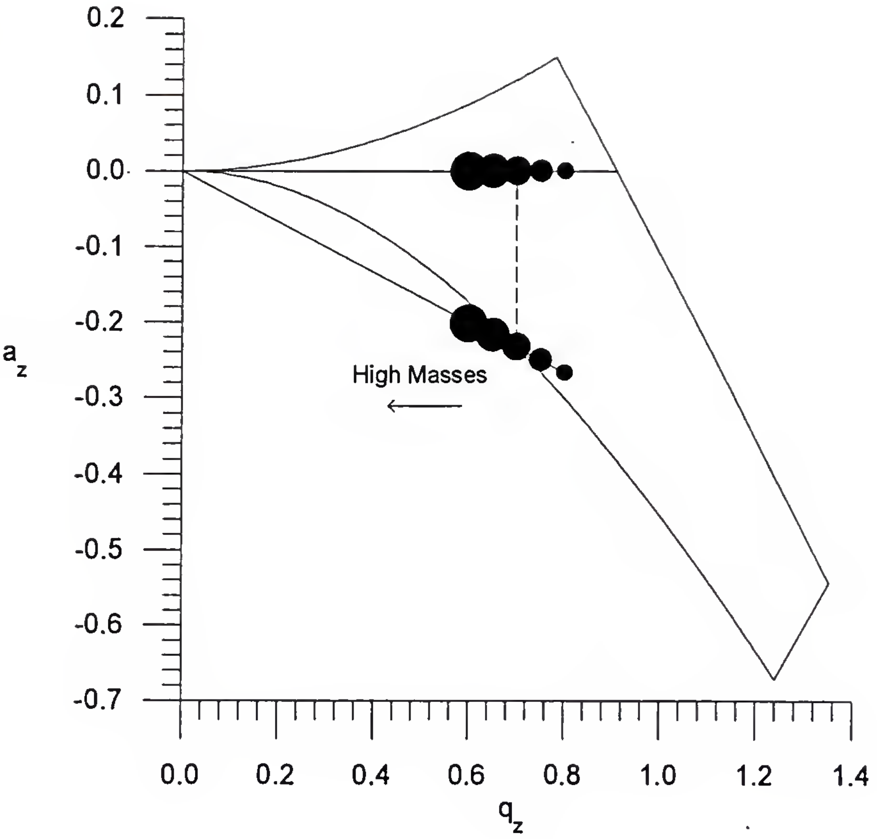
0.2
0.1
0.0
-0.1
-0.2
-0.3
-0.4
-0.5
-0.6
-0.7
a_z
High Masses
0.0
0.2
0.4
0.6
0.8
1.0
1.2
1.4
q_z

(b)

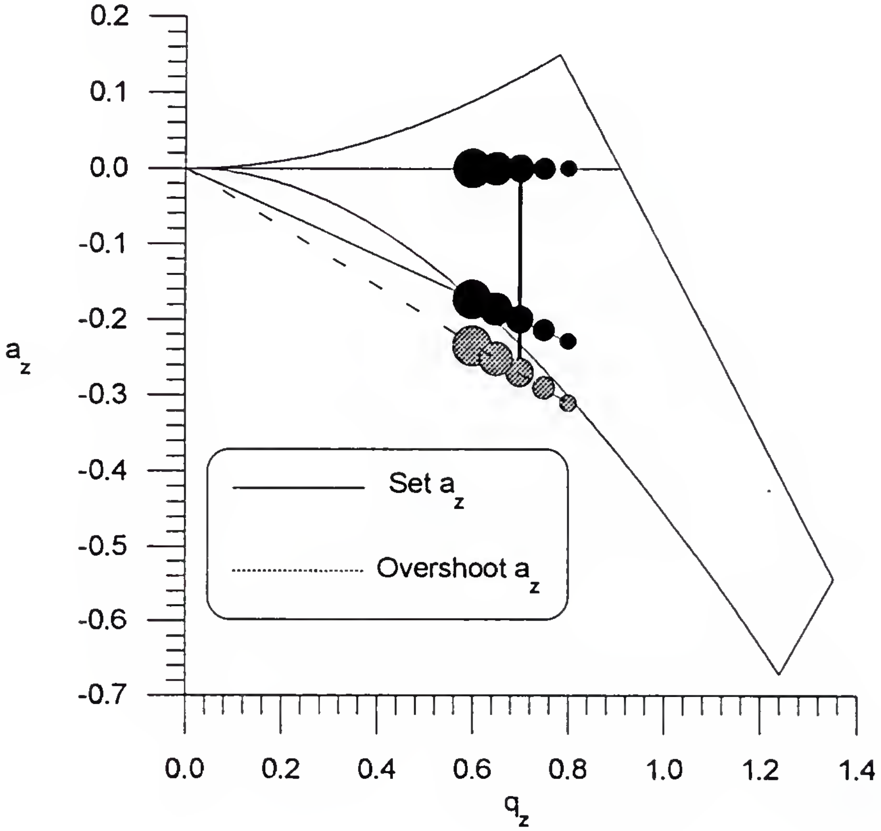
0.2
0.1
0.0
-0.1
-0.2
-0.3
-0.4
-0.5
-0.6
-0.7
a_z
Set a_z
Overshoot a_z
0.0
0.2
0.4
0.6
0.8
1.0
1.2
1.4
q_z

depicted in Figure 3-4a, the ideal DC voltage change used to approach to the $\beta_z=0$ stability boundary allows the higher m/z ions to be ejected from the QITMS without loss of the m/z ion of interest. The overshoot of the power supply, however, will cause the ions of interest also to go past the stability boundary. This effect can be seen in Figure 3-4b, which depicts the effect of the overshoot on the position of the ion in the stability region. As the requested DC voltage nears the boundary, the overshoot actually can cause the m/z of interest to leave the stable region for a short time and thus decrease the ion intensity. The overshoot can be as large as 15% of the voltage step size. A digital oscilloscope trace for single-step DC voltage is shown in Figure 3-5. The trace shows the DC voltage changing from 0 to 130 V ($a_z=0.00$ to $a_z=-0.200$ for m/z 100). In this case the overshoot on the ITS-40 (the ITMS is comparable) is approximately 6% but can be as much as 15% of the voltage change. The voltage decays to the set voltage in approximately 60μs; thus, ions of the m/z of interest leave the stability diagram during the isolation process. To prevent this loss the DC voltage must be set to a value lower than theoretically predicted. This has the effect of keeping the ions away from the stability boundary (except for the brief overshoot) and therefore lowers the isolation efficiencies. The short duration and large amplitude of the overshoot of the DC power supply prevents approaching the stability edge very closely.

The loss of the ion signal before the theoretical boundary for single-step DC voltage may also be explained by losses due to the ion cloud expansion.

Figure 3-5. Oscilloscope traces for changing the DC voltage on an ITS-40 from 0 to 130 V. The desired voltage is reached by one large voltage change. The overshoot can be as large as 15% of the desired value.

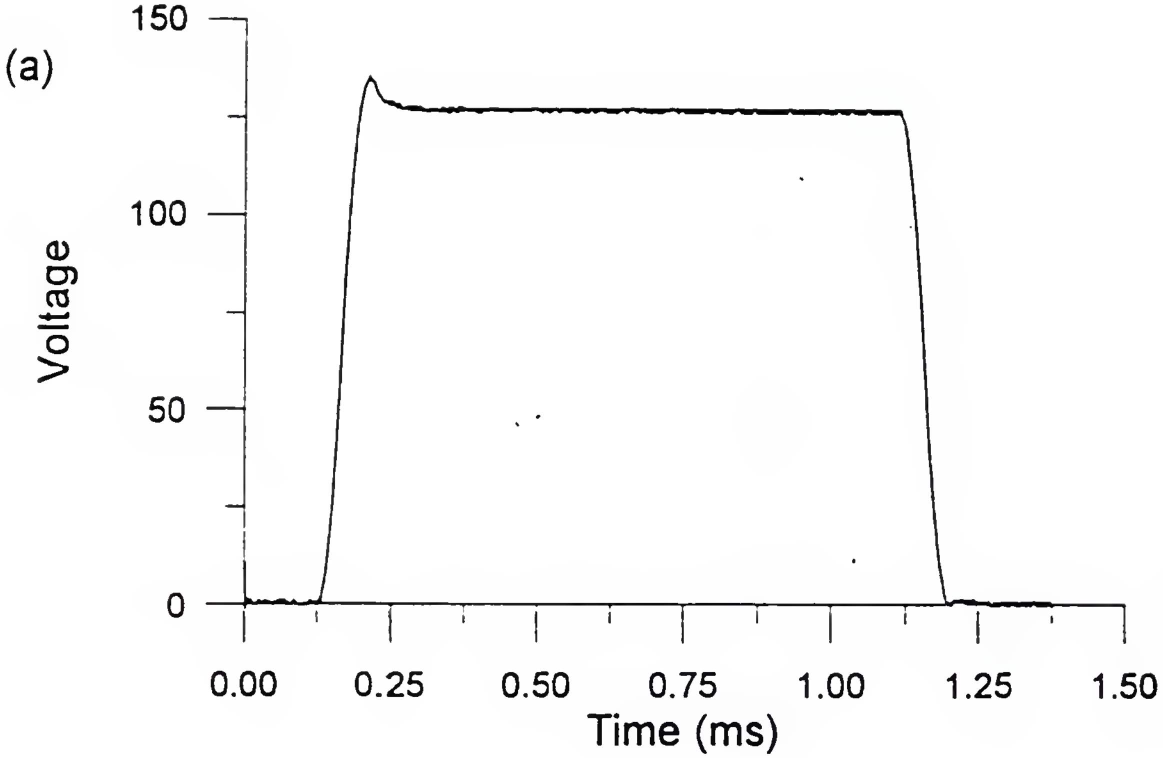
(a)
Voltage
150
100
50
0
0.00
0.25
0.50
0.75
1.00
1.25
1.50
Time (ms)

The abrupt change of the DC voltage also might cause the orbits to change drastically. This abrupt change coupled with the already large orbits associated with a_z values close to the stability boundaries can cause the loss of ion signal. For example, Figure 3-6 shows the simulated ion trajectories for q_z=0.710 while (a) a_z=0.0 and (b) a_z=-0.235. Notice that as the a_z value becomes more negative the ion orbit expands in the z direction. Further simulations of the effect of the rate at which the a_z value is changed would help to investigate this phenomena.

Currently, the major reason for the loss of ion signal upon approaching the β_z=1 boundary with a single DC step is not known. It is believed that the aforementioned factors are the primary causes for the ion signal loss; however, there could be more factors that have not yet been determined. The combination of the two effects were alleviated, to a large extent, with the use of small, slow DC steps associated with ramped DC voltages.

Figures of Merit for Isolation

Two figures of merit have been defined to determine the efficiency of an isolation technique[6]. They are the efficiency of isolation (E_{is}), the percentage of the ion of interest that remains in the QITMS after isolation, and the efficiency of ejection (E_{ej}), the percentage reduction in the neighboring ions after isolation. The two efficiencies are defied as

Figure 3-6. Simulation showing the trajectories for m/z 100 at q_z=0.710 while (a) a_z=0.00 and (b) a_z=-0.235. The trap geometry is as follows r_0=0.1cm, z_0=0.707 with a 10% stretch. The simulations were performed using SIMION v. 6.0 from Idaho National Engineering Lab, 1995. Notice the larger z excursion near the β_z=1 boundary.

(a)

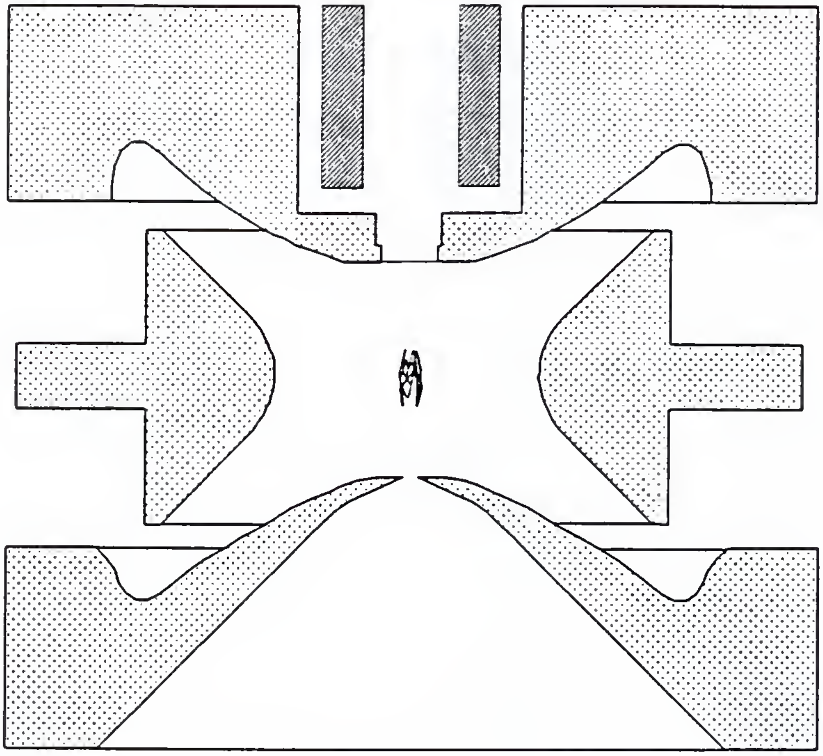

(b)

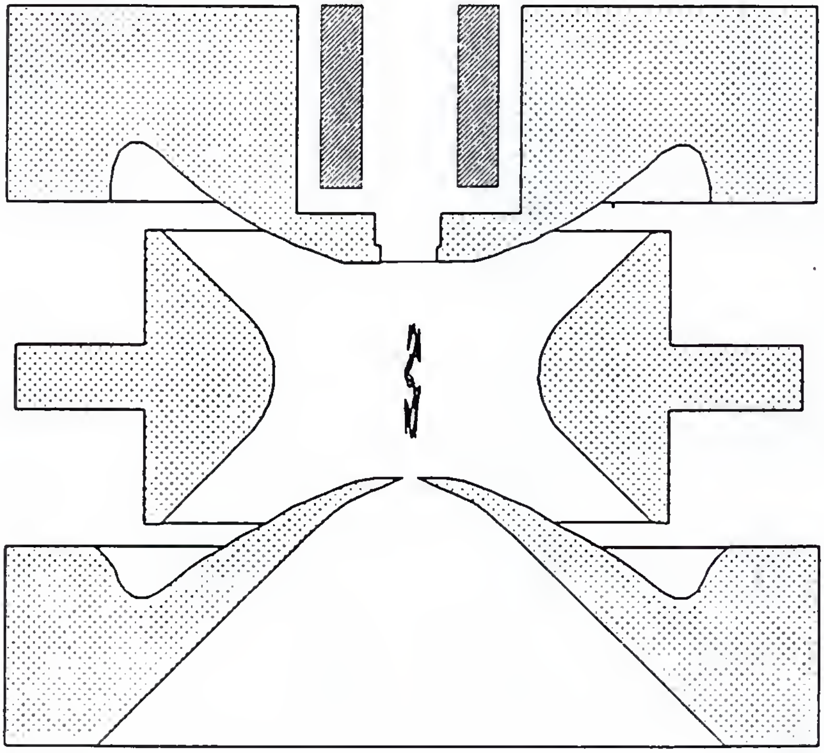

$$E_{is} = \left(\frac{I_p}{I_p^o}\right) * 100\% \qquad (3\text{-}1)$$

$$E_{ej} = \left[1 - \left(\frac{I_{p+n}}{I_{p+n}^o}\right)\right] * 100\% \qquad (3\text{-}2)$$

where the subscripts p, and p+n on I (intensity) denote the m/z of interest and the nearest neighbor above and below the ion of interest, respectively; the superscript ^{o} denotes the ion intensity before isolation.

Isolation Efficiencies

The m/z 56 fragment ion, $C_4H_8^+$, from 1-octene was chosen for comparison due to the fact that the neighboring ions (m/z 55 and 57) were of approximately the same intensities as the m/z 56 ion. The isolation figures of merit for the m/z 56 ion using ramped and single-step DC voltage are shown in Figure 3-7. Ideal isolation would have both E_{is} and E_{ej} equal to 100% (i.e., the upper right of the plots). As can be seen when the a_z is being changed with a fixed $q_{z,}$ the ideal case was not achieved.

Examination of the isolation and ejection efficiencies for higher masses (Figure 3-7a) shows that for ramped DC voltage E_{ej} can be greater than 90% with an E_{is} of 80%. In comparison, to achieve E_{is} equal to 80% for single-step

Figure 3-7. Plot of the efficiencies for isolation of m/z 56 and ejection of (a) m/z 57 and (b) m/z 55 of 1-octene using ramped and single-step DC voltage methods.

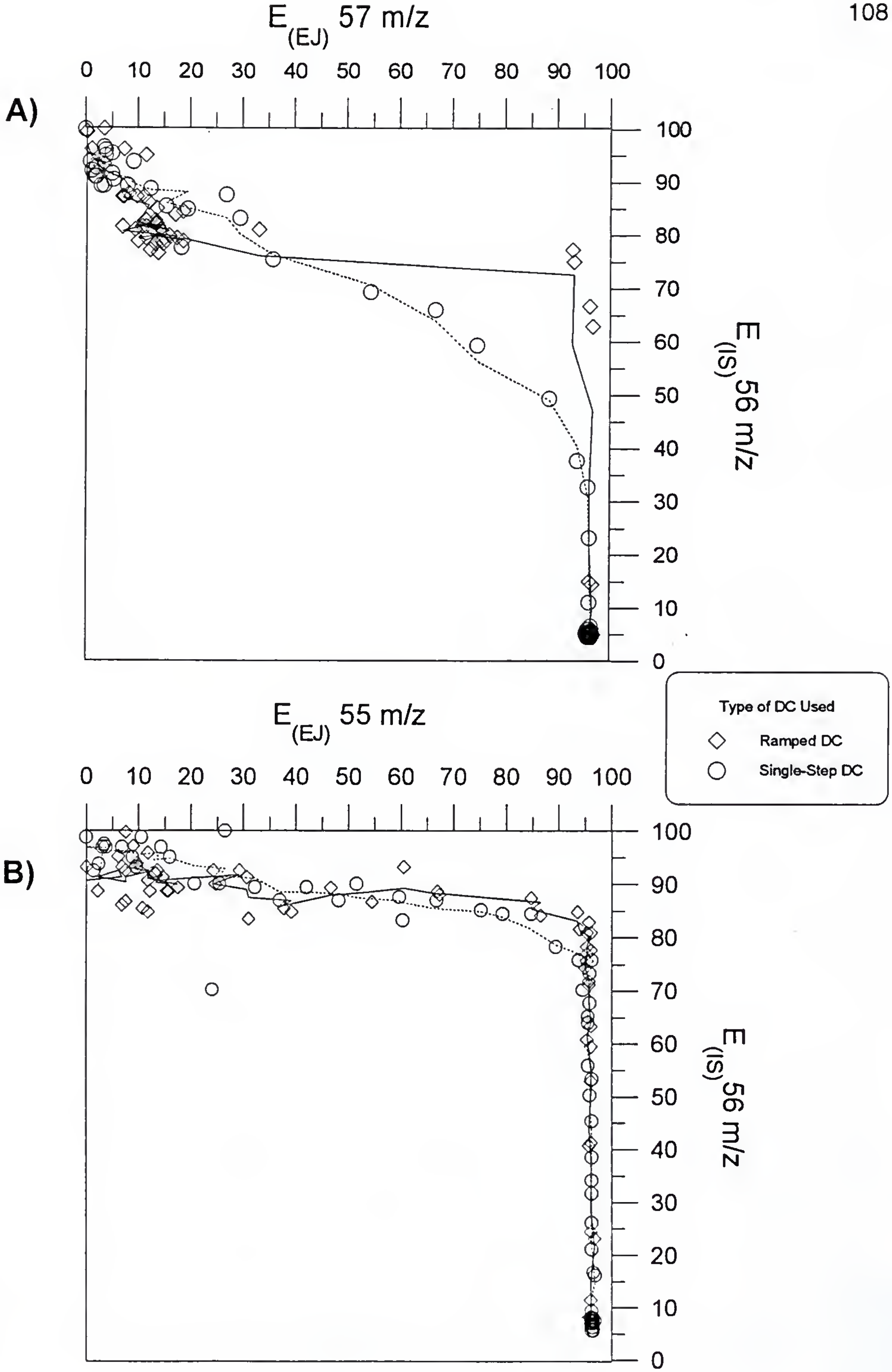
A)
$E_{(EJ)}$ 57 m/z
0 10 20 30 40 50 60 70 80 90 100
$E_{(IS)}$ 56 m/z
100 90 80 70 60 50 40 30 20 10 0
B)
$E_{(EJ)}$ 55 m/z
0 10 20 30 40 50 60 70 80 90 100
$E_{(IS)}$ 56 m/z
100 90 80 70 60 50 40 30 20 10 0
Type of DC Used
◇ Ramped DC
○ Single-Step DC

DC voltage, E_{ej} was seen to be less then 40%. The results for low mass ejection are shown in Figure 3-7b. Although the overall efficiencies are higher than for the high mass ejection, it clearly demonstrates that ramped DC voltages improve E_{is} when E_{ej} is greater than 70%.

Ramped DC methods showed an improvement in isolation and ejection efficiencies by as much as 50% over single-step DC methods. The loss of isolation efficiencies for single-step DC voltage suggest that the edge of the stability diagram is not being efficiently reached by this method. Ramped DC voltage, in contrast, was able to efficiently reach the stability boundary which can, in part, be attributed to eliminating the overshoot.

The trace in Figure 3-8a is a digital oscilloscope trace for single-step DC voltage. The trace shows the DC voltage changing from 0 to 130V (a_z=0.00 to a_z=-0.200 for m/z 100). Figure 3-8b depicts a simple method to overcome the overshoot that can be used on instruments not equipped with ramped DC voltage. The method uses two steps of voltage to reach the desired value. The first step is used to bring the ions near the area of the stability boundary; the second step moves the ions to the stability boundary. During the second step, it is important to keep the voltage change less then 100VDC to prevent overshoot from causing ion loss. This was seen to improve the isolation efficiencies to approximately that of ramped DC voltage. The time necessary for this method, however, is dramatically increased (more then two times) due, in part, to the time necessary to let the voltage stabilize during the first large

Figure 3-8. Oscilloscope traces for changing the DC voltage on an ITMS from 0 to 130 V. The desired voltage is reached by (a) one large voltage change and (b) two steps of voltage change with an initial change of 90 V.

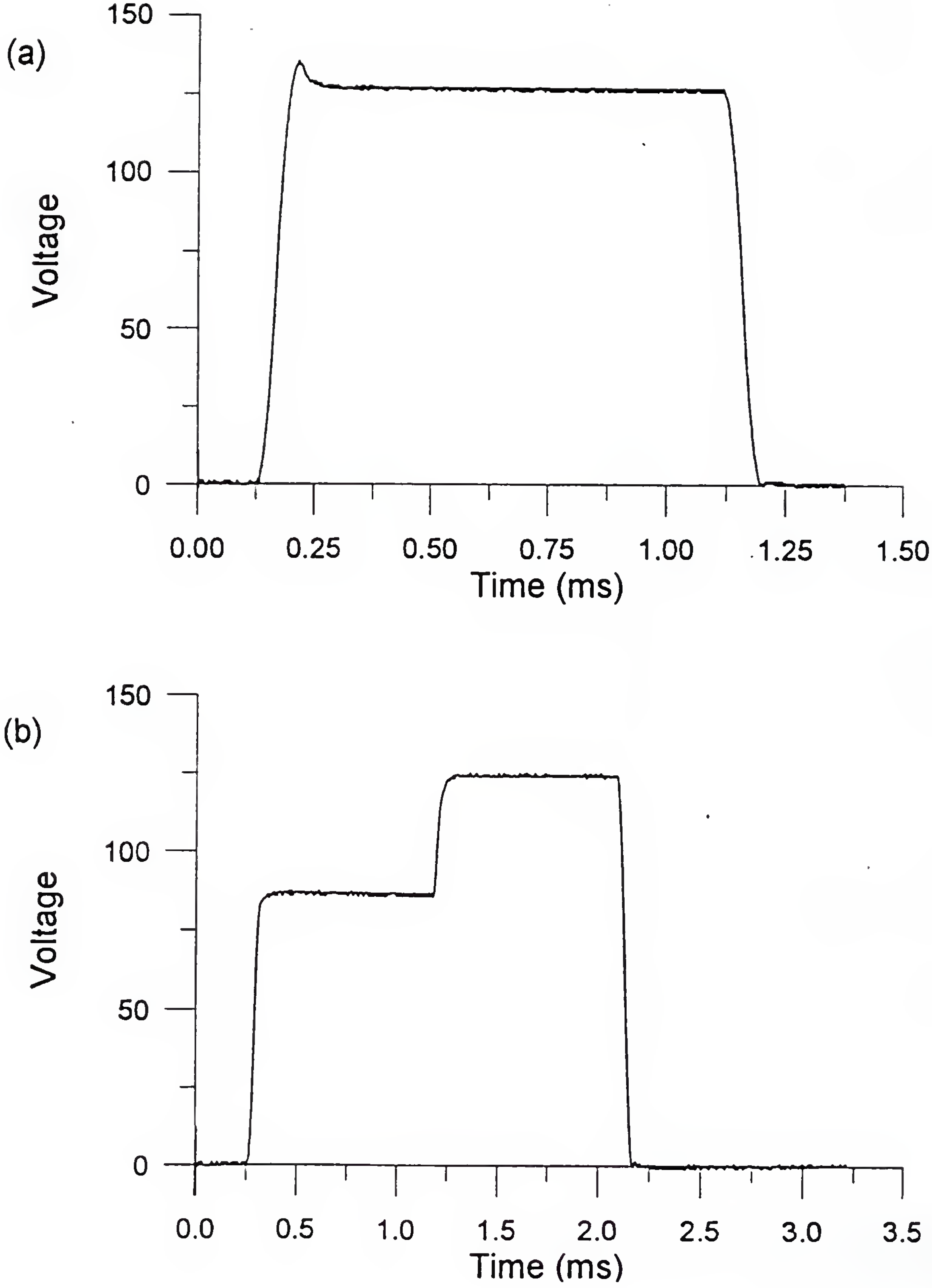
(a)
150
100
50
0
Voltage
0.00
0.25
0.50
0.75
1.00
1.25
1.50
Time (ms)
(b)
150
100
50
0
Voltage
0.0
0.5
1.0
1.5
2.0
2.5
3.0
3.5
Time (ms)

DC step. Additional time is needed for this technique over the ramped method because of the time for necessary for the hardware to start a new table in a scan function.

Summary

The use of ramped DC voltage improves isolation efficiencies by as much as 50% over single-step DC voltage methods. This improvement can be explained by the improved ability to place the ions close in close proximity to the stability boundary, enabling the ejection of the neighboring ions while maintaining the ion of interest. The overshoot and possibly the ion cloud expansion associated with conventional single-step DC methods inhibits the placement of the ions close to the stability boundary, decreasing isolation efficiencies. It was not determined from these experiments which factor caused the greater loss of ion signal, ion cloud expansion or overshoot of the DC voltage. Both factors, however, seem to influence isolation on the QITMS.

An alternative approach that can be used to help alleviate the problems associated with the single-step DC is the use two or more separate steps of DC voltage to reach the correct voltage. The first step must places the a_z value into the region of the stability boundary; the second step is kept small enough to minimize any overshoot or expansion of the ion cloud. The technique was shown to improve isolation efficiencies and is useful for instruments lacking the software for ramped DC voltages.

CHAPTER 4
MASS-SELECTIVE AUTOMATIC GAIN CONTROL

Introduction

On the quadrupole ion trap mass spectrometer, increasing the ionization time to increase the number of ions formed and thus the sensitivity can result in poor resolution, decreased collision-induced dissociation efficiency, and incorrect mass assignment due to ion-ion interactions (space charge). To overcome these problems, Finnigan MAT developed automatic gain control (AGC) [8] which is a method to automatically adjust the ionization time based on the number of ions detected in a prescan. AGC is limited, however, when two or more compounds of widely varying concentrations are present in the trap simultaneously. Since the total number of ions detected in the prescan is used to set the ionization time, a minor component may form too few ions to be detected.

This chapter of the dissertation discusses a method which was developed to overcome this limitation of AGC, called mass-selective automatic gain control (MSAGC). Mass-selective AGC uses two-step isolation during the prescan to adjust automatically the ionization time dependent upon the number of ions of only a single m/z. The chapter shows an example of using the new technique to overcome the problems of using AGC with co-eluting compounds. The technique, however, can also be used for complex sample mixtures or to control the number of parent or fragment ions formed during GC/MS/MS[29]. Included in this chapter is a comparison of MSAGC to AGC.

Set Ionization Time

The response of the QITMS is dependent on the ionization time used to form ions. This can graphically be seen in Figure 4-1. The x-axis is the amount of sample (arbitrary units), while the y-axis is the (arbitrary) number of ions formed. For this example it is assumed that 100 ions must be stored in the QITMS to be detected. Notice that to reach this detection limit for an ionization time of 0.1 ms, 1K units of the sample must be introduced into the trap. Only 10 units of the sample is needed, however, with an ionization time of 10 ms. A limitation to using longer ionization times is the onset of space charge (see Chapters 5 and 6 for more details about space charge effects). Notice that the 10 ms ionization time reaches the space charge region at 20K units of the sample, while 2M units of the sample can be introduced before reaching space charge for 0.1 ms ionization time. It also is important to note that the slope of the log-log response lines are 45°, implying that an increase in the amount of sample introduced produces a proportional increase in the number of trapped ions.

Figure 4-1. The response of the ion trap mass spectrometer for set ionization times. The space charge region is placed in an arbitrary location. Adapted from reference number 7.

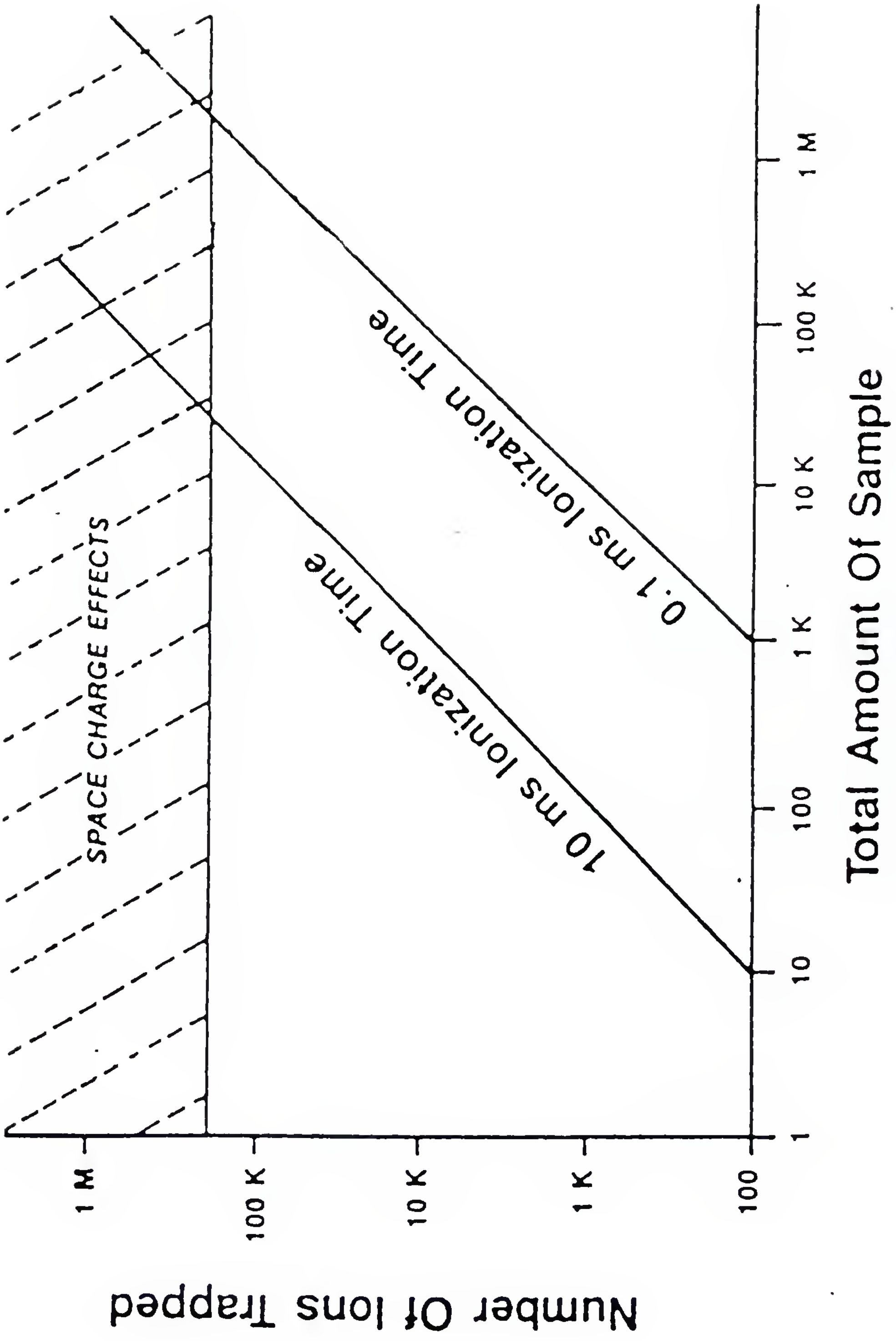
SPACE CHARGE EFFECTS
10 ms Ionization Time
0.1 ms Ionization Time
Number Of Ions Trapped
1 M
100 K
10 K
1 K
100
Total Amount Of Sample
1
10
100
1 K
10 K
100 K
1 M

Variable Ionization Time (AGC)

Automatic gain control is a method to adjust automatically the ionization time depending upon the total number of ions detected in the ion trap. The response of AGC is depicted graphically in Figure 4-2. Notice that the maximum ionization time of 25 ms is used until the number of trapped ions is just below the space charge region. The ionization time is then decreased to keep the number of ions trapped constant, until the minimum ionization time (10μs) is reached. The usable linear dynamic range is thus increased from 3 orders of magnitude without AGC to over 5 orders of magnitude with AGC. The AGC scan function, depicted in Figure 4-3, has two sections, prescan and analytical scan. During the prescan, ions are formed for a given time (Table 1), the resulting ions are detected (Table 2), and subsequently the variable ionization time used in the analytical scan (Table 3) is calculated by the equation[30].

$$IT_a = IT_p \times \frac{TIC_T}{TIC_M} \times SF \tag{4-1}$$

Where IT_a = calculated ionization time, IT_p = ionization time of the prescan, TIC_T = target total ion current, TIC_M = Measured total ion current of the prescan, and SF = scaling factor. The mass spectrum is then acquired in Table 4.

As can be seen from examination of equation 4-1, the total number of ions detected in the prescan dictates the ionization time. For example, the

Figure 4-2. The response of the ion trap mass spectrometer with AGC. Notice that the ionization time decreases to keep the number of ions out of the space charge region. Adapted from reference number 7.

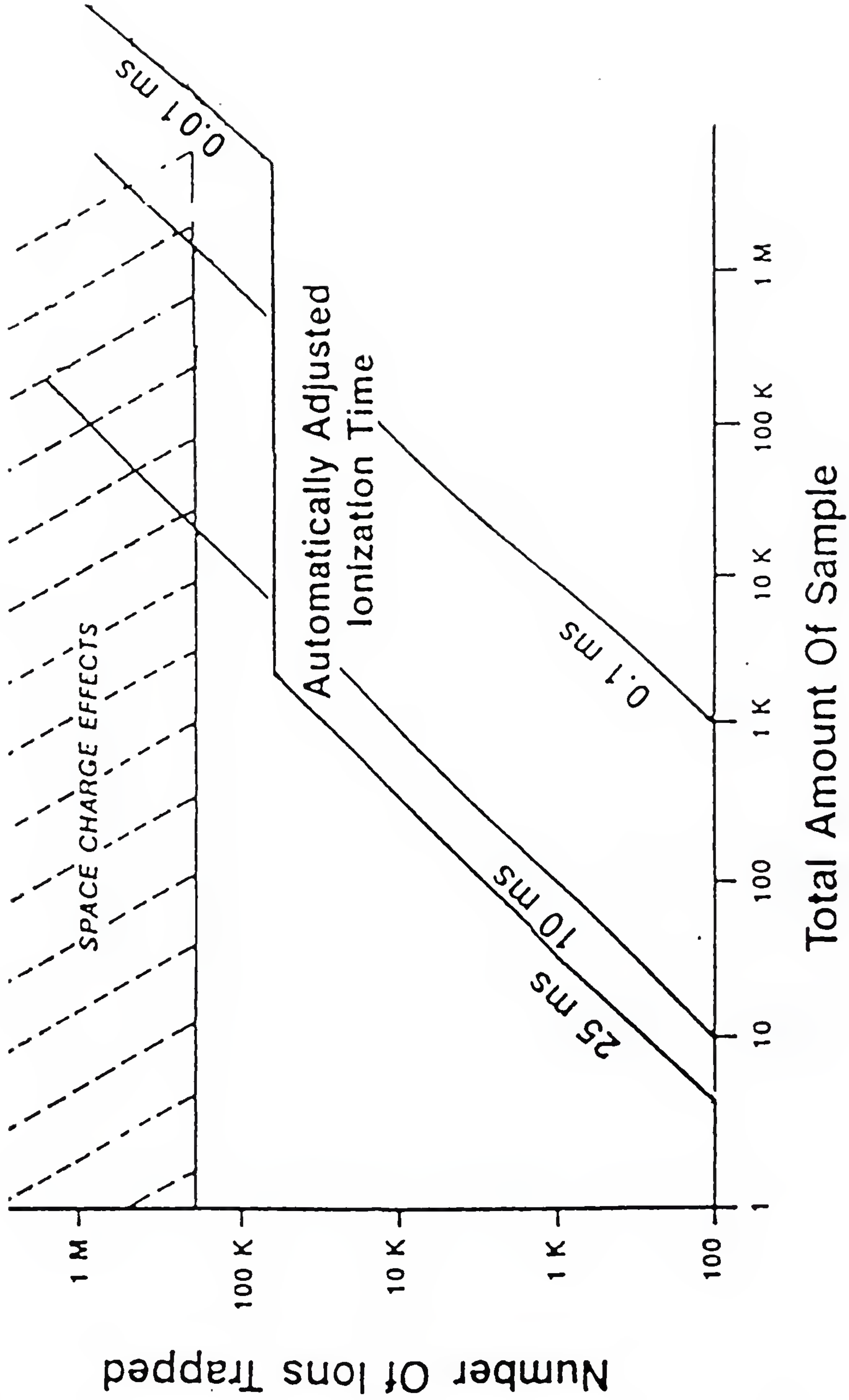
Number Of Ions Trapped
1 M
100 K
10 K
1 K
100
Total Amount Of Sample
1
10
100
1 K
10 K
100 K
1 M
SPACE CHARGE EFFECTS
Automatically Adjusted
Ionization Time
0.01 ms
0.1 ms
10 ms
25 ms

Figure 4-3. AGC scan function depicting the RF voltage and ion intensity detected. Notice the two sections of the scan function: prescan and analytical scan.

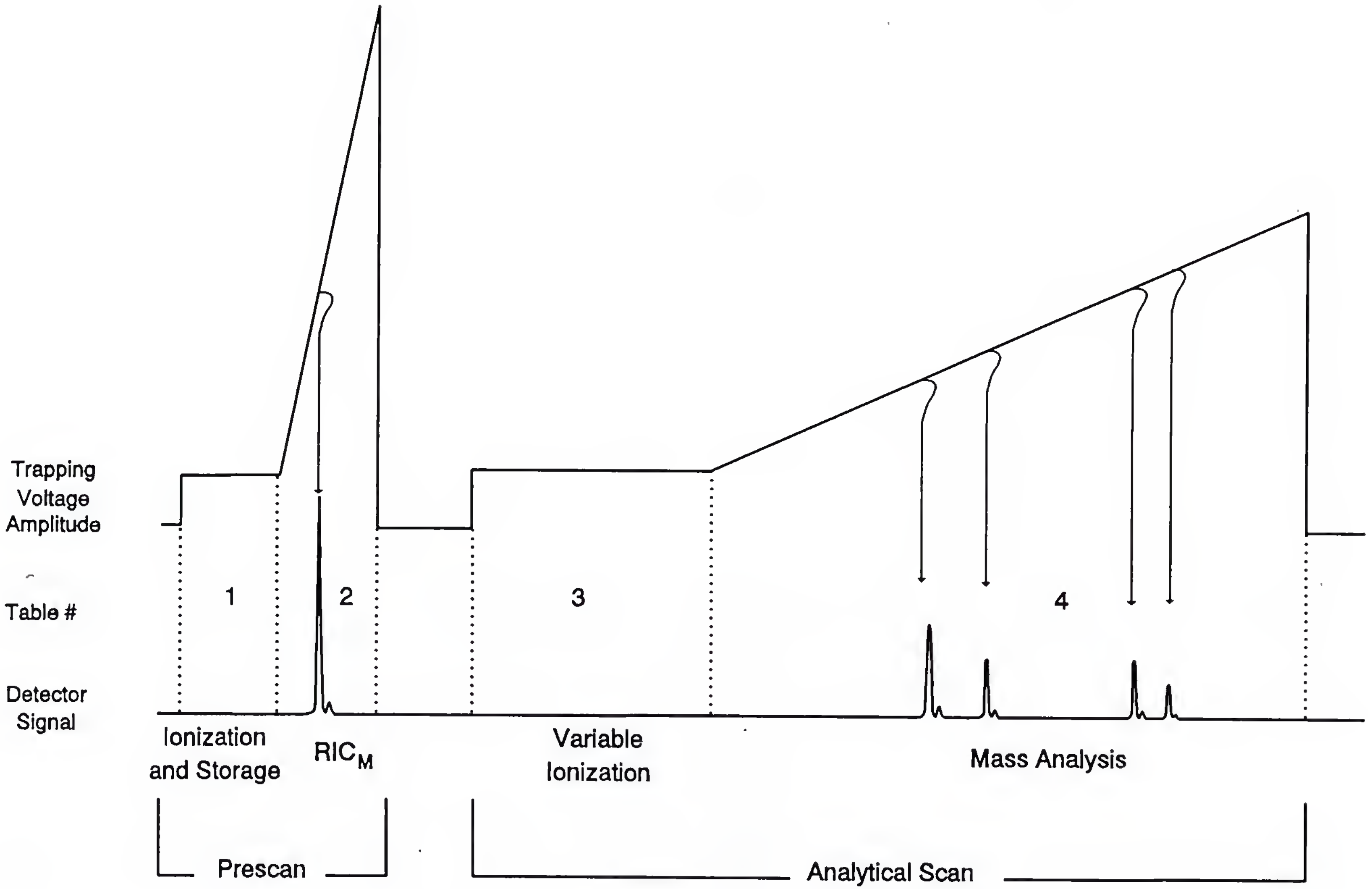
Trapping Voltage Amplitude
Table #
Detector Signal
1
2
3
4
Ionization and Storage
RIC$_M$
Variable Ionization
Mass Analysis
Prescan
Analytical Scan

larger the number of ions detected, the shorter the calculated ionization time ($IT_{a\text{-}min}$ of 10 µs). Conversely, a low number of detected ions increases the calculated ionization time ($IT_{a\text{-}max}$ of 25 ms). The ion intensity is then scaled on the SAP board by multiplying by the scaling factor $IT_{a\text{-}max}/IT_a$. This has the effect of scaling the ion intensity to the maximum ionization time, having assumed a linear relationship between ion intensity and ionization time.

A major limitation of AGC stems from the basis that the total number of ions detected (above a background m/z cutoff) in the prescan is used to determine the ionization time to be used in the analytical scan. This can make it difficult or, in some cases, impossible to detect the small number of ions at a given m/z formed from a minor component when other compounds are present in larger abundance. In other words, when a large number of ions are detected in the prescan, the ionization time decreases which can cause the loss of intensity for compounds that are present in low abundance. An example is shown in Figure 4-4, in which furan was bled into the QITMS at a constant rate; dimethyl disulfide was then inject onto the GC column. Notice that as the dimethyl disulfide (molecular ion at m/z 94) eluted, the AGC decreased the ionization time to such an extent that all of the furan molecular ion signal (m/z 68) was lost. This can be a major problem if the furan is the compound of interest.

A technique that was developed in our laboratory on a Finnigan ITMS to overcome the limitations of AGC for co-eluting compounds used alternating

Figure 4-4. Chromatogram showing the effect of AGC. Furan was bled into the ion trap vacuum manifold at a constant rate (manifold pressure = 4×10^{-7} torr) during the entire run. Dimethyl disulfide was injected onto the GC column in the splitless mode. Notice the complete loss of the furan ion signal as dimethyl disulfide elutes due to a large decrease in the ionization time.

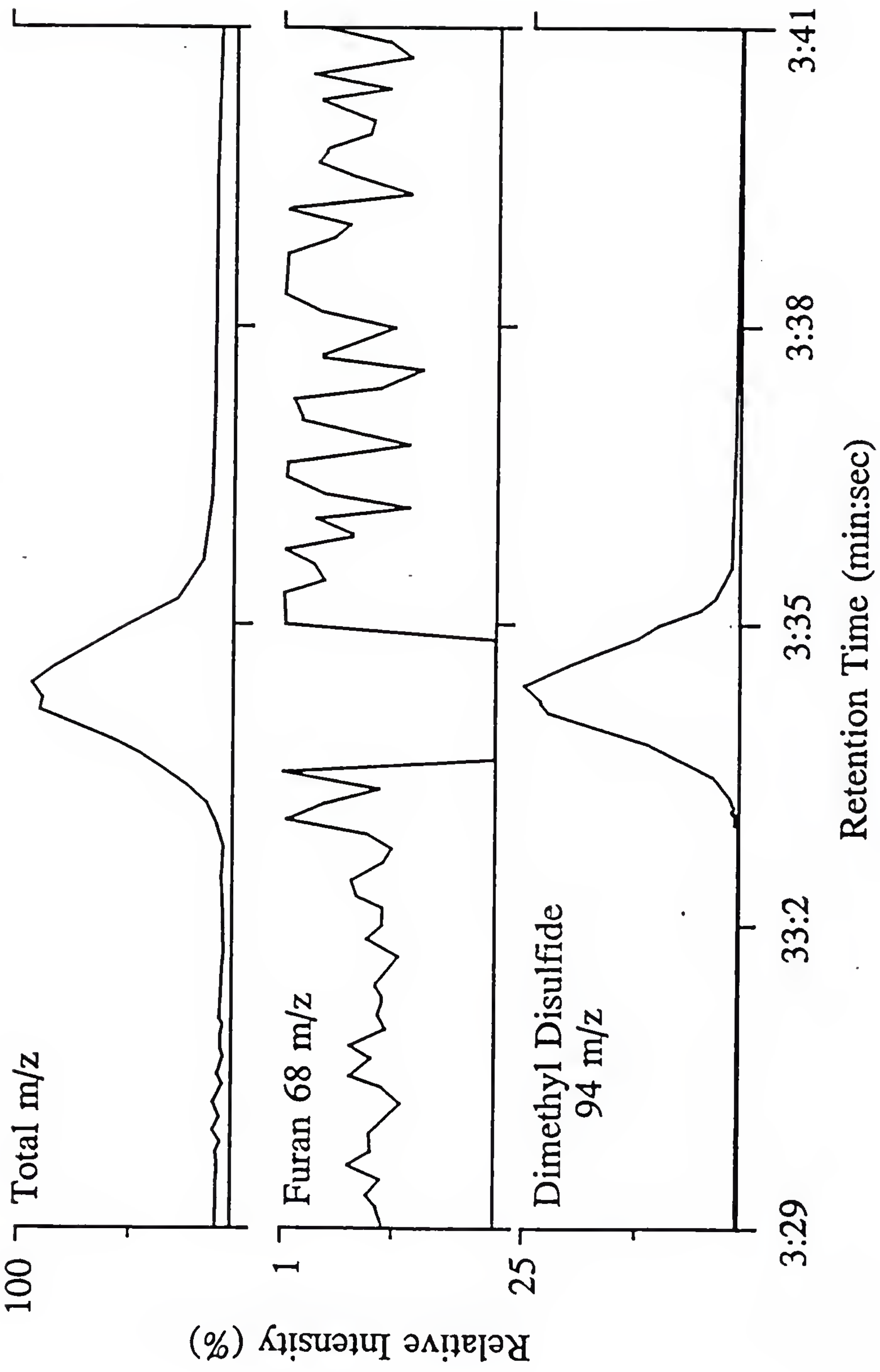
Total m/z
Furan 68 m/z
Dimethyl Disulfide
94 m/z
100
1
25
Relative Intensity (%)
3:29
33:2
3:35
3:38
3:41
Retention Time (min:sec)

RF/DC isolation[31]. This technique, however, required extensive setup, including manual selection of the ionization time, and FORTH programming to implement. Many techniques have been used to selectively "fill" the ion trap with ions of a particular m/z range to reduce space charge effects, including white noise[14], filtered noise fields[17], and SWIFT[16]; however, these methods do not adjust the ionization time.

Mass-selective Automatic Gain Control

This chapter explains the development of a mass-selective AGC technique specifically for co-eluting compounds, including complex mixtures. In contrast to AGC, this technique allows the control of the ionization time to be based upon a single m/z ion. In this manner, the ionization time is dependent only on the abundance of an ion of interest. The ability to adjust automatically the ionization time based upon a single ion intensity helps alleviate the AGC discrimination against ions of low abundance. The MSAGC scan function is shown in Figure 4-5. Notice that it again is made up of two parts; the prescan and analytical scan. Mass-selective AGC isolates and detects a narrow m/z range of ions during the AGC prescan to calculate the correct ionization time to use, which produces a large linear dynamic range for the selected analyte in addition to improving the flexibility of the instrument.

Figure 4-5. MSAGC scan function depicting the RF voltage and ion intensity detected. Two-step isolation is used during the prescan to store and detect only the ion of interest.

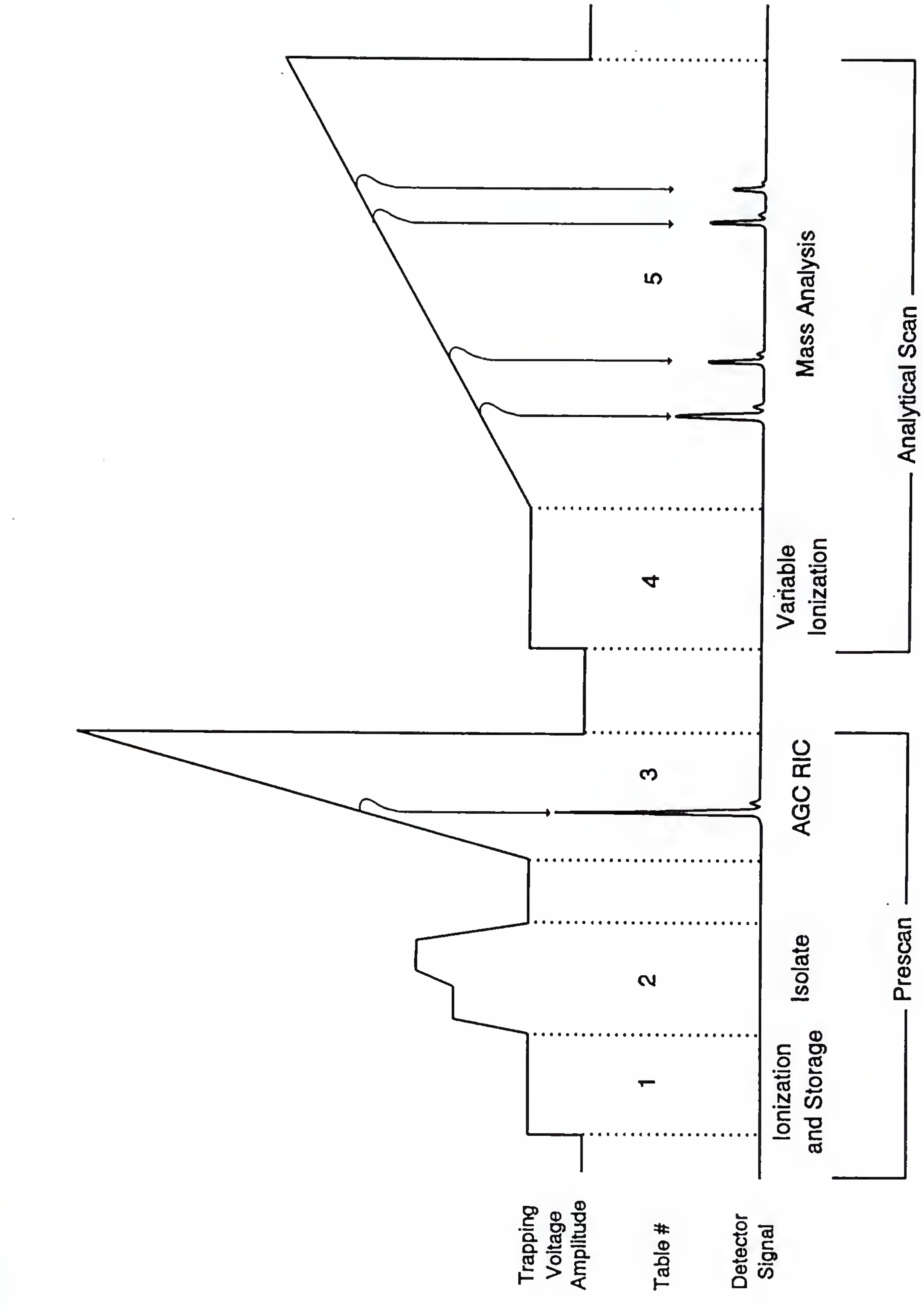
Trapping Voltage Amplitude
Table #
Detector Signal
1
2
3
4
5
Ionization and Storage
Isolate
AGC RIC
Variable Ionization
Mass Analysis
Prescan
Analytical Scan

Experimental

The objective of these experiments was to determine the feasibility of using MSAGC to control the ion population during a GC run. The use of an analyte compound and its isotopically labeled analog at varying concentration levels served as a general model of co-eluting compounds. This approach is widely used for the accurate quantitation of analytes by GC/MS. Both AGC and MSAGC were evaluated in this study.

Instrumentation

All data were collected on a Finnigan MAT (San Jose, CA, USA) quadrupole ion trap mass spectrometer (ITS-40). The routines used Gatorware, described in Chapter 2 of this dissertation. The optimal values (determined experimentally) for the AGC target total ion current (25,000), scaling factor (1), AGC ionization time (200µs), and maximum ionization time (25,000µs) were used for all experiments.

Timing Diagram

As can be seen in Figure 4-5, MSAGC used two-step isolation [12,13] during the AGC prescan to mass select a single ion for use in the calculations. Mass-selective AGC used the same calculations as AGC to determine the ionization time. The target total ion current and scaling factor were adjusted for the MSAGC prescan to give the best resolution and response while, preventing space charge (as listed above). The subsequent calculated ionization time (10 - 25,000 μs) was used for the analytical scan.

Compounds

The compound obtained from Sandoz Research Institute is shown in Figure 4-6. The analyte, as shown, incorporated one ^{13}C and three deuteria (giving a molecular weight of M+4). The internal standard incorporated a second ^{13}C and three more deuteria (M+8); the asterisks denote the sites of isotopic labeling. The analyte has a base peak of m/z 195, the internal standard has a base peak of m/z 199. Dilutions were made in 5% isopropanol in hexane. All compounds were used without further purification.

Results and Discussion

Mixtures composed of 525 ng of the analyte and 1.0, 4.0, 12, 43, 150, and 525 ng of the internal standard were used to generate the log-log calibration curve in Figure 4-7a under AGC conditions; all injections were performed in triplicate. The most important thing to note is that for the two lowest concentrations (1.0 and 4.0 ng) only one of the three injections produced a detectable ion signal, due to the low ionization time.

The mass spectrum at Point B (4.0ng internal standard) on the AGC calibration curve (Figure 4-8a) shows the loss of intensity for the m/z 199 ion. The ionization time (16 μs) is approximately the same as for Point A (525ng

Figure 4-6. Structure of the compound (molecular weight M+4) used for the experiments on co-eluting peaks. The asterisks (*) denote the sites for additional isotopic labeling in the internal standard (M+8).

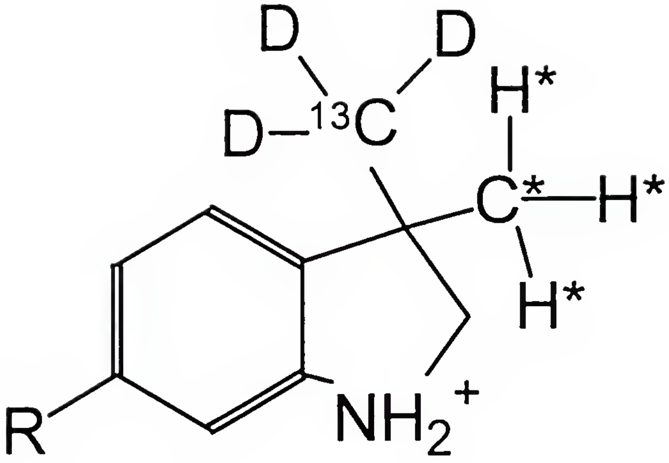
D
D
D
13C
H*
C*
H*
H*
R
NH2+

Figure 4-7. Calibration curves for m/z 199 (internal standard) for (a) AGC and (b) MSAGC. Point A coresponds to 525 ng of the compound and its internal standard. Point B corresponds to 525 ng of the compound and 4 ng of the internal standard. Average of triplicate injections are shown, with error bars corresponding to ±1 standard deviation.

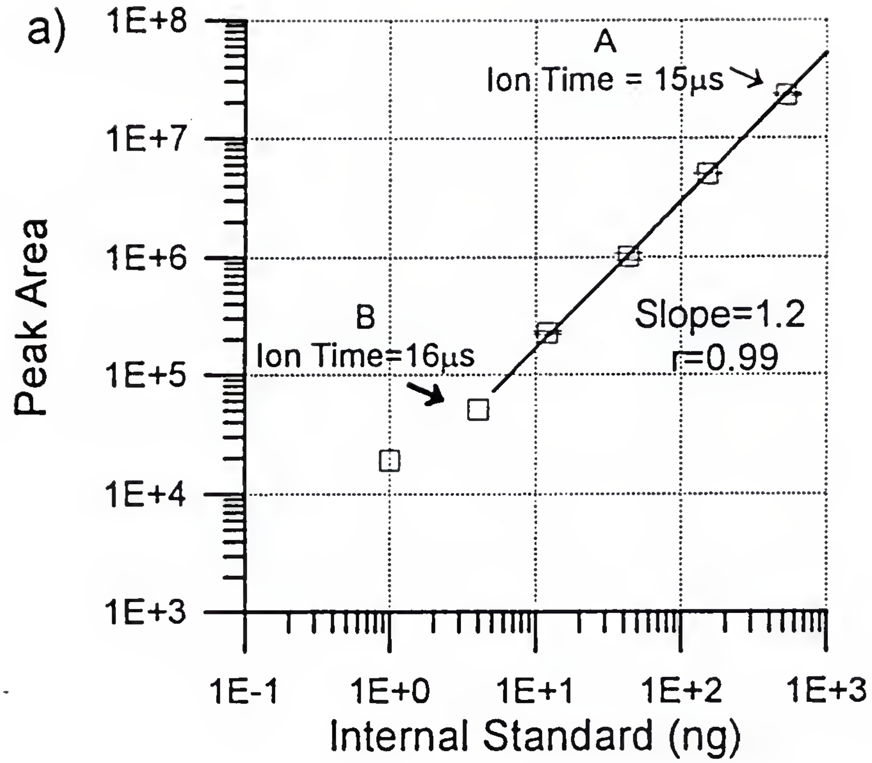
a)
A
Ion Time = 15µs
B
Ion Time=16µs
Slope=1.2
r=0.99
Peak Area
1E+8
1E+7
1E+6
1E+5
1E+4
1E+3
1E-1
1E+0
1E+1
1E+2
1E+3
Internal Standard (ng)

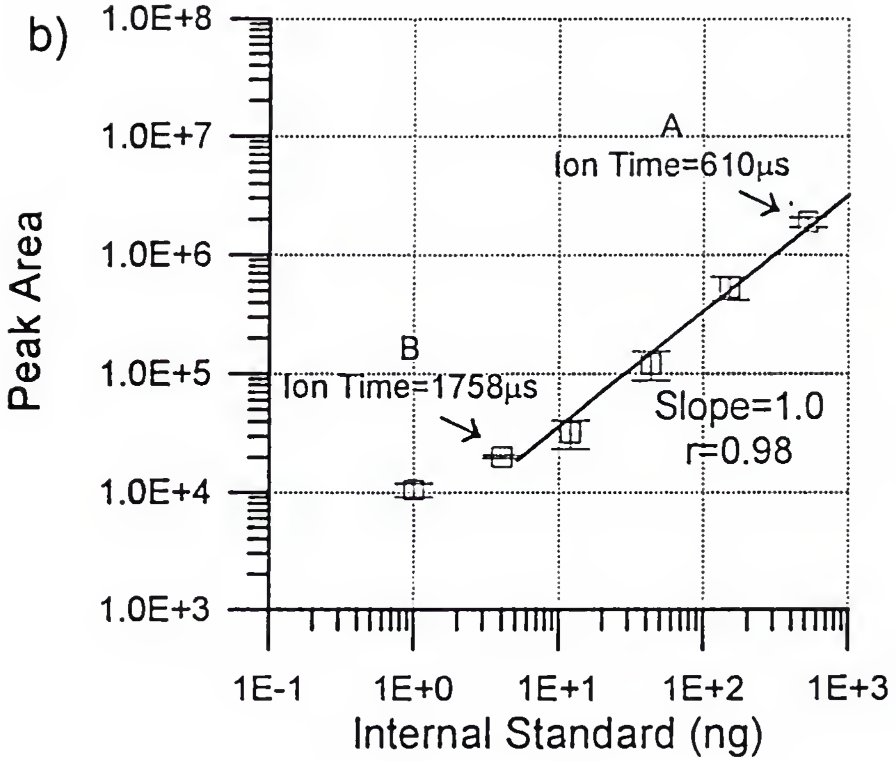
b)
A
Ion Time=610µs
B
Ion Time=1758µs
Slope=1.0
r=0.98
Peak Area
1.0E+8
1.0E+7
1.0E+6
1.0E+5
1.0E+4
1.0E+3
1E-1
1E+0
1E+1
1E+2
1E+3
Internal Standard (ng)

Figure 4-8. Mass spectra of 525 ng of compound with 4.0 ng of the co-eluting internal standard. The mass spectra are for (a) AGC and (b) MSAGC.

a)

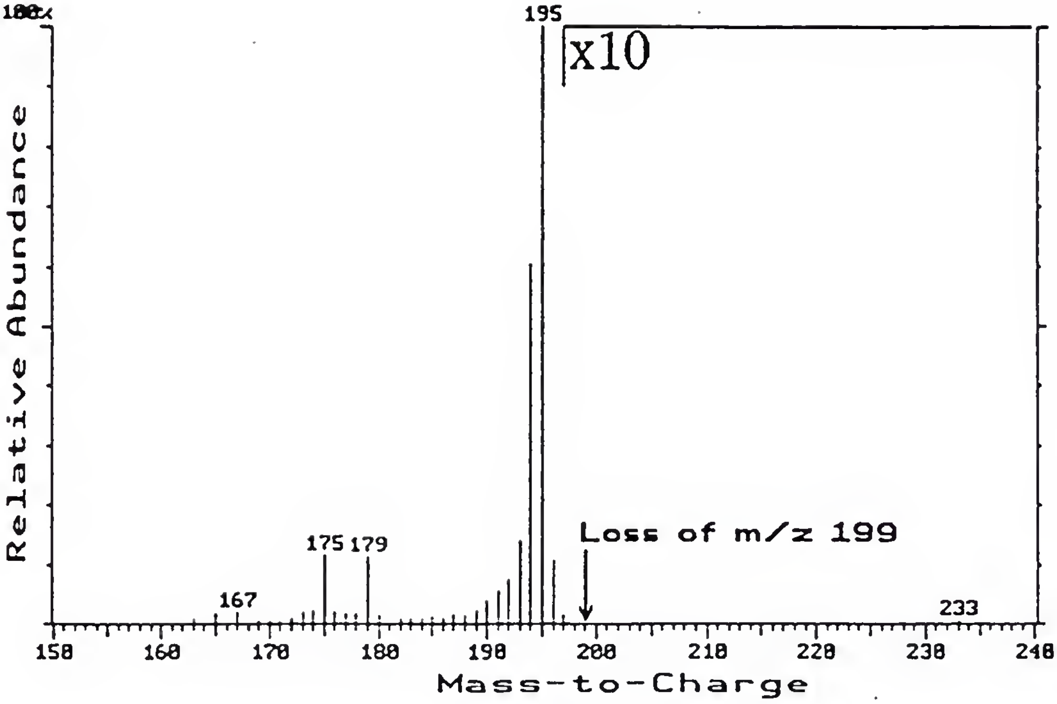
100%
195
x10
Relative Abundance
175
179
167
Loss of m/z 199
233
150
160
170
180
190
200
210
220
230
240
Mass-to-Charge

b)

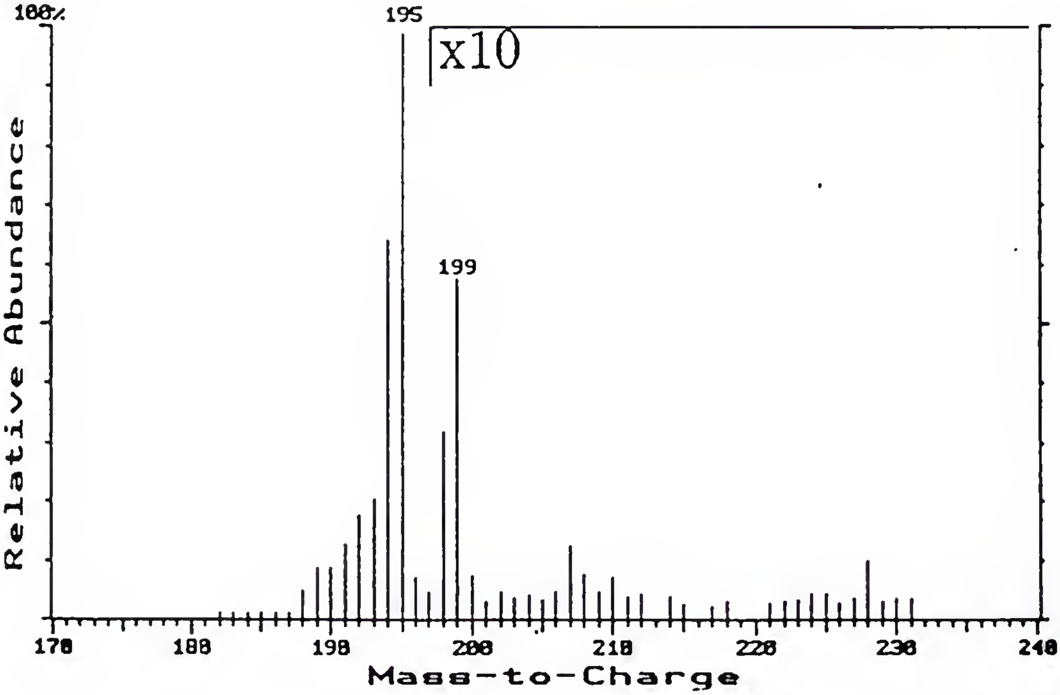
100%
195
x10
199
Relative Abundance
170
180
190
200
210
220
230
240
Mass-to-Charge

internal standard), which confirms that the ionization time is primarily determined by the m/z 195 ion intensity.

The same mixtures that were used for the AGC calibration curve were used to construct the MSAGC calibration curve (Figure 4-7b). The most important difference from the AGC calibration curve, however, is that all three injections for the two lowest concentrations (1.0 and 4.0 ng) produced ion intensities significantly above the background. The ionization time was also seen to increase with a decrease in the sample concentration which demonstrates that the calculated ionization time is based to a large extent on the m/z of interest.

The peak at m/z 199, which was not seen using AGC (Figure 4-8a), is observed in the mass spectrum at Point B on the MSAGC calibration curve (Figure 4-8b). The ionization time for this spectrum increased to 1758μs, thus yielding a higher m/z 199 ion intensity. A limitation of this method is that the higher ionization times can cause space charge for ions of lower m/z.

Summary

It was shown that it is feasible to automatically adjust the ionization time based upon a single m/z during a GC/MS run. This was accomplished by the use of mass-selected automatic gain control to control the ionization time to used during the analytical scan based upon a narrow m/z range stored in the QITMS. The range can be as small as a single m/z. Mass-selective AGC was shown to produce a linear calibration curve even when the analyte was not the most abundant compound. The longer ionization times used during MSAGC permits detecting the minor component more reliably. The use of the technique was shown for co-eluting compounds; however, the method can also be used to control the ionization time based upon the parent or fragment ions for GC/MS/MS[29].

CHAPTER 5
STABILITY DIAGRAM BOUNDARIES

Introduction

Ion isolation in the quadrupole ion trap mass spectrometer (QITMS) typically uses combinations of RF and DC voltages to approach the boundaries of the stability diagram (see chapters 1 and 3). Therefore, changes in the position of the boundaries will affect the isolation efficiencies. Similarly, storage efficiencies in a QITMS require the selection of a_z, q_z combinations that do not correspond to non-linear resonances[30], which may induce unwanted ejection or collision-induced dissociation (CID). Any change in the stability diagram could affect the position of the non-linear resonance lines and make them difficult to avoid.

This chapter focuses on the examination of the actual boundaries of the stability diagram, using ramped RF and DC voltages to accurately determine them. The positions of the stability boundaries for different mass-to-charge (m/z) ratios and different ion populations are examined.

Background

Previous studies have examined the position of the stability boundaries [32-44]. The results of the studies showed that increases in stored ion populations (achieved by increasing ionization times) produced large shifts of the stability diagram. These shifts were attributed to ion-ion interactions or space charge. The effects of space charge were modeled by the addition of a DC potential upon the electrodes of the ion trap [41,41]. The addition of the DC potential caused the actual a_z value to differ from that theoretically predicted thus, shifts of the stability diagram were observed.

Fisher [41] and Schwebel *et al.* [42] have developed two models which describe the effect of space charge in the QITMS. The methods employ a space-charge-induced potential (ϕ_i) to predict the influence of space charge on the operation of the ion trap. In the case of Fisher, the magnitude of the shift has been developed as

$$\Delta a_z = \frac{-8e\pi\rho_{max}}{m\Omega^2} \qquad (5\text{-}1)$$

and

$$\Delta a_r = \frac{-4e\pi\rho_{max}}{m\Omega^2} \qquad (5\text{-}2)$$

In the treatment by Schwebel, the space-charge potential is of the same form as the pseudopotential well, and was determined to differ only in the magnitude of the numerical coefficients, specifically

$$\Delta a_z = \frac{-32e\pi\rho_{max}}{3m\Omega^2} \tag{5-3}$$

(32/3 = 10.7 versus Fisher's 8) and

$$\Delta a_r = \frac{-8e\pi\rho_{max}}{3m\Omega^2} \tag{5-4}$$

(8/3 = 2.7 versus Fisher's 4) where e is equal to the charge of an electron, ρ_{max} is the maximum charge density, and Ω is the drive frequency. The models both show a defocusing in the r and z directions. The Schwebel model would show a larger defocusing of the ions in the z direction compared to the model of Fisher. Additionally, the Schwebel *et al.* model suggests that the stability diagram will move to larger a_z values, while the Fisher model suggest the opposite. A detailed derivation can be found in the articles by Schwebel *et al.* [42] and Fisher [41] along with the text by March [9].

Todd *et al.*[32] and March *et al.*[40] attempted to match their experimental results with the values theoretically predicted by Fisher[41], Schwebel[42], and Dehmelt[44]. Although their experimental results showed some agreement with theoretical predictions, the experimental results could not be completely explained. The experiment done by Todd *et al.*[32] determined the actual boundary positions of the stability diagram by observing ion intensities at different a_z,q_z values. A example showing the typical stability diagram determined by Todd is shown in Figure 5-1. Shifts of the stability boundaries were observed to be inversely proportional to the m/z stored ($\Delta q_{z(edge)}=1/\Delta m$). Other researchers [40-42, 44] examined shifts in the frequencies of the stored ions and then calculated the shifts of the boundaries based upon the change in the ion frequencies. Frequency shifts are discussed in Chapter 6 of this dissertation. The different researchers also employed different experimental setups. For example Fisher[41] used screen mesh for the fabrication of the electrodes. The experimental setups used by the different researchers, including us, are listed in Table 5-1. Under the heading Method technique refers to how the a_z,q_z combinations were reached. For example, we ionized at the same a_z,q_z combination then ramped to the stability boundary; while Todd ionized at the a_z,q_z combinations that was being investigated. The pulse detection method employed by Todd and March was by application of a large DC voltage to one endcap electrode to either "suck" or "push" the ions out of the trap to the detector. Resonance detection is a method that uses a tuned circuit to measure the change in impedance caused by the ion cloud passing close to the electrodes. Examination of the

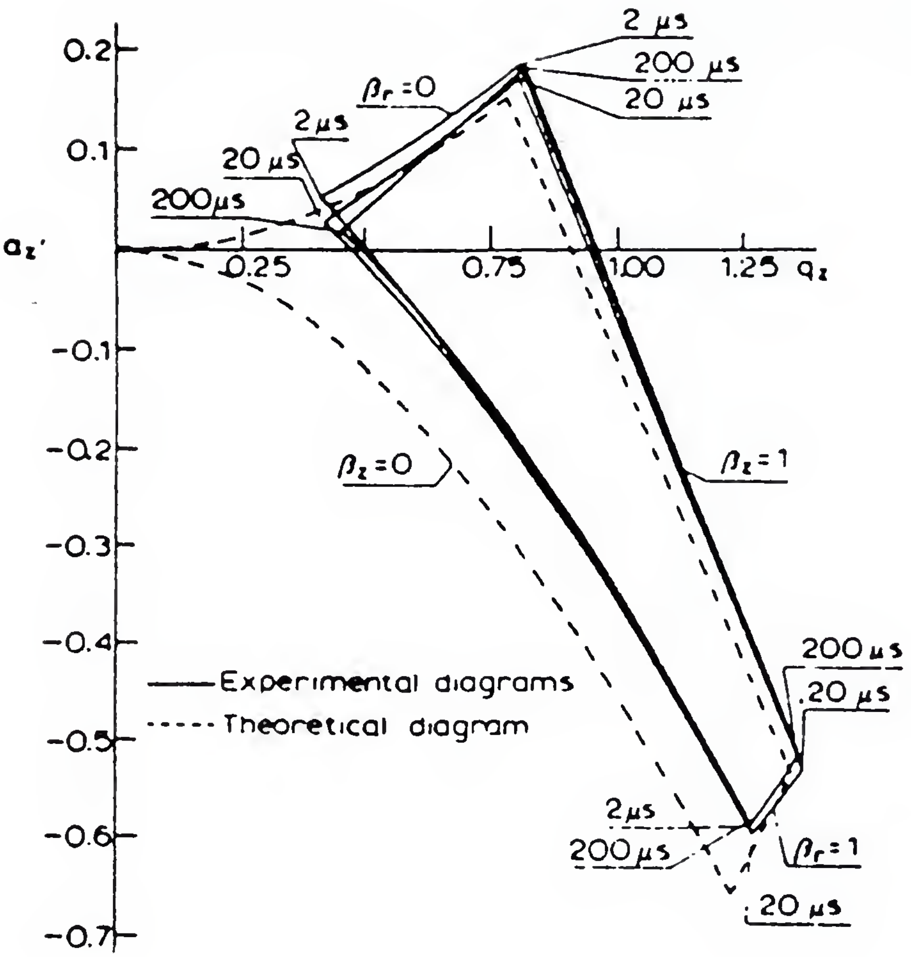

Figure 5-1. Experimentally determined stability diagram[32]. The diagram shown by the dashed line is the theoretical diagram. The experimental diagram was determined using Ne^+ ionized for the different times shown.

Table 5-1. Experimental Setup of Our and Previous Studies.

Method	Griffin	Todd	March	Fisher	Schwebel
Ionization	endcap	ring	endcap	endcap	endcap
Technique	Ion→Point	Ion=Point	Ion=Point	Set RF	Set DC
Detection	Scan	Pulse	Pulse	Swept DC	Swept RF
Detect with	Multiplier	Quad(Mult)	Quad	Resonance	Resonance
He buffer	No	No	No	No	No
Species	Ar^+, $C_4H_4O^+$, $C_4H_4S^+$, $C_4H_8{}^+$	Ne^+, Ar^+	Ar^+ and 9 ions from 2-propanol		
Isolation	No(Yes)	No	No	No	No
Freq (MHz)	1.05	0.85(2.85)	1.6	0.500	0.400
Auxiliary Frequency	Axial Modulation	No	Ejection (one endcap)	Resonance (excite)	Resonance (excite)
Map Type	a_z, q_z	a_z, q_z	Freq	Freq	Freq
Edge Det	experimental (10% max)	experimental (loss of signal)	Theory (N/A)	Theory (N/A)	Theory (N/A)
Material	Chrome	Stainless	Stainless	Brass	s.s. mesh
z_o(cm)	0.793 (stretched)	0.707	0.707	1.414	0.025
Results	No Shifts detected	Shifts due to: Ion Time Store Time mass-to-charge	Shifts due to: Ion Time	Shifts due to: Ion Time	Shifts due to: Ion Time

table reveals that we and Todd were the only ones to investigate the actual position of the stability diagram. We were the only researcher to not change the ionization, isolation and detection steps during the experiments.

Objectives

The objectives of this work were to map the position of the boundaries of the stability diagram. In conjunction with this, comparisons to theory were done. This research reexamined the work done by Todd *et al.* with particular attention paid to the $\beta_z=0$ stability boundary. This boundary is of importance because ejection of higher mass ions during two-step isolation requires that the m/z of interest be placed in close proximity to this boundary. In addition, ion trap analysis often require placing ions at ow q_z values, in the vicinity of the $\beta_z=0$ boundary; for example, CID is typically done at a $q_z=0.3$, while mass range extension often requires a $q_z<0.3$. With the stability diagram depicted in Figure 5-1, it would be impossible to accurately predict where to perform CID or mass range extension.

Experimental

The experiments discussed in this chapter are in three parts. The first part used the argon ion, m/z 40, to determine the position of the entire stability diagram for different ion populations. The position of the stability boundaries at $q_z=0.7$ and 0.85 for different compounds and different ion populations were investigated in more detail in the second part of the experiments. The third part examines the isolation efficiencies of different ions at different ion populations. A summary of the experimental setups used for these experiments is listed in Table 5-2.

Instrumentation

All experiments used Gatorware. Argon was bled directly into the QITMS via a modified GC transfer line. The liquid compounds, furan and butanol, were bled into the manifold through a Negretti leak valve on the CI gas line to give an uncorrected gauge reading of 4.0×10^{-7}torr.

Scan Function

The scan function used to examine the stability boundaries is shown in Figure 5-2. After ionization at $a_z=0.0$, $q_z=0.2$ (Table 1) the ions isolated (Table 2) and then were moved to various a_z, q_z values via an RF and DC ramp and stored for 2ms (Table 3). The ions were then ramped to $a_z=0.0$, $q_z=0.3$ and cooled for 5ms (Table 4). Acquisition (Table 5) was performed using a mass-selective instability scan with axial modulation at 485kHz. Only Table 3 was changed during the experiments.

Table 5-2. Experimental overview

Ionization: Electron Ionization -- via endcap electrode

Detection Mode: Mass-selective Instability Scan

Buffer Gas: None

Ions Studied: Mapping Entire Stability Diagram -- Centroid Data
- m/z 40 (Ar^+) -- Not Isolated

Detailed Study and Isolation Efficiencies -- Profile Data
- m/z 40 (Ar^+) -- Isolated
- m/z 42 ($C_3H_6^+$ from butanol) -- Isolated
- m/z 56 ($C_4H_8^+$ from butanol) -- Isolated
- m/z 68 ($C_4H_4O^+$ from furan) -- Isolated

Ionization Times: Mapping Entire Stability Diagram
- 0.2, 5, 10, and 40 ms

Detailed Study
- 0.5, 1, 10, and 80 ms

Isolation Efficiencies
- 0.5 to 80 ms with increments of 0.5ms

Figure 5-2. Scan function used for determining the stability boundaries. The only changes during the experiments occur during table 3.

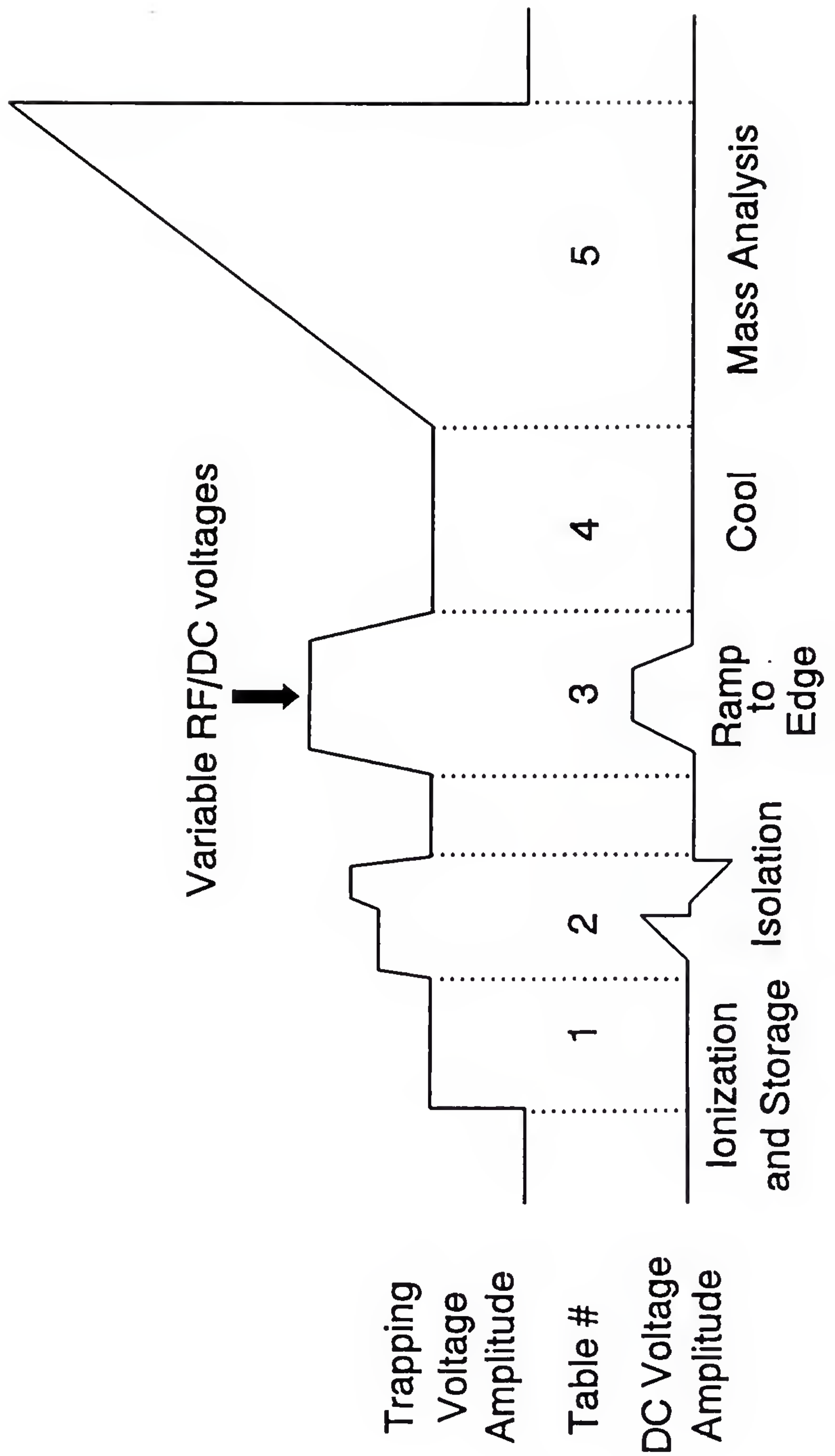
Variable RF/DC voltages
Trapping Voltage Amplitude
Table #
DC Voltage Amplitude
1
2
3
4
5
Ionization and Storage
Isolation
Ramp to Edge
Cool
Mass Analysis

Mapping of Entire Stability Diagram

Slices of the stability diagram were taken along constant q_z lines (Figure 5-3). As indicated by the large dashed lines in Figure 5-3 the entire stability diagram was examined with q_z slices of 0.05 and a_z steps of 0.01. The smaller dotted lines indicate the region of the stability diagram that also was examined with finer resolution (q_z slices of 0.01 and a_z steps of 0.001); this enabled a close examination of the upper apex and the β_z=0 stability boundary where large shifts were previously seen. Centroid data were collected for the Ar^+ ion, m/z 40. The boundary was considered the point that the intensity was 10% of the maximum value of the constant q_z slice. All of the experiments were performed without helium buffer gas.

Detailed Examination of Boundaries

The position of the stability boundaries at q_z=0.7 and 0.85 were investigated in more detail for four different ions; this was accomplished by taking slices of the stability diagram with a_z step sizes of 0.0005. The experiments were performed without helium buffer gas. Profile data were collected for the ions $C_4H_8^+$ (m/z 56) from butanol, $C_3H_6^+$ (m/z 42) from butanol, Ar^+ (m/z 40), and $C_4H_4O^+$ (m/z 68) from furan for this part of the investigation.

Figure 5-3. Diagram depicting the slices of the stability diagram examined. The smaller dashed lines indicate the region where high resolution experiments also were performed.

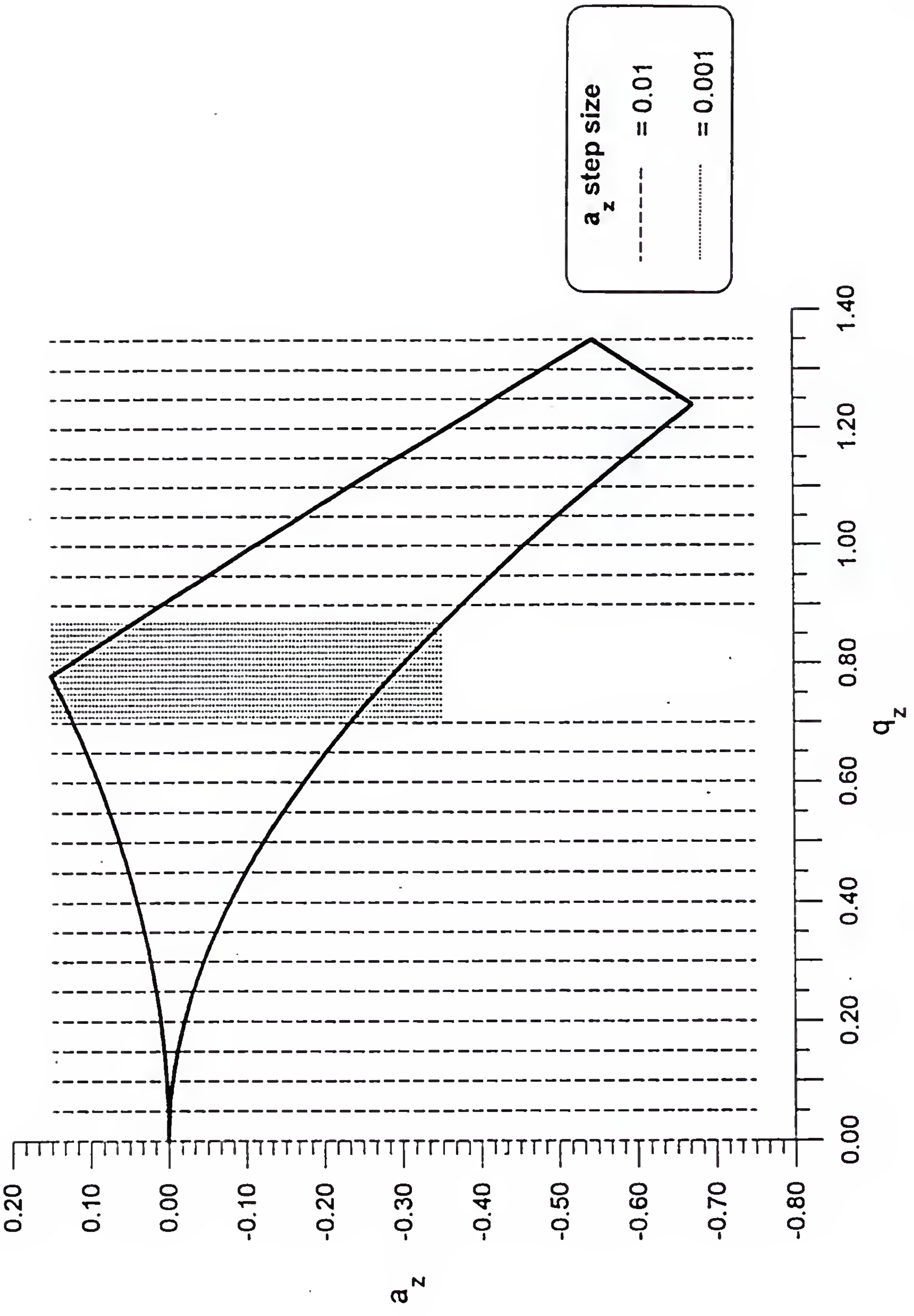

a_z step size
= 0.01
= 0.001
a_z
0.20
0.10
0.00
-0.10
-0.20
-0.30
-0.40
-0.50
-0.60
-0.70
-0.80
q_z
0.00
0.20
0.40
0.60
0.80
1.00
1.20
1.40

Isolation Efficiencies

The isolation efficiencies for two-step isolation were investigated without helium. The ionization times investigated ranged from 0.5 to 80 ms with increments of 0.5 ms. Profile data were collected for the ions $C_4H_8^+$ (m/z 56) from butanol, $C_3H_6^+$ (m/z 42) from butanol, Ar^+ (m/z 40), and $C_4H_4O^+$ (m/z 68) from furan.

Results and Discussion

The results of the experiments are presented in three sections. The first section examines all of the boundaries of the stability boundary. This work focused on the effects of different ionization times and thus, different ion populations on the entire stability region. The second section is a detailed study of two sections of the stability boundaries. In particular, a close examination at q_z=0.70 and 0.85 for different compounds and different ion populations was performed. The isolation efficiencies for different species and ionization times are the focus of the third section.

Mapping Entire Stability Diagram

The boundaries of the stability diagram for Ar^+ ions formed with different ionization times are seen in Figure 5-4. The areas of higher resolution are shown in figure 5-5. As is evident in Figures 5-4 and 5-5, there was no shifting of the stability diagram.

Figure 5-4. Experimentally determined stability diagram for Ar^+ with no helium. The solid line denotes the theoretical stability boundaries.

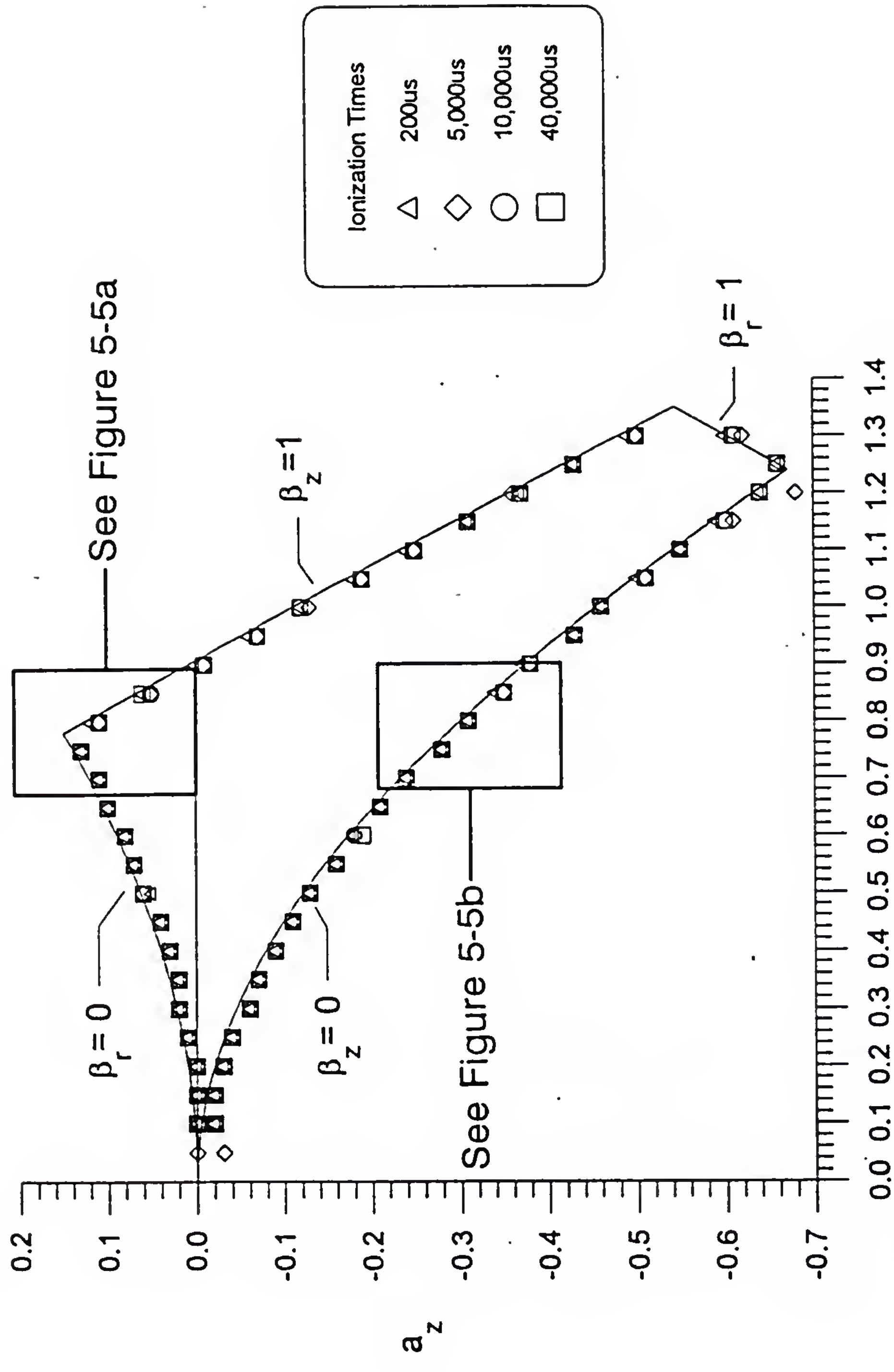
a_z
0.2
0.1
0.0
-0.1
-0.2
-0.3
-0.4
-0.5
-0.6
-0.7
q_z
0.0
0.1
0.2
0.3
0.4
0.5
0.6
0.7
0.8
0.9
1.0
1.1
1.2
1.3
1.4
See Figure 5-5a
See Figure 5-5b
$\beta_r = 0$
$\beta_z = 0$
$\beta_z = 1$
$\beta_r = 1$
Ionization Times
△ 200us
◇ 5,000us
○ 10,000us
□ 40,000us

Figure 5-5. Blown-up sections (a) upper apex (b)bottom left of Figure 5-4. The solid line denotes the theoretical boundary.

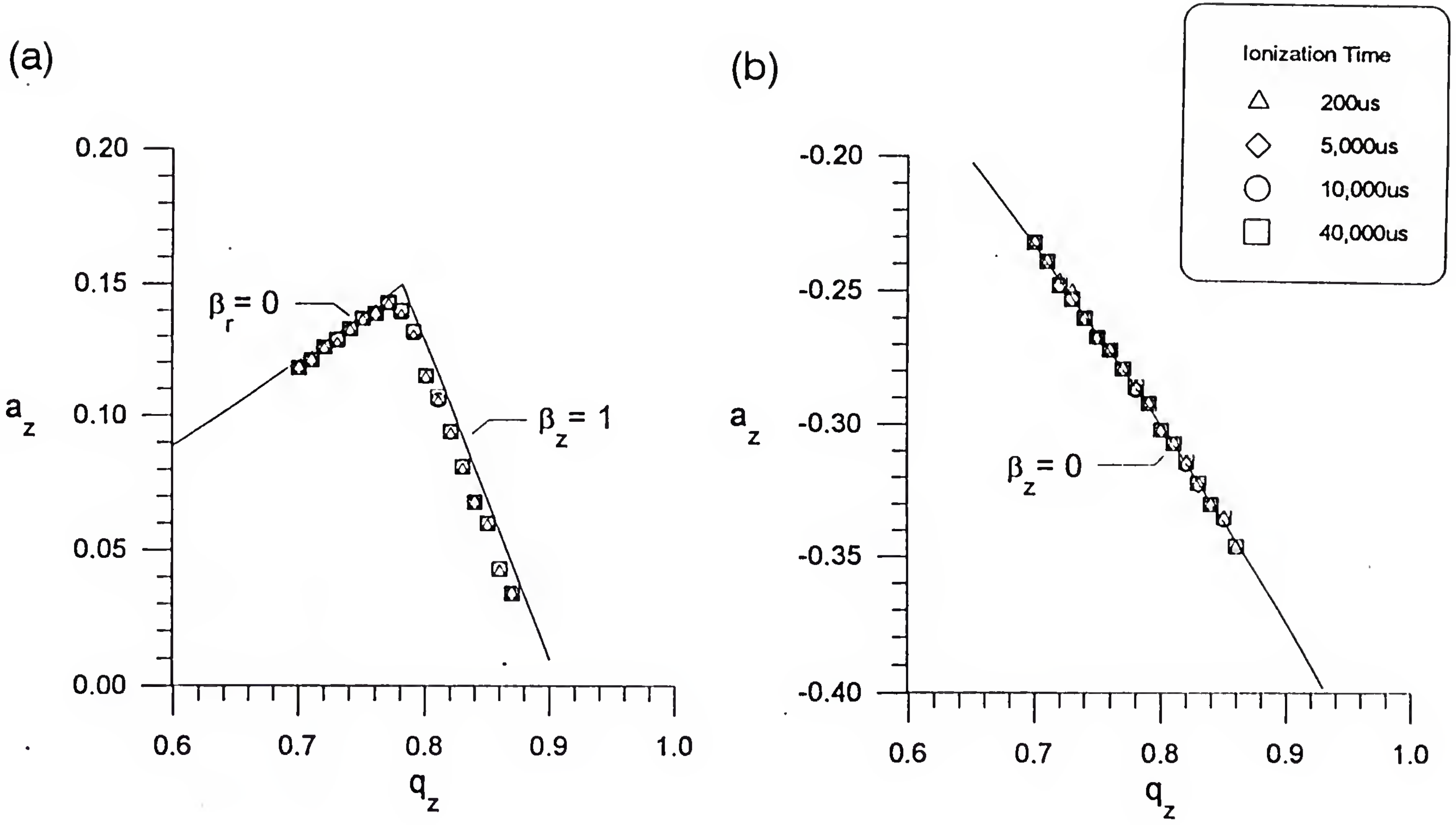
(a)
a_z
0.20
0.15
0.10
0.05
0.00
0.6
0.7
0.8
0.9
1.0
q_z
$\beta_r = 0$
$\beta_z = 1$
(b)
a_z
-0.20
-0.25
-0.30
-0.35
-0.40
0.6
0.7
0.8
0.9
1.0
q_z
$\beta_z = 0$
Ionization Time
△ 200us
◇ 5,000us
○ 10,000us
□ 40,000us

The normalized intensities for one vertical slice of the stability diagram, at q_z=0.70, is shown in Figure 5-6. The boundaries of the stability region, 10% of maximum, for ionization times varying over a range of 200 all lie on top of each other with no detectable shift. It is interesting to note that some changes occur somewhere between the ionization times of 5 and 10 ms. The differences, however, are within the stability diagram associated with non-linear resonances[30]. The lower ionization times (0.2 and 5 ms) showed less ion loss from the non-linear resonances at β_z=1/2 and 1/3, as shown by the larger normalized ion signal between a_z=-0.15 and a_z=-0.07. As the ion population increased, the affected area of the non-linear resonance also increased. However, the a_z position of the minimum value was not seen to shift.

To further show the effects of ion population on the stability diagram, topographical maps are shown for ionization times of 0.2 and 10ms in Figures 5-7 and 5-8, respectively. The theoretical stability diagram is the solid line superimposed onto the topographical map. Notice that the edges of the stability diagram are sharp and correspond to the theoretical values. Also of interest is the inability to store ions below a q_z of 0.05 due to the weak trapping field. The decrease of ion intensity to the lower right of q_z=0.9, a_z=0.0 was seen because of the large number of non-linear resonance lines[30] that must be crossed to reach the area.

Figure 5-6. Single slice of the stability diagram for Ar^+ q_z=0.70 without helium. The slice shown is depicted in the inset. The major non-linear resonances are indicated.

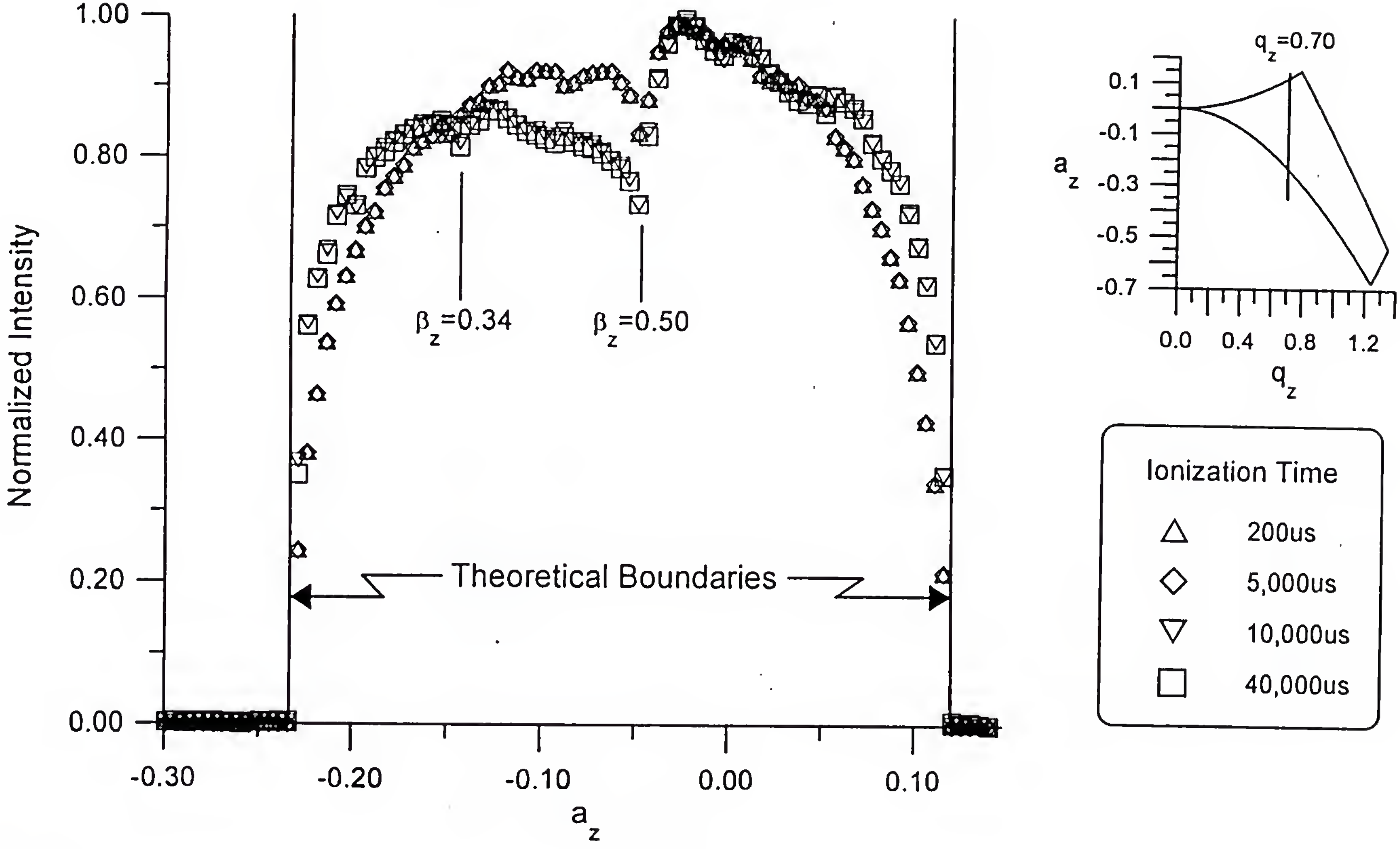
1.00
0.80
0.60
0.40
0.20
0.00
Normalized Intensity
-0.30
-0.20
-0.10
0.00
0.10
a_z
$\beta_z=0.34$
$\beta_z=0.50$
Theoretical Boundaries
$q_z=0.70$
0.1
-0.1
-0.3
-0.5
-0.7
a_z
0.0
0.4
0.8
1.2
q_z
Ionization Time
△ 200us
◇ 5,000us
▽ 10,000us
□ 40,000us

Figure 5-7. Topographical map showing the entire stability diagram for Ar^+ without helium. The map is for 0.2 ms ionization time. The solid line is the theoretical location of the stability boundaries.

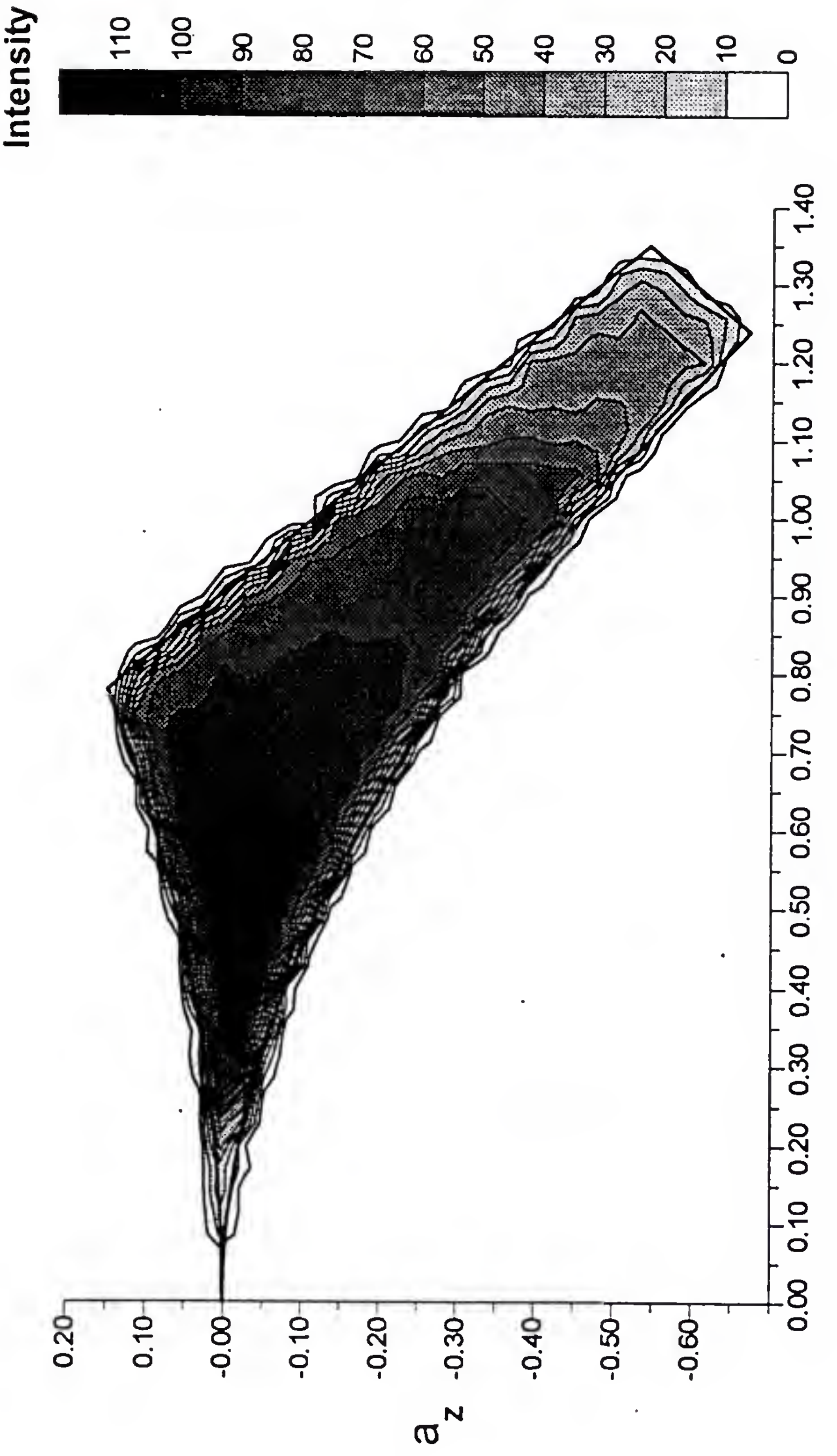
Intensity
110
100
90
80
70
60
50
40
30
20
10
0
a_z
0.20
0.10
-0.00
-0.10
-0.20
-0.30
-0.40
-0.50
-0.60
q_z
0.00
0.10
0.20
0.30
0.40
0.50
0.60
0.70
0.80
0.90
1.00
1.10
1.20
1.30
1.40

Figure 5-8. Topographical map showing the entire stability diagram for Ar^+ without helium. The map is for 10 ms ionization time. The solid line is the theoretical location of the stability boundaries.

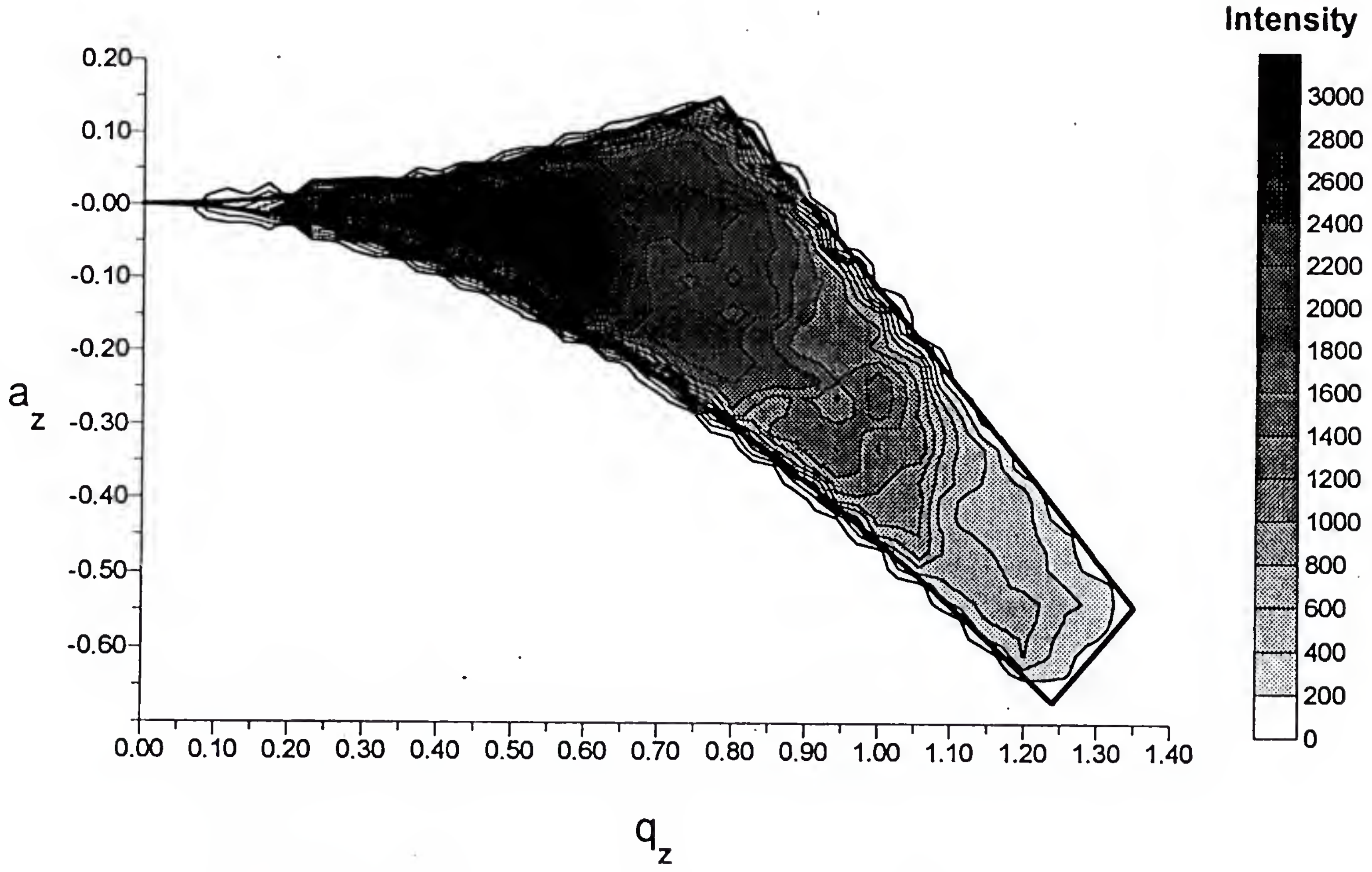
Intensity
3000
2800
2600
2400
2200
2000
1800
1600
1400
1200
1000
800
600
400
200
0
0.20
0.10
-0.00
-0.10
-0.20
-0.30
-0.40
-0.50
-0.60
a_z
0.00
0.10
0.20
0.30
0.40
0.50
0.60
0.70
0.80
0.90
1.00
1.10
1.20
1.30
1.40
q_z

Detailed Study

The experimentally determined position of the stability boundary (defined as q_z=0.710, a_z=-0.2336) at q_z=0.70 for different ions with an ionization time of 0.5 ms is shown in Figure 5-9. The dashed line denotes the theoretical position of the stability boundary. The bars indicate the average position of two independently run experiments for ionization times of 0.5ms. The furan (m/z 68) and butanol (m/z 56) ions correspond well with theory. The figure suggests that the deviation from theory increases with decreasing m/z. This trend, however, is not reproducible between experiments. In addition, the position of the boundary is so close to theory that no bases can be made for determining any overall trend. The shifts for Ar^+ are a lot larger than seen in Figure 5-5b; this is probably due, at least in part, to a difference in the calibration of the RF voltage. The RF voltage calibration could also account for the m/z 40 and 42 being farther from theory then the larger m/z ions. The calibration for lower RF voltages might not have been as accurate.

The effect that ion population has on the position of the stability boundary for q_z=0.70 can be seen in Figure 5-10. The deviation in the boundary, Δa_z was found with respect to shortest ionization time (0.5 ms), rather than with respect to the theoretical boundary. This was to enable a more detailed look in any changes in the boundary which would be lost with the large deviations from theory. The dashed line denotes the step size that was taken in the a_z value; any values less then 0.0005 a_z units were

Figure 5-9. Location of the stability boundary for different mass-to-charges at $q_z=0.700$. The dotted line denotes the theoretical position of the boundary.

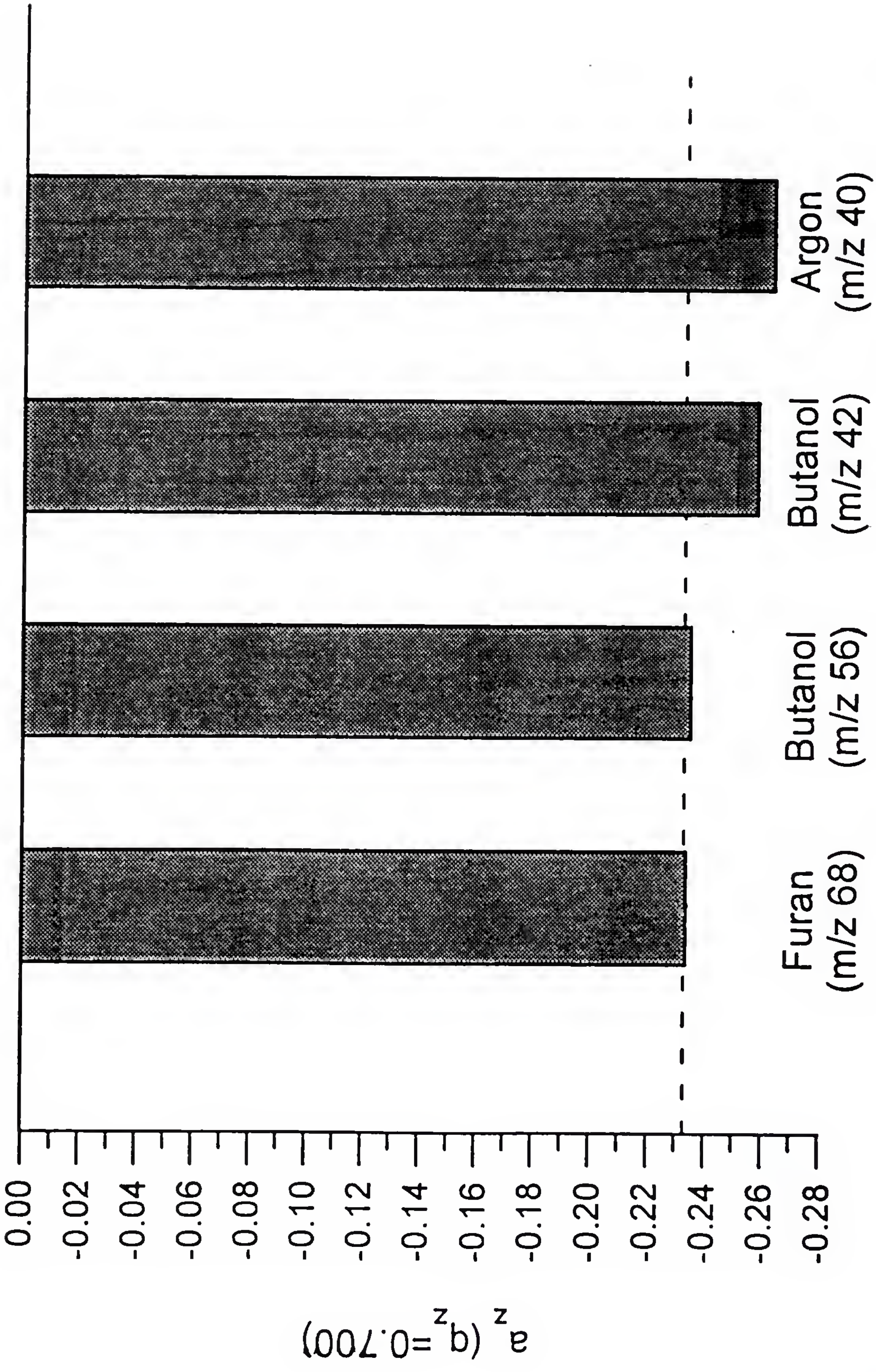
a_z (q_z=0.700)
0.00
-0.02
-0.04
-0.06
-0.08
-0.10
-0.12
-0.14
-0.16
-0.18
-0.20
-0.22
-0.24
-0.26
-0.28
Furan (m/z 68)
Butanol (m/z 56)
Butanol (m/z 42)
Argon (m/z 40)

Figure 5-10. Change in the a_z value for different ionization times (q_z=0.700). The changes are measured with respect to 0.5 ms ionization times. The dotted line denotes the step size that was used for these experiments.

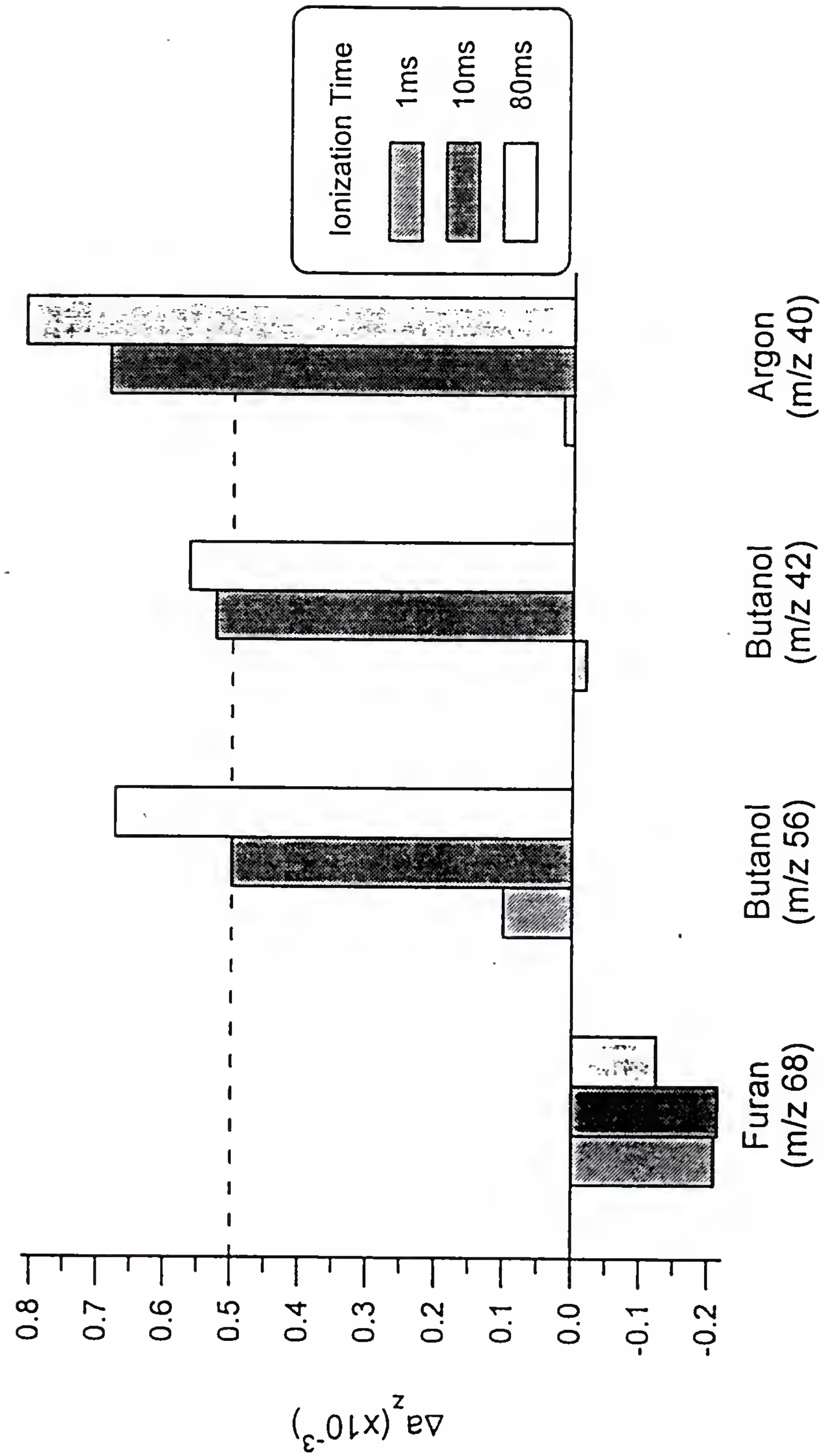
Δa_z (x10^-3)
0.8
0.7
0.6
0.5
0.4
0.3
0.2
0.1
0.0
-0.1
-0.2
Furan (m/z 68)
Butanol (m/z 56)
Butanol (m/z 42)
Argon (m/z 40)
Ionization Time
1ms
10ms
80ms

interpolated. For the most part, at higher ionization times the change in a_z was seen to increase. This trend, however, is not seen for m/z 68 of furan. The stability diagram was seen to shift in the opposite direction than for the other ions. The shifts in ion population are seen to be too small to show up in the data such as those in Figure 5-5.

The stability boundary was also examined for $q_z=0.85$. The results are shown in Figure 5-11. The solid line, again, denotes the theoretical position of the stability boundary; an ionization time of 0.5 ms was used in each case. As can be seen in the figure there is no apparent trend based on the m/z of the ion. It is interesting to note that the largest deviation from theory occurs with Ar^+ while the smallest occurs with $C_3H_6^+$ (m/z 42) from butanol. The Δa_z for different ionization times at $q_z=0.85$ is plotted in Figure 5-12 with respect to that for 0.5 ms ionization time. As can be seen, there is no trend based upon ion population. Any shifting of the boundaries is less than the experimental step size, depicted by the dotted lines.

Isolation Efficiency

To determine the effect that the stability diagram shifts have upon two-step isolation, the isolation efficiencies for different ions and ionization times were calculated (equation 3-1) and plotted (Figure 5-13). Notice that the largest variation in the isolation efficiency occurs between different ions. There is no apparent trend based upon m/z of the ions, as well as no appreciable

Figure 5-11. Location of the stability boundary for different mass-to-charges at $q_z=0.850$. The dotted line denotes the theoretical position of the boundary.

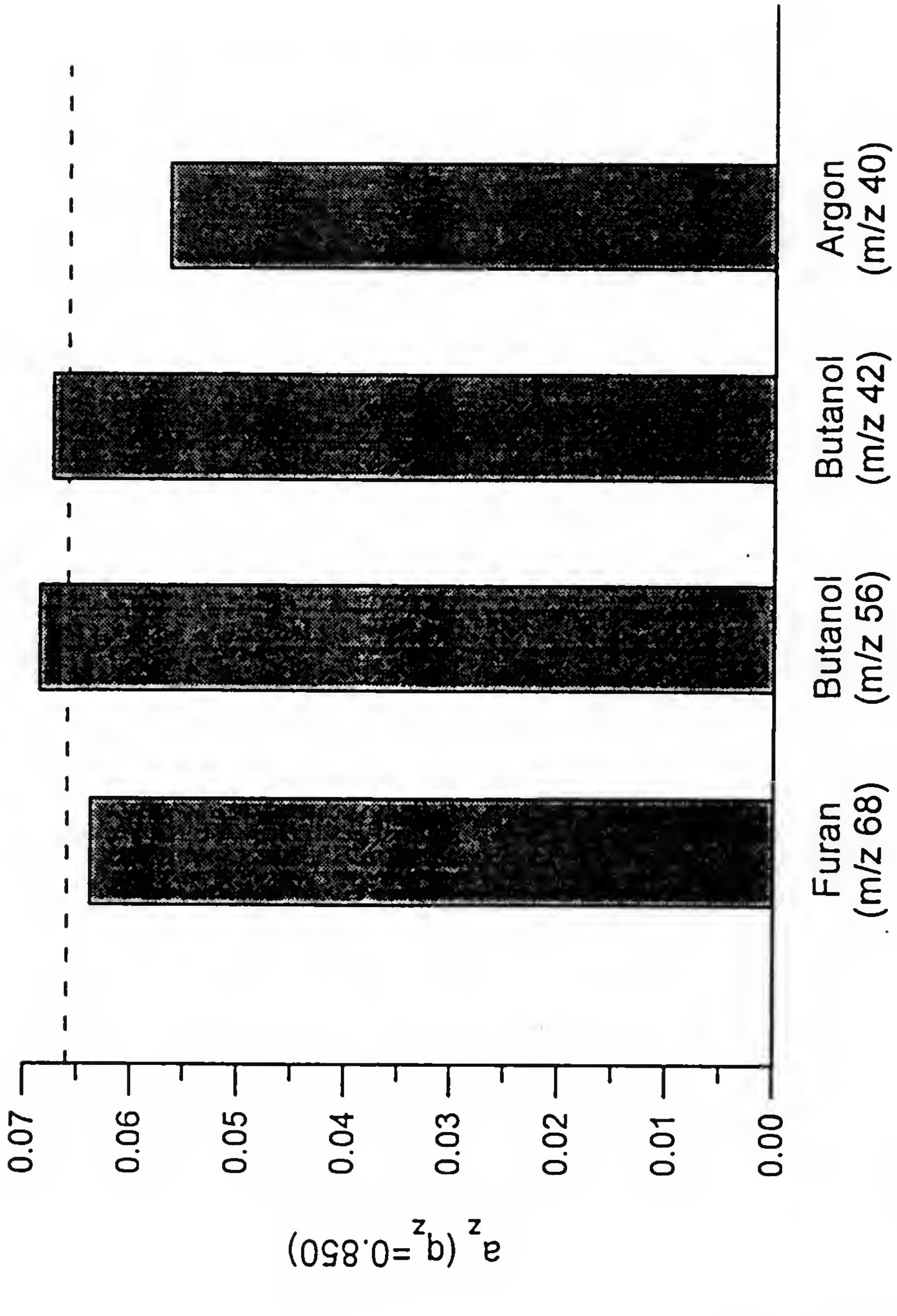
a_z (q_z=0.850)
0.07
0.06
0.05
0.04
0.03
0.02
0.01
0.00
Furan (m/z 68)
Butanol (m/z 56)
Butanol (m/z 42)
Argon (m/z 40)

Figure 5-12. Change in the a_z value for different ionization times (q_z=0.850). The changes are measured with respect to 0.5 ms ionization times. The dotted lines denotes the step size used for these experiments.

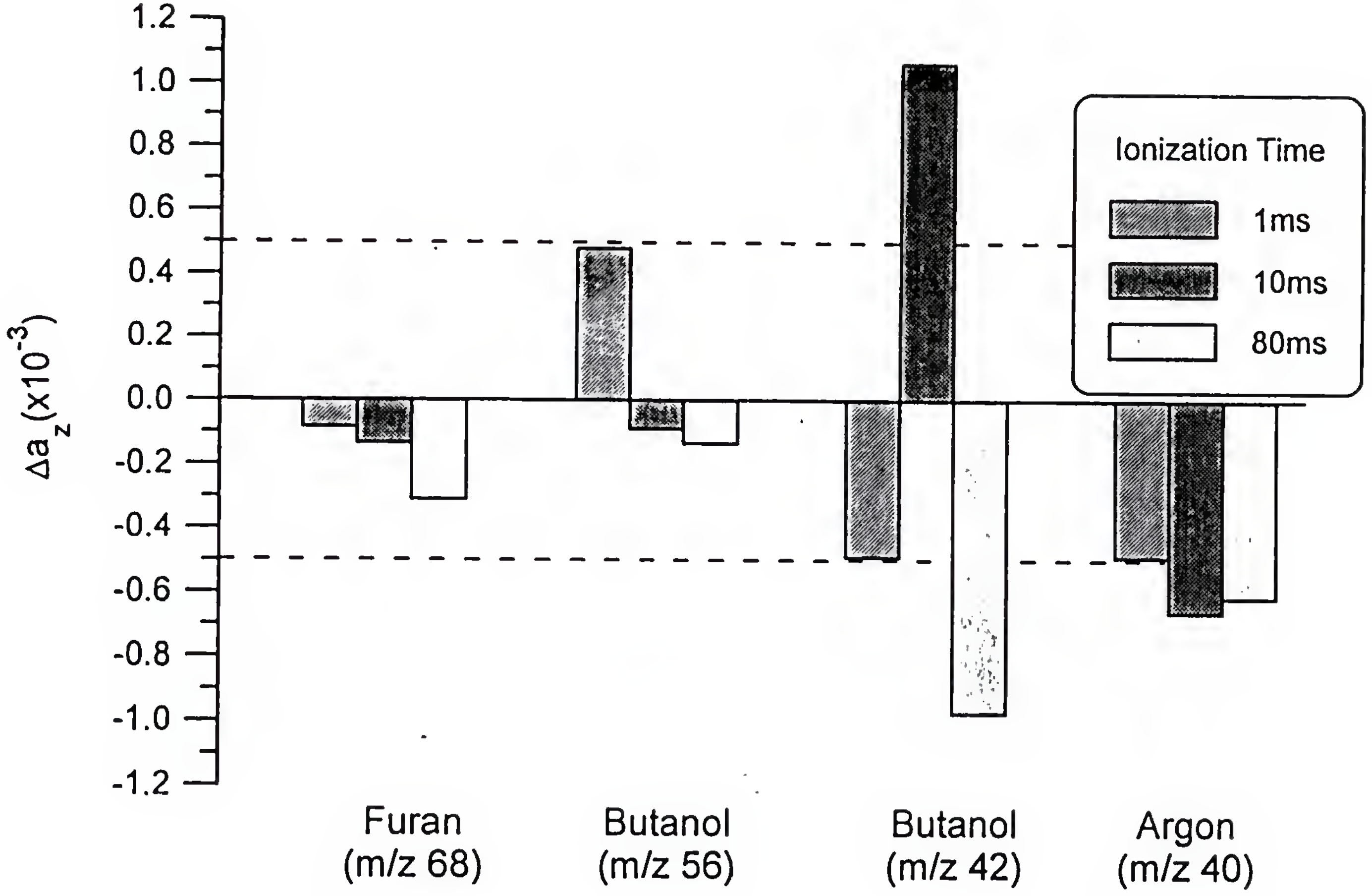

1.2
1.0
0.8
0.6
0.4
0.2
0.0
-0.2
-0.4
-0.6
-0.8
-1.0
-1.2
$\Delta a_z (\times 10^{-3})$
Furan (m/z 68)
Butanol (m/z 56)
Butanol (m/z 42)
Argon (m/z 40)
Ionization Time
1ms
10ms
80ms

Figure 5-13. Isolation efficiencies for different ion populations and mass-to-charges. Isolation efficiency is defined in equation 3-1.

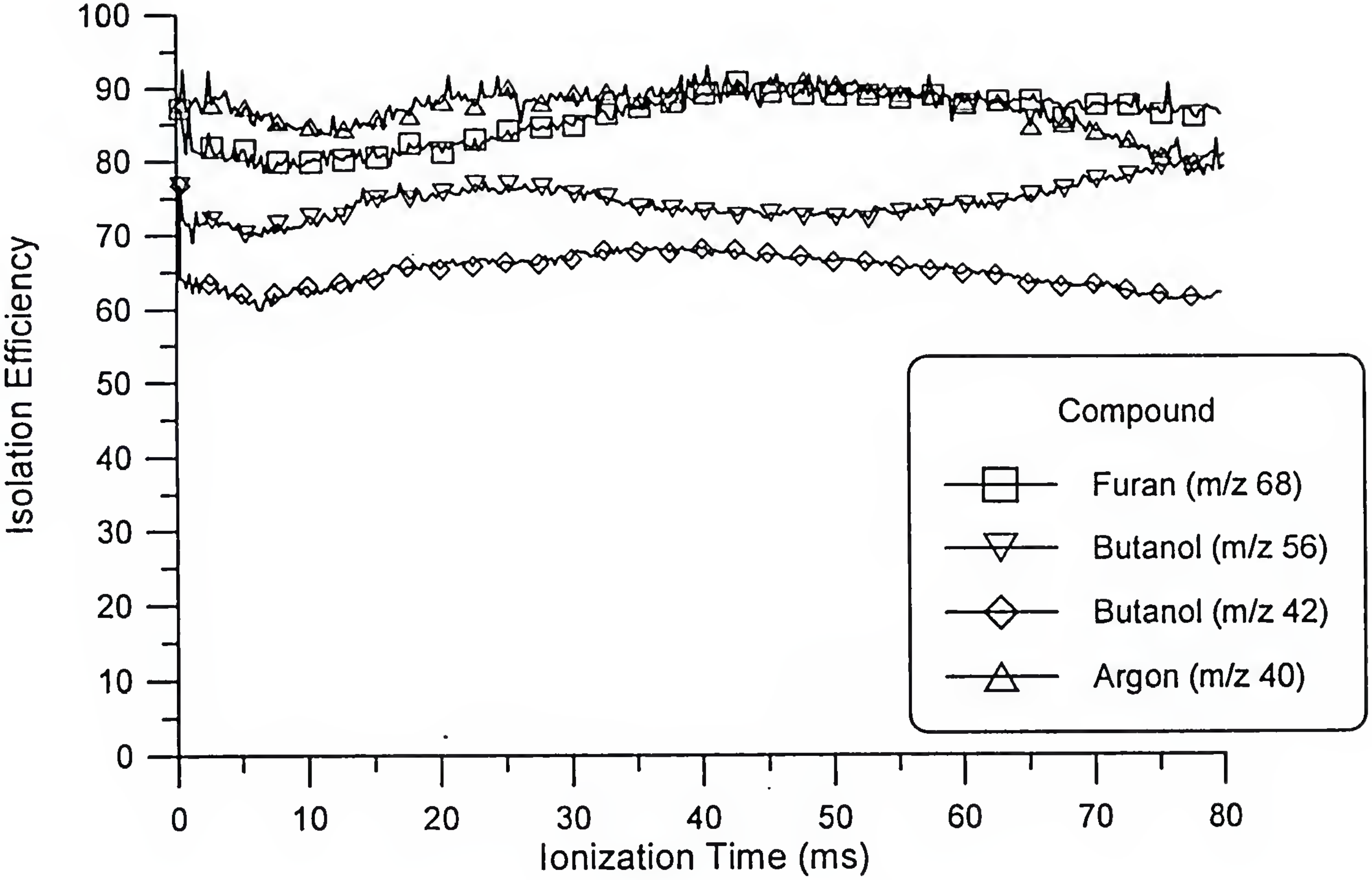
100
90
80
70
60
50
40
30
20
10
0
Isolation Efficiency
0
10
20
30
40
50
60
70
80
Ionization Time (ms)
Compound
Furan (m/z 68)
Butanol (m/z 56)
Butanol (m/z 42)
Argon (m/z 40)

change based upon the ion population. The cyclic nature associated with the ionization time for each m/z also was not seen to be reproducible for different m/z, and may simply reflect drift over the period of the experiment (approximately 12 hrs for each set of data).

Summary

The experimentally determined stability diagram boundaries match those theoretically predicted. No significant reproducible shifts of the boundaries due to ion population or mass-to-charge were detected. The movement of the stability diagram was seen to be within experimental error, as well as not following any detectable trend.

The two-step isolation method using RF and DC voltages to approach the stability boundary were seen not to be affected by the number of ions stored and isolated in the quadrupole ion trap. Differences were seen in the isolation efficiency for different ions. There was not seen, however, any trend based on mass-to-charge.

Non-linear resonance effects were enhanced with increases in ion population, as expected [30]. Large ion losses caused by non-linear resonances were seen with increasing ion population. The width of the areas effected by the non-linear resonances also were seen to increase with larger ion populations; however, the a_z value corresponding to the bottom of the well did not shift.

The work shown in this chapter showed no agreement with that shown by Todd (Figure 5-1). It is interesting to note that the position that Todd showed to be out side of the stability region ($q_z < 0.5$, $a_z = 0.00$) was seen to be were the highest intensities were recorded for these experiments (Figures 5-7 and 5-8). The reasons for the large discrepancies are not fully known, however, the experimental setup of Todd varied greatly from ours, see Table 5-1. In addition, Todd used a non-stretched ion trap manufactured in house while we used a stretched Finnigan ion trap. The losses seen by Todd could also be do to non-linear resonances. An additional point is that Todd injected the electrons through the ring electrode, while we injected them through an endcap. The large voltages applied to the ring electrode can affect the ability of the electrons to enter and ionize compounds in the ion trap.

Along with Todd we were not able to correlate our experimental results with the theory of Fisher or Schwebel. This can be explained by the fact that Fisher and Schwebel examine frequency shifts and then correlated those to changes in a_z; while Todd and we investigated effect of actually changing the a_z parameters. Frequency shifts are examined in Chapter 6 of this dissertation.

CHAPTER 6
EFFECTS OF ION POPULATION ON SECULAR FREQUENCY

Introduction

To perform tandem mass spectrometry on the quadrupole ion trap mass spectrometer (QITMS) the frequency of ion motion, or secular frequency, must be known. The most common method for MS/MS on the QITMS is collision-induced dissociation (CID) which involves the application of an auxiliary frequency to the endcap electrodes. To cause fragmentation, the auxiliary frequency must equal the secular frequency of the ions. Many factors have been shown to affect the efficiency with which CID can be performed on the QITMS.

This chapter discusses investigation into factors that affect the secular frequency and thus CID on the QITMS. The investigations included the determination of how ion population and ion m/z affects the secular frequency. Additional studies were performed to determine if the storage parameters, i.e., q_z, a_z, affect the secular frequency to deviate from theory.

Background

There are many factors that influence the secular frequency of ions. These include ion population and m/z of the ions stored in the QITMS. The shifts have been shown to affect CID efficiency [6] during a GC run. The change in the CID efficiency occurs because the ion population can vary by orders of magnitude as compounds elute. As the ion population varies the secular frequency shifts away from the auxiliary frequency which causes a decrease in the CID efficiency. To overcome this problem, many methods which apply a range of frequencies (rather than a single frequency) to the endcap electrodes have been developed. These methods include broad band[15], white noise[14], and stored-waveform inverse Fourier Transform (SWIFT)[16]. These methods, however, are difficult, time-consuming, and expensive to implement. Therefore, MSAGC was developed to control the number of ions stored in the QITMS, as shown in Chapter 4. The method controls the ionization time and thus the ion population continuously during a GC run. Mass-selective AGC, however, must be set up and optimized for each m/z that will undergo CID. This can make it time-consuming to implement.

The effect of different ion populations on the secular frequency is shown in Figure 6-1. The figure shows the frequency profiles for furan at three

Figure 6-1. Three ion profiles for different ion populations. The ion probe used was the $C_4H_4O^+$ ion of furan (m/z 68) at $q_z=0.85$ and $a_z=0.00$. The auxiliary freuqency was 0.100 mV_{0p} with the starting phase equal to zero.

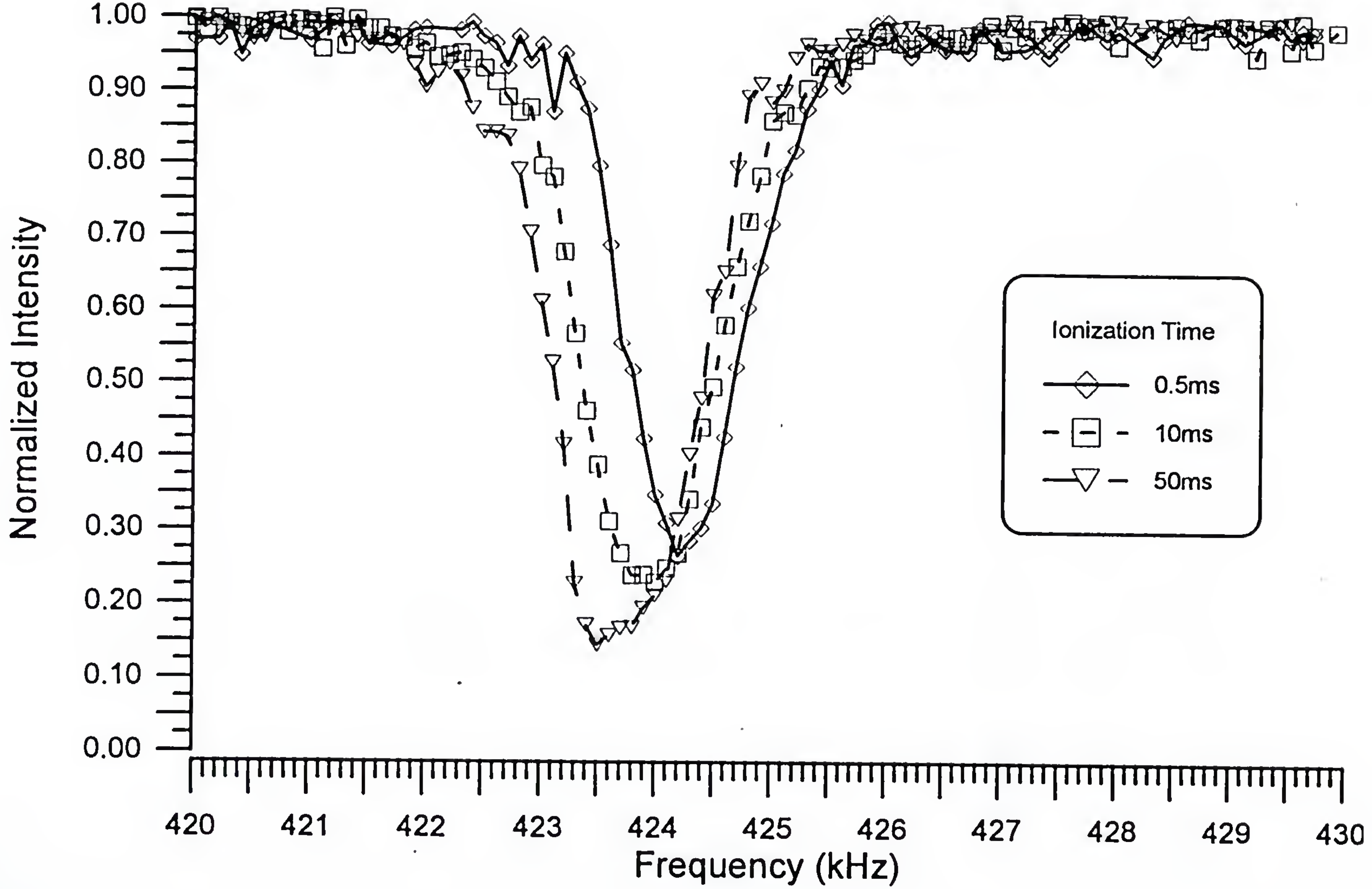

Normalized Intensity
1.00
0.90
0.80
0.70
0.60
0.50
0.40
0.30
0.20
0.10
0.00
420
421
422
423
424
425
426
427
428
429
430
Frequency (kHz)
Ionization Time
0.5ms
10ms
50ms

different ionization times. The data were collected by ionizing for a set time, applying a given frequency to the endcaps, then collecting the ion intensity. The process is then repeated for a different frequency until the entire frequency profile is collected. After which, the ionization time is increased and the whole process is repeated. The dip in the ion intensity corresponds to the secular frequency. Notice that as the ionization time increases, i.e., increased ion population, the secular frequency decreases. In this case we see a decrease in the secular frequency of 0.6 kHz for a change in ionization times from 0.5 to 50 ms. To perform CID on the QITMS the auxiliary frequency applied to the endcap electrodes must equal to the secular frequency. As can be seen from Figure 6-1 the variation in the secular frequency with ion population has so far made it impossible to accurately predict the secular frequency.

The frequency shifts have been related to movement of iso-β lines of the stability diagram. In addition, the frequency shifting has been modeled by Fisher[41] and Schwebel *et al.*[42] as an induced DC potential to the ring electrode, see Chapter 5. From the above models the βz can be determined by

$$\beta_z = (a_z)^{\frac{1}{2}} \quad \text{or} \quad \beta_z^2 = a_z \tag{6-1}$$

The amount that the a_z shifts can therefore be expressed by the size of the shifting of the iso-β lines by the equation

$$\Delta(\beta_z)^2 = (\beta_z^t)^2 - (\beta_z^e)^2 = a_z^t - a_z^e = \Delta a_z \qquad (6\text{-}2)$$

where the superscripts t and e denote theoretical and experimental values, respectively. Additionally, the secular frequency can be determined for the β_z value by the equation

$$\omega_o = \frac{\beta_z \Omega}{2} \qquad (6\text{-}3)$$

where Ω is the frequency of the RF voltage applied to the ring electrode, and w_o is the secular frequency. If this equation is substituted into equation 6-1 the change in a_z can be related to the change in the secular frequency:

$$\Delta a_z = \frac{4}{\Omega^2} |(\omega_z^t)^2 - (\omega_z^e)^2| \qquad (6\text{-}4)$$

Objectives

This work has examined the correlation between the secular frequencies determined experimentally and those obtained by theory. The work primarily focused on the effects of different ion populations on the secular frequency, with additional work on the effect of m/z on the secular frequency. These studies were performed at different q_z values, with a_z=0.00, to determine any effect of ion placement in the stability diagram on the secular frequency.

Experimental

The experiments focused on examining the secular frequencies for ions at three different ion populations, i.e., low, medium and high. The same ion populations were examined for ions of three different m/z, each originating from a different compound. The method used for determining the secular frequency is shown in Figure 6-2. Shown is a frequency profile of the m/z 56 fragment ion ($C_4H_8^+$) of butanol at q_z=0.205, a_z=0.00, with no helium. A program was written in C++ included in Gatorwork to determine the secular frequency by finding the two points that are 20% greater than the minimum value; interpolation was used when necessary. The average value of the two 20% points was said to be the secular frequency, 83.51kHz in the case of Figure 6-2.

Scan Function

The scan function used for these experiments is shown in Figure 6-3. The scan function was made of three major sections. The ions were formed at q_z=0.20 and a_z=0.00. The m/z of interest was then isolated using two-step isolation (see Chapter 1 and 3). The ion was placed at the q_z value to be investigated and the corresponding frequency was then applied. A subsequent mass-instability scan was used for detection.

Figure 6-2. The method used to determine the secular frequency. The frequency profile shown is for the $C_4H_8{}^+$ fragment ion from butanol (m/z 56) at q_z=0.205 and a_z=0.00. The middle point corresponding to 20% above the minimum value was said to be the secular frequency.

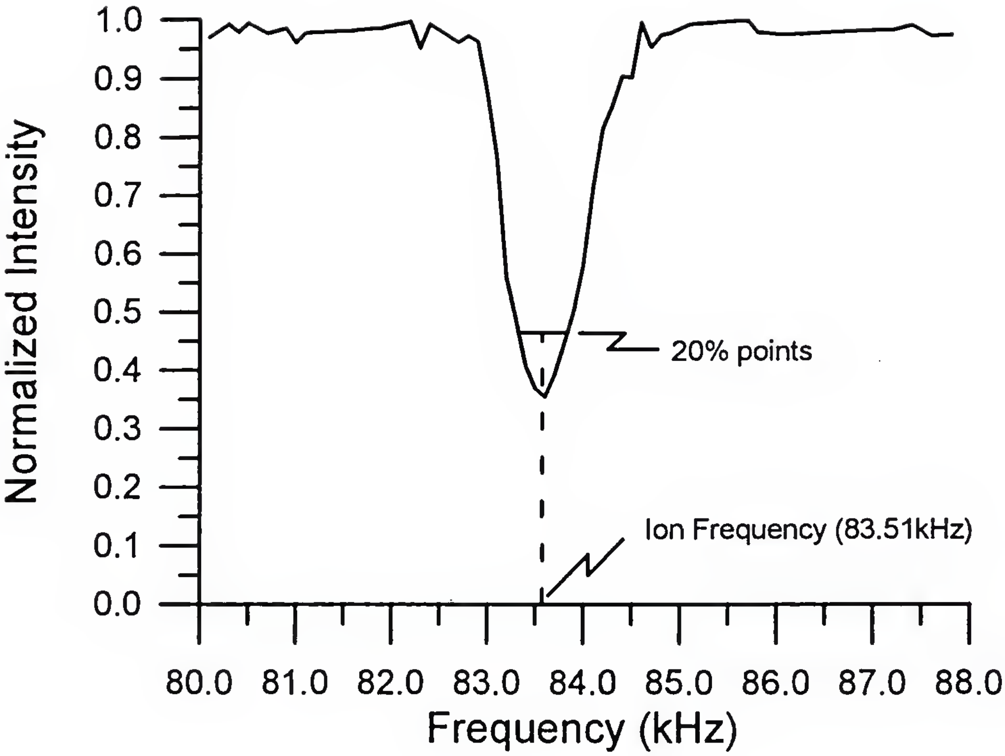
Normalized Intensity
1.0
0.9
0.8
0.7
0.6
0.5
0.4
0.3
0.2
0.1
0.0
20% points
Ion Frequency (83.51kHz)
80.0
81.0
82.0
83.0
84.0
85.0
86.0
87.0
88.0
Frequency (kHz)

Figure 6-3. Scan function used to obtain the frequency profiles. The only section that was changed during the experiments was the resonant excitation section.

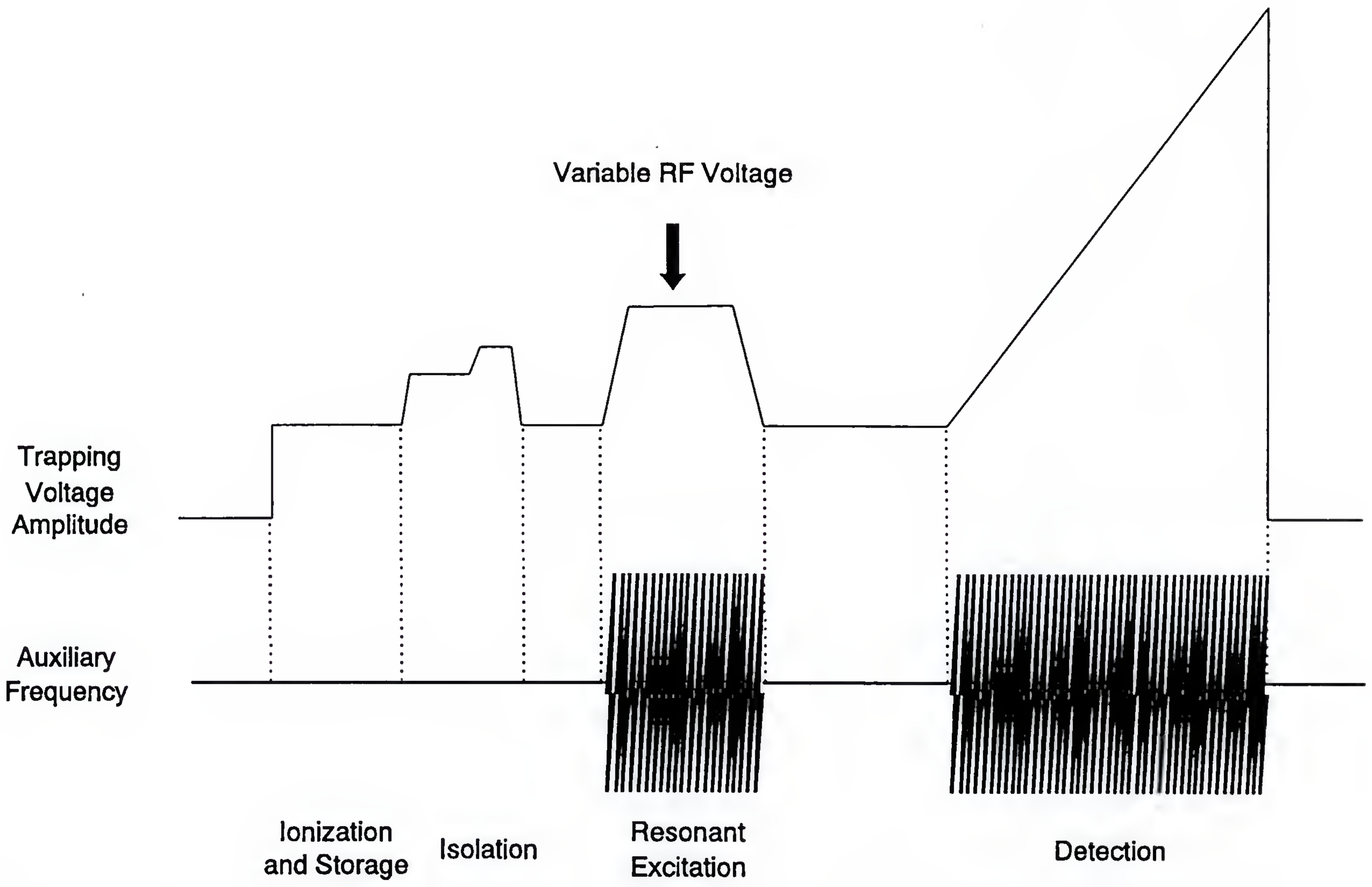
Variable RF Voltage
Trapping Voltage Amplitude
Auxiliary Frequency
Ionization and Storage
Isolation
Resonant Excitation
Detection

Acquisition of Frequency Profile

During the resonant excitation section the q_z value and the auxiliary frequency could be changed. The method changed the q_z value, obtain a frequency profile, then moved the ion to a new q_z value. This was accomplished by setting the q_z value to that under investigation (i.e., q_z=0.30), after which, the auxiliary frequency was turned on at a given frequency (i.e., 119kHz); the mass spectrum was subsequently collected. The frequency was then incremented to a new value (i.e., 119.1kHz) and the cycle repeated until the entire frequency profile was collected. The q_z value was then changed (i.e., q_z=0.35) and a new frequency profile was collected. Table 6-1 lists the q_z values investigated along with the frequency range and step size that were used for these experiments.

Ion Populations

To perform these experiments, constant ion populations were used instead of the more common method of constant ionization times. This was accomplished by PIF-PTHEN routines added to the FORTH/Procedure language; see Chapter 2 for details and examples. The ion populations that were used for these experiments were 1,000, 5,000, 30,000 ion counts, collected in profile mode. Constant ion populations was used to enable comparisons between different ions.

Table 6-1. Experimental parameters to obtain a frequency profile.

q_z value	Frequency Range (kHz)	Frequency Step Size (kHz)
0.20	70 - 90	0.100
0.25	90 - 110	0.100
0.30	119 - 139	0.100
0.35	140 - 160	0.100
0.40	162 - 182	0.100
0.45	180 - 200	0.100
0.50	200 - 220	0.100
0.55	223 - 243	0.100
0.60	249 - 269	0.100
0.65	275 - 295	0.100
0.70	300 - 320	0.100
0.75	330 - 350	0.100
0.80	365 - 385	0.100
0.85	410 - 430	0.100

Compounds

Ions from three compounds were used for these investigations. They were the $C_4H_8^+$ ion from butanol (m/z 58), $C_4H_4O^+$ from furan (m/z 68), and $C_4H_4S^+$ from thiophene (m/z 84). Profile data were collected for all of the experiments.

Results and Discussion

The data obtained from these experiments can be examined by three different methods. The first is to compare the experimental secular frequency to the theoretical values. Determination of the change in a_z values that are associated with the change in frequency (from equation 6-4) is a second method. The final method used to scrutinize the data was to determine the change in the q_z value associated with the change in frequency, that is, assuming that the space charge induces change in the RF field (q_z) rather than the DC field (a_z).

Frequency Comparisons

The experimental secular frequency can be compared to the theoretical secular frequency. The comparison will enable any trends based upon ion population, m/z, or q_z value to be seen. The theoretical frequency was determined using the iterative approach that is discussed by March[9] and equations 1-3 and 6-3. A C++ program was written to automatically calculate the theoretical secular frequency that corresponds to each q_z value investigated.

Plots showing the experimentally determined secular frequencies at different q_z values for the three different ions are shown in Figures 6-4 to 6-6. Notice that for each of the ions the experimental secular frequencies differ from the theoretical values. The plot for the furan $C_4H_4O^+$ ion, Figure 6-5, shows the most consistent offset for each q_z value. This can be seen by comparisons of the plots for the $C_4H_4^+$ ion of butanol and the $C_4H_4S^+$ ion of thiophene, Figures 6-4 and 6-6, respectively, to that of $C_4H_4O^+$. It can further be seen that for low q_z values $C_4H_8^+$ and $C_4H_4O^+$ had experimental secular frequencies that are almost equal. For higher q_z, however, the secular frequencies of butanol and furan are approximately the same. To further see this trend the secular frequencies for q_z=0.30 and q_z=0.70 for three different ion populations are depicted in Figure 6-7. To better see any trends between the different ions plots of the change in frequency versus the q_z are shown Figure 6-8 for ion populations of 30,000 counts. Notice that for each case there is a peak associated with the largest frequency shift. These peaks shift to lower q_z values for larger m/z ions. For example, the largest peak associated with $C_4H_8^+$ is located at q_z=0.6; the largest peak for $C_4H_4S^+$, however, is located at q_z=0.3. These five plots also show the lack of shifts of the secular frequencies for different ion populations.

Figure 6-4. Frequency dependence of the butanol ion (m/z 56) without helium buffer gas. The solid line denotes the theoretical values.

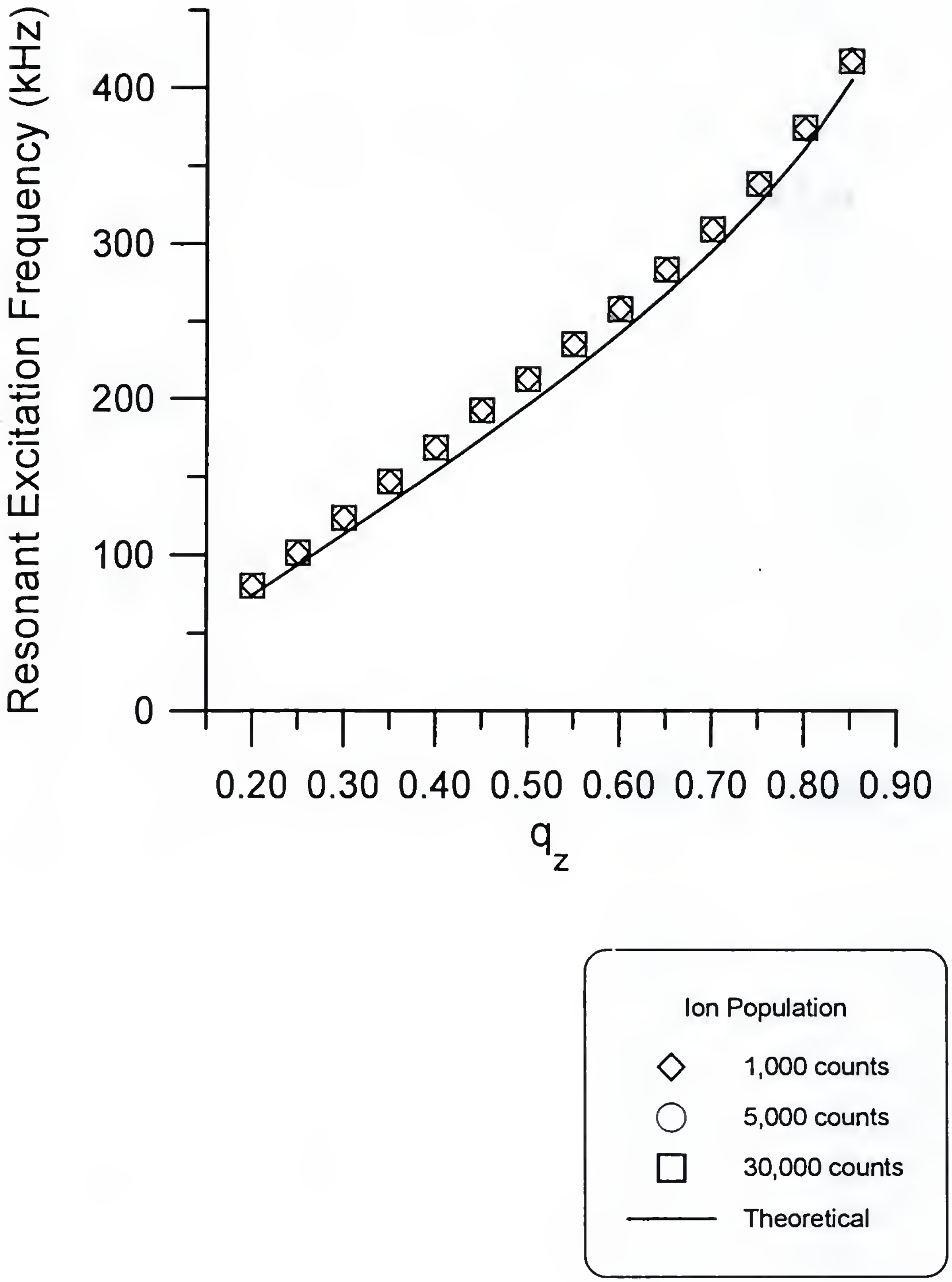
Resonant Excitation Frequency (kHz)
0
100
200
300
400
0.20
0.30
0.40
0.50
0.60
0.70
0.80
0.90
q_z
Ion Population
◇ 1,000 counts
○ 5,000 counts
□ 30,000 counts
Theoretical

Figure 6-5. Frequency dependence of the furan ion (m/z 68) without helium buffer gas. The solid line denotes the theoretical values.

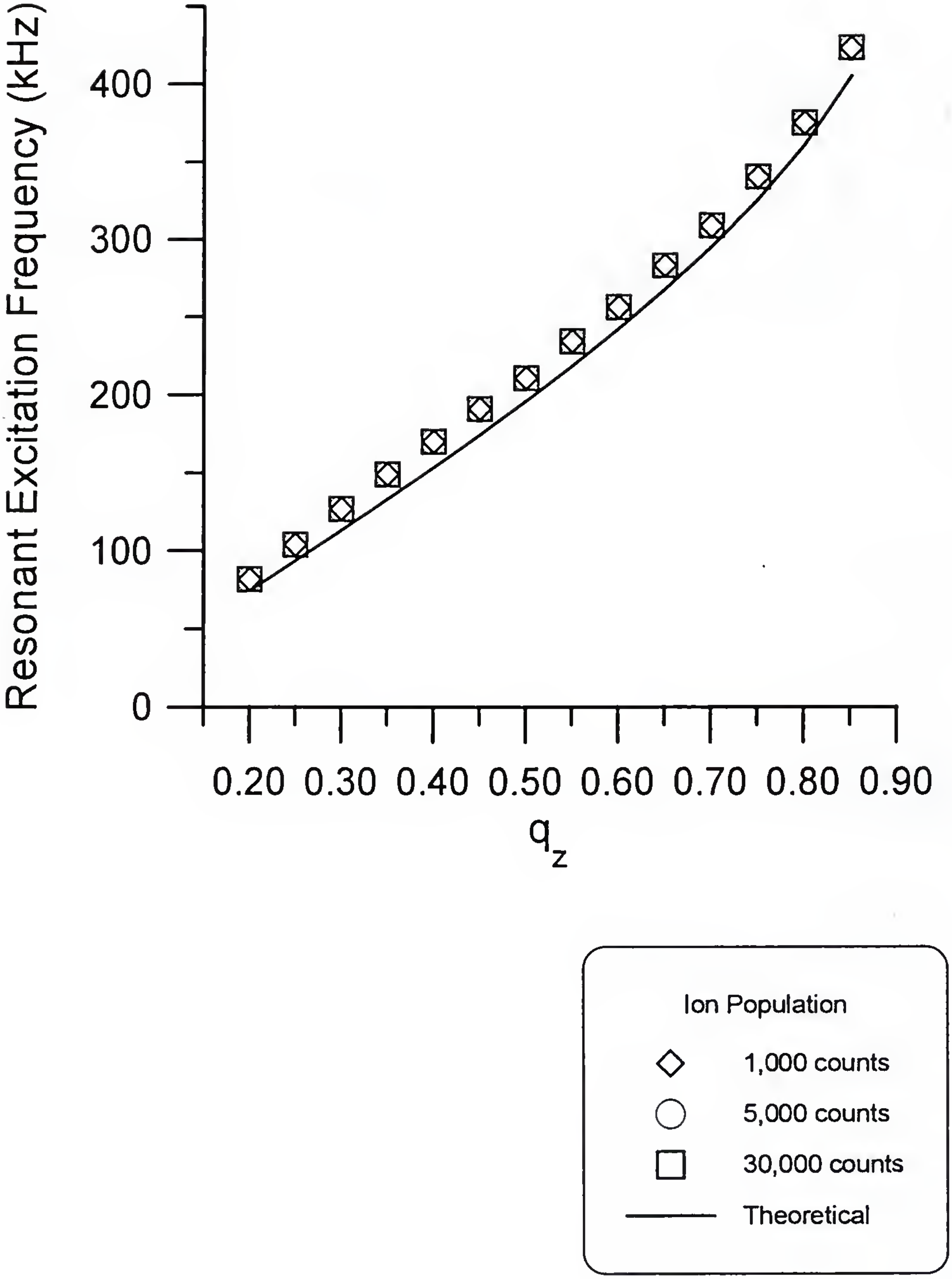
Resonant Excitation Frequency (kHz)
0
100
200
300
400
0.20
0.30
0.40
0.50
0.60
0.70
0.80
0.90
q_z
Ion Population
◇ 1,000 counts
○ 5,000 counts
□ 30,000 counts
Theoretical

Figure 6-6. Frequency dependence of the thiophene ion (m/z 84) without helium buffer gas. The solid line denotes the theoretical values.

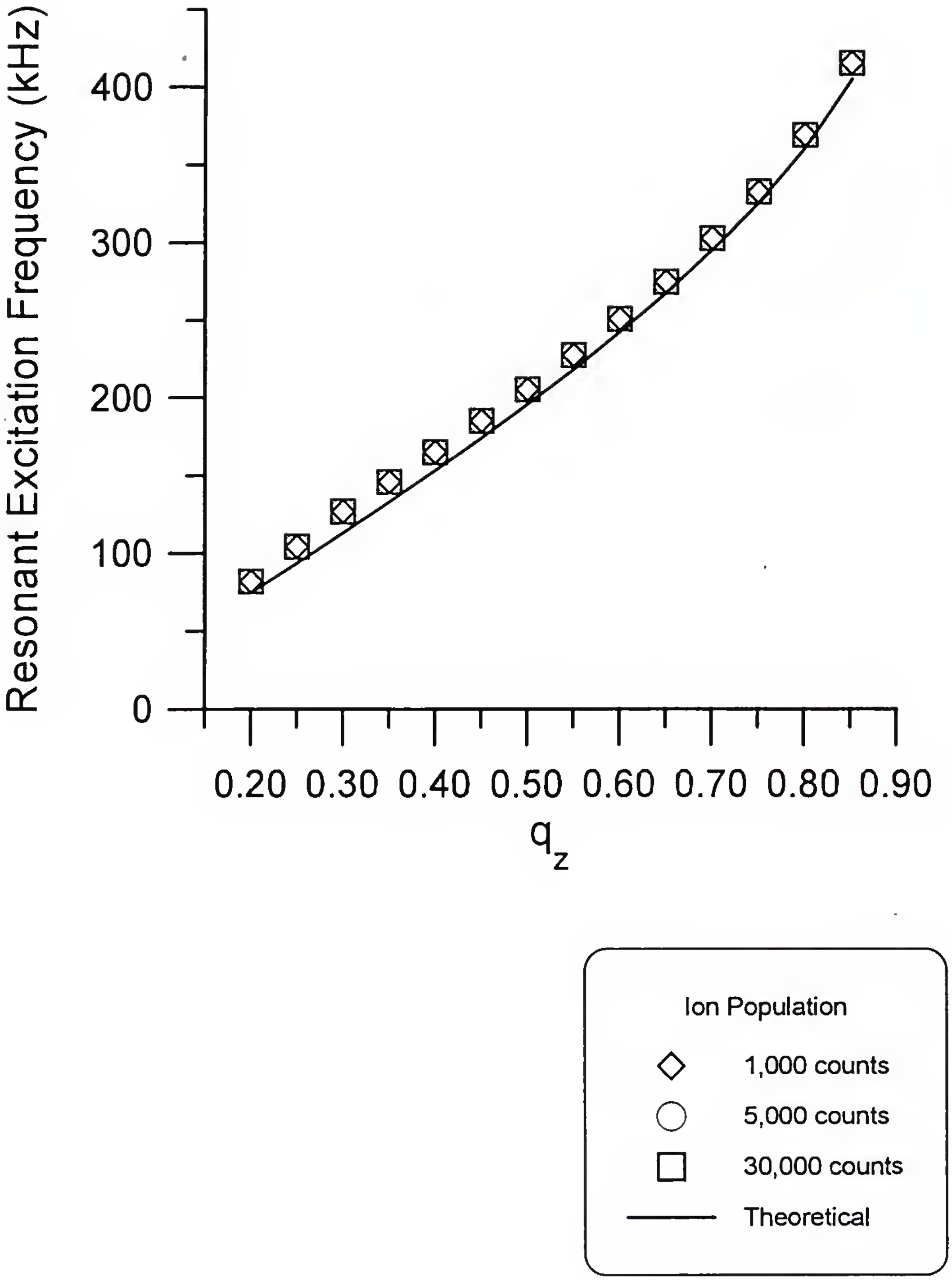
Resonant Excitation Frequency (kHz)
0
100
200
300
400
0.20
0.30
0.40
0.50
0.60
0.70
0.80
0.90
q_z
Ion Population
◇ 1,000 counts
○ 5,000 counts
□ 30,000 counts
Theoretical

Figure 6-7. The effect of ion population on the secular frequency. The secular frequencies for (a) $q_z=0.30$ and (b) $q_z=0.70$ are depicted for a range of ion populations.

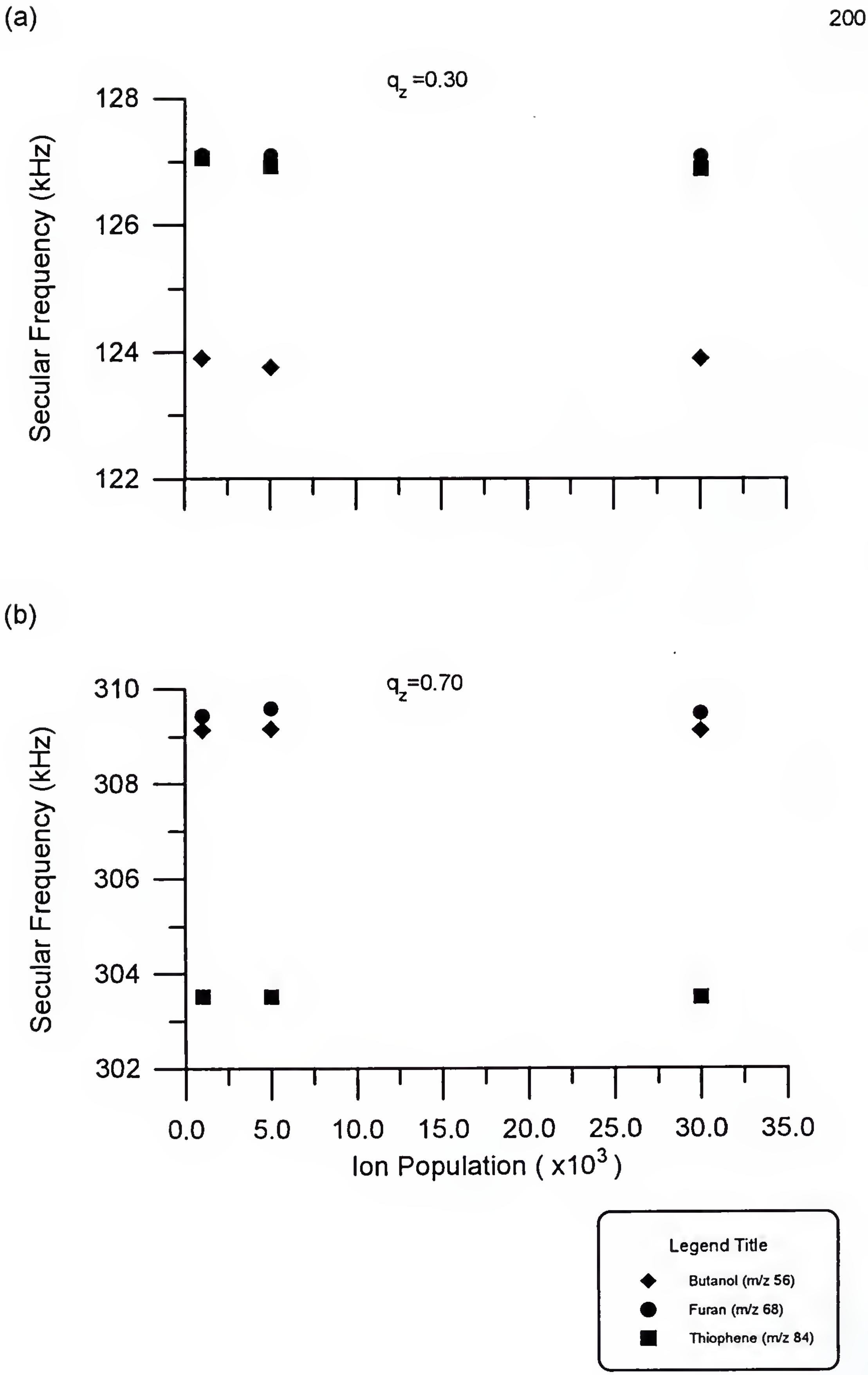
(a)
q_z =0.30
128
126
124
122
Secular Frequency (kHz)
(b)
q_z=0.70
310
308
306
304
302
Secular Frequency (kHz)
0.0
5.0
10.0
15.0
20.0
25.0
30.0
35.0
Ion Population (x10^3)
Legend Title
◆ Butanol (m/z 56)
● Furan (m/z 68)
■ Thiophene (m/z 84)

Figure 6-8. The change of frequency versus set q_z values. The ion probes are (a) $C_4H_8^+$, (b) $C_4H_4O^+$, and (c) $C_4H_4S^+$ for ion populations of 30,000 counts.

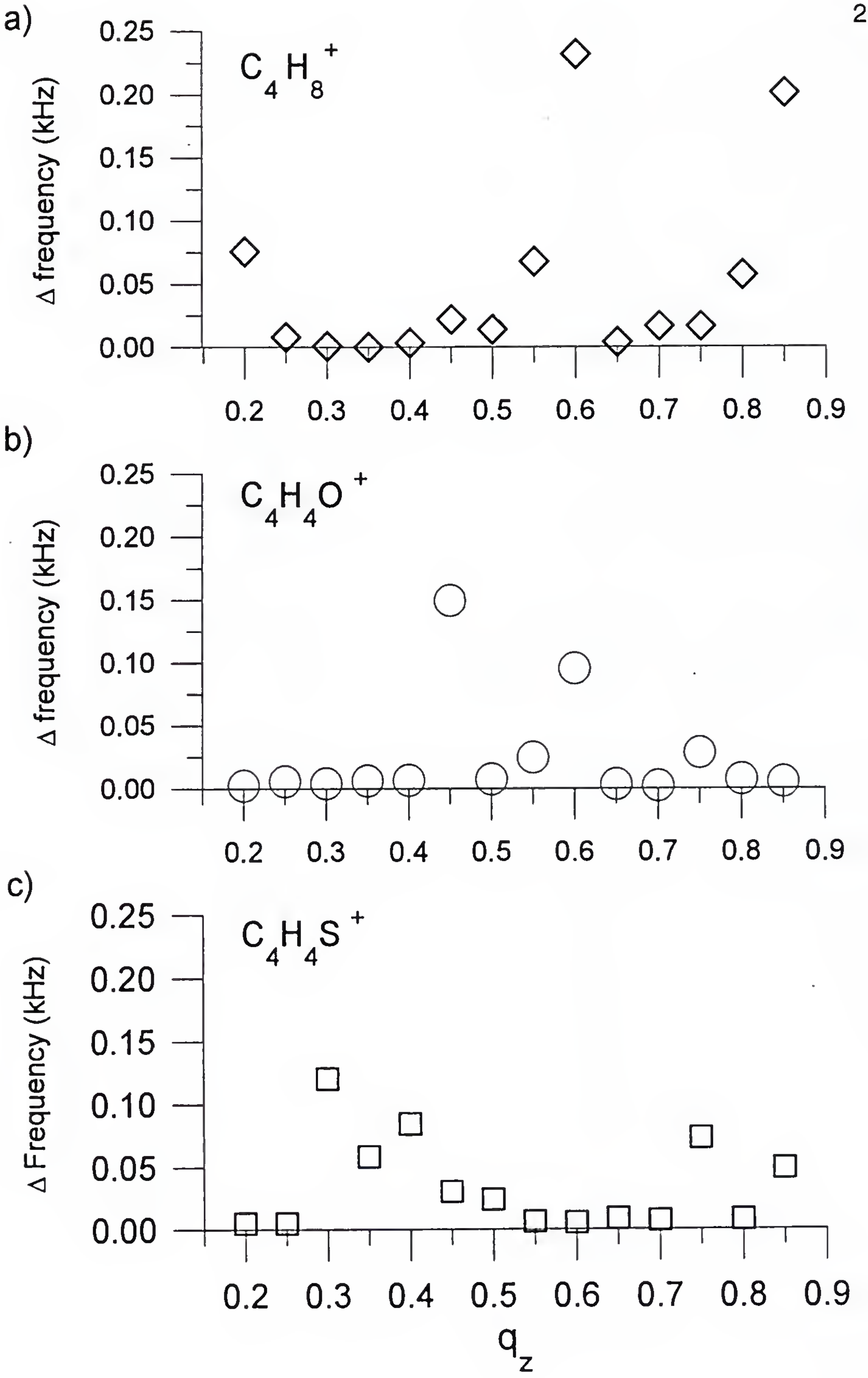
a)
$C_4H_8^+$
Δ frequency (kHz)
0.25
0.20
0.15
0.10
0.05
0.00
0.2
0.3
0.4
0.5
0.6
0.7
0.8
0.9
b)
$C_4H_4O^+$
Δ frequency (kHz)
0.25
0.20
0.15
0.10
0.05
0.00
0.2
0.3
0.4
0.5
0.6
0.7
0.8
0.9
c)
$C_4H_4S^+$
Δ Frequency (kHz)
0.25
0.20
0.15
0.10
0.05
0.00
0.2
0.3
0.4
0.5
0.6
0.7
0.8
0.9
q_z

Changes in a_z Values

By using the theoretical models of Fisher[41] and Schwebel[42], as discussed above, the change in the apparent a_z value can be calculated. This has been done for the different ion populations and q_z values. The results for the three different ions are plotted in Figures 6-9 to 6-11. The solid lines indicate the position of the stability boundaries if no shifting occurred. It is interesting to note that the trends at low and high q_z values are similar for each of the ions. The higher q_z values have larger deviations from theory, while the low q_z values correspond more closely. All three plots show a leveling out of the shift in at middle q_z values. The small dips in the curves for butanol and furan at q_z=0.50 and q_z=0.60 appear to correspond to non-linear resonances. The plot for thiophene, however, showed no, or very little, effect due to the non-linear resonances and thus the plateau region is larger.

Changes in q_z Values

The theory developed by Fisher[41] and Schwebel[42] assumed that all changes in the secular frequency were due to a change in the a_z value (DC field). The q_z value (RF field), however, could be affected by ion population or m/z of the ions stored in the QITMS. To show this effect the experimental q_z values, based on the experimental secular frequencies, were calculated. This is a simplified approach that assumes that the a_z value does

Figure 6-9. The effect of different storage parameters, i.e., q_z values, on the a_z values for $C_4H_8^+$ from butanol (m/z 56) without helium. The Δa_z was determined by the secular frequency [equation 6-4].

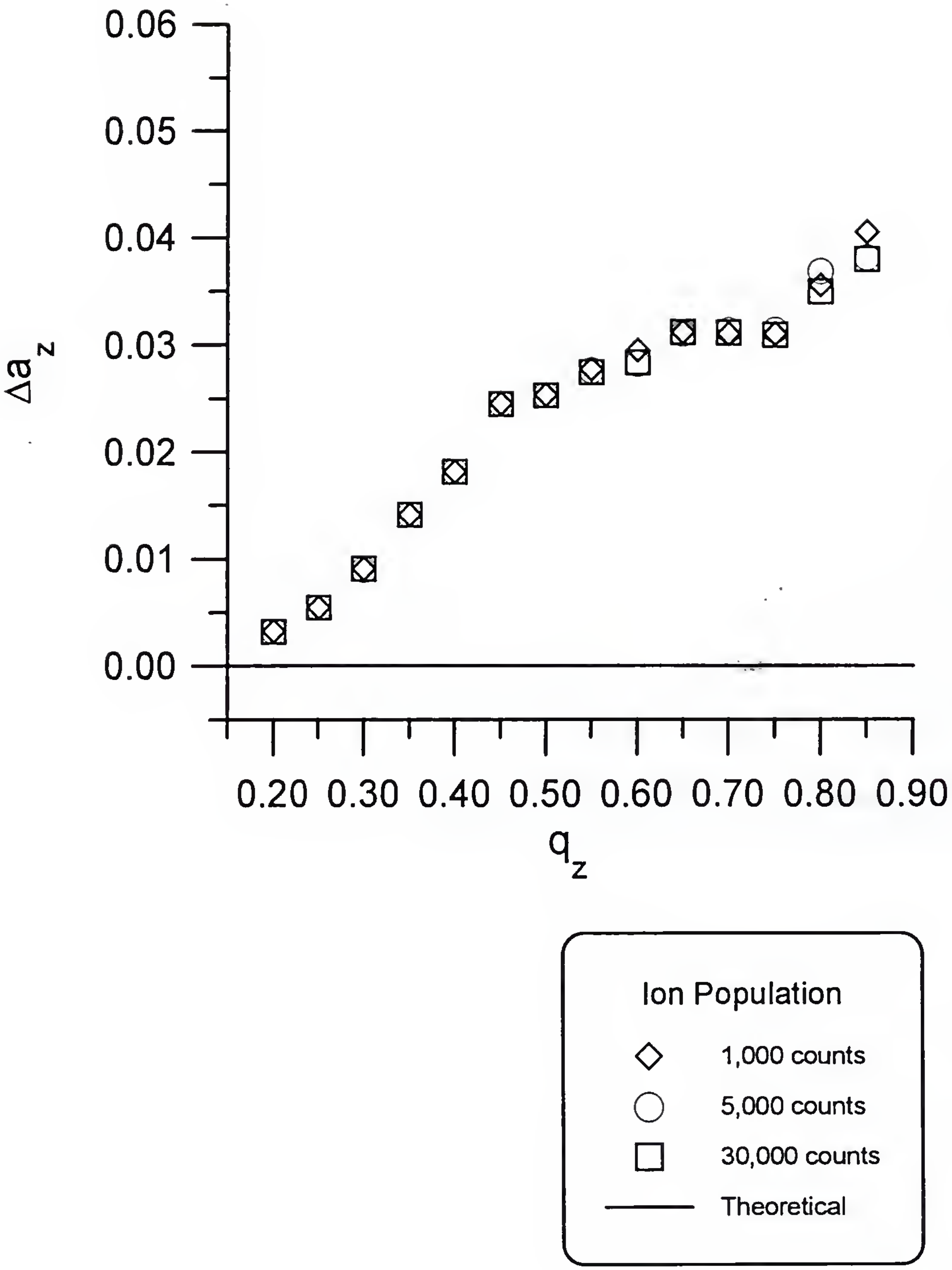
0.06
0.05
0.04
0.03
0.02
0.01
0.00
Δa_z
0.20
0.30
0.40
0.50
0.60
0.70
0.80
0.90
q_z
Ion Population
◇ 1,000 counts
○ 5,000 counts
□ 30,000 counts
Theoretical

Figure 6-10. The effect of different storage parameters, i.e., q_z values, on the a_z values for $C_4H_4O^+$ from furan (m/z 68) without helium. The Δa_z was determined by the secular frequency [equation 6-4].

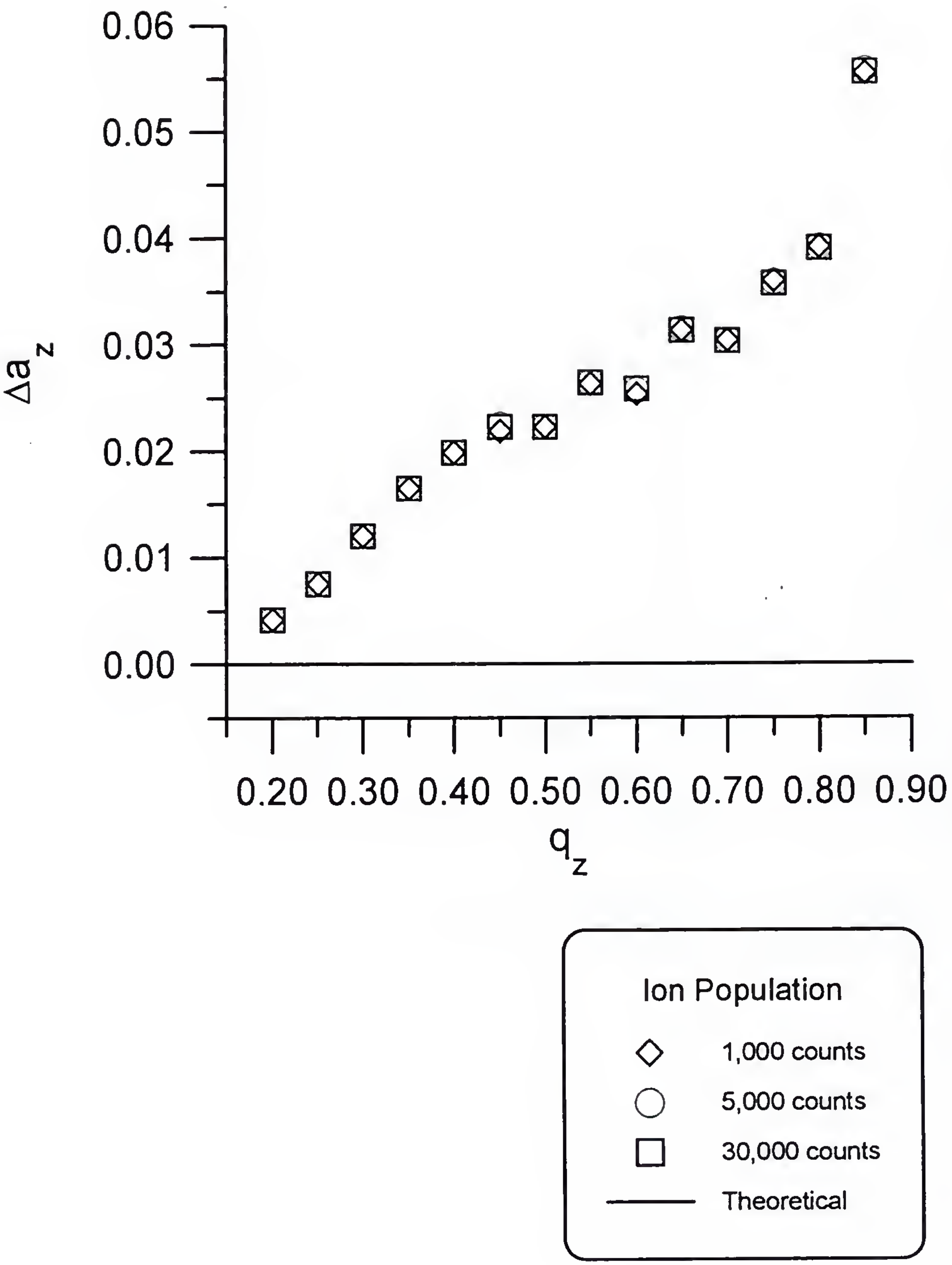
0.06
0.05
0.04
0.03
0.02
0.01
0.00
Δa_z
0.20
0.30
0.40
0.50
0.60
0.70
0.80
0.90
q_z
Ion Population
◇ 1,000 counts
○ 5,000 counts
□ 30,000 counts
Theoretical

Figure 6-11. The effect of different storage parameters, i.e., q_z values, on the a_z values for $C_4H_4S^+$ from thiophene (m/z 84) without helium. The Δa_z was determined by the secular frequency [equation 6-4].

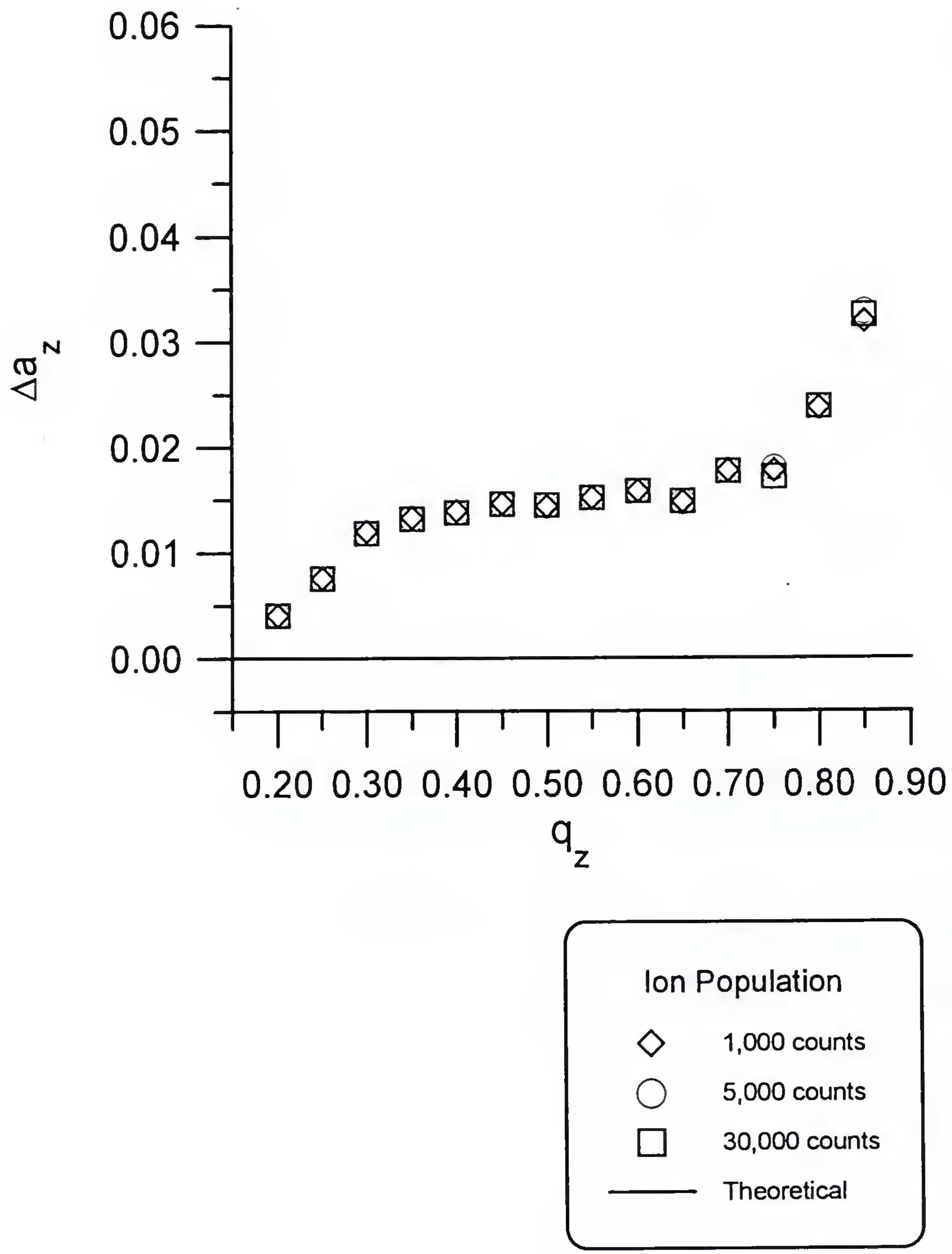
0.06
0.05
0.04
0.03
0.02
0.01
0.00
Δa_z
0.20
0.30
0.40
0.50
0.60
0.70
0.80
0.90
q_z
Ion Population
◇ 1,000 counts
○ 5,000 counts
□ 30,000 counts
Theoretical

not vary, but rather the q_z value. In actuality both the q_z and q_z values maybe affected by the ion population and m/z. This method of examining the data, however, is a simple way to discover any overall trends. The results showing the experimentally determined q_z values versus the theoretical, or set, q_z values for the three ions are plotted in Figures 6-12 to 6-14. The solid line in each plot indicates the ideal or theoretical response. All ions exhibited a maximum deviation from theory away from the edges of the stability diagram. The maximum deviations appear to shift to lower q_z values for higher m/z. This trend is seen more clearly in Figure 6-15 which is a plot of Δq_z vs. q_z for the different compounds. For example, the maximum shift for $C_4H_8{}^+$ is at approximately q_z=0.45 versus q_z=0.40 $C_4H_4O^+$ and q_z=0.30 for $C_4H_4S^+$. This trend could arise from the limitations of RF voltage calibration rather than any fundamental parameters of the QITMS. Current versions of the instrument (including Gatorware), however, do not enable new methods of RF voltage calibration to be investigated due to software limitations. This error in calibration also could account for the offset of the experimentally determined secular frequencies from theory.

Summary

This chapter described methods that were used to examine the secular frequency of ions stored in the QITMS. The results obtained did not show the expected shifts of the ion frequency based on ion population. Shifts, however,

Figure 6-12. The deviation of the experimentally determined q_z value from theory for the butanol ion (m/z 56) without helium. The solid line denotes the theoretical response which was calculated using the iterative approach.

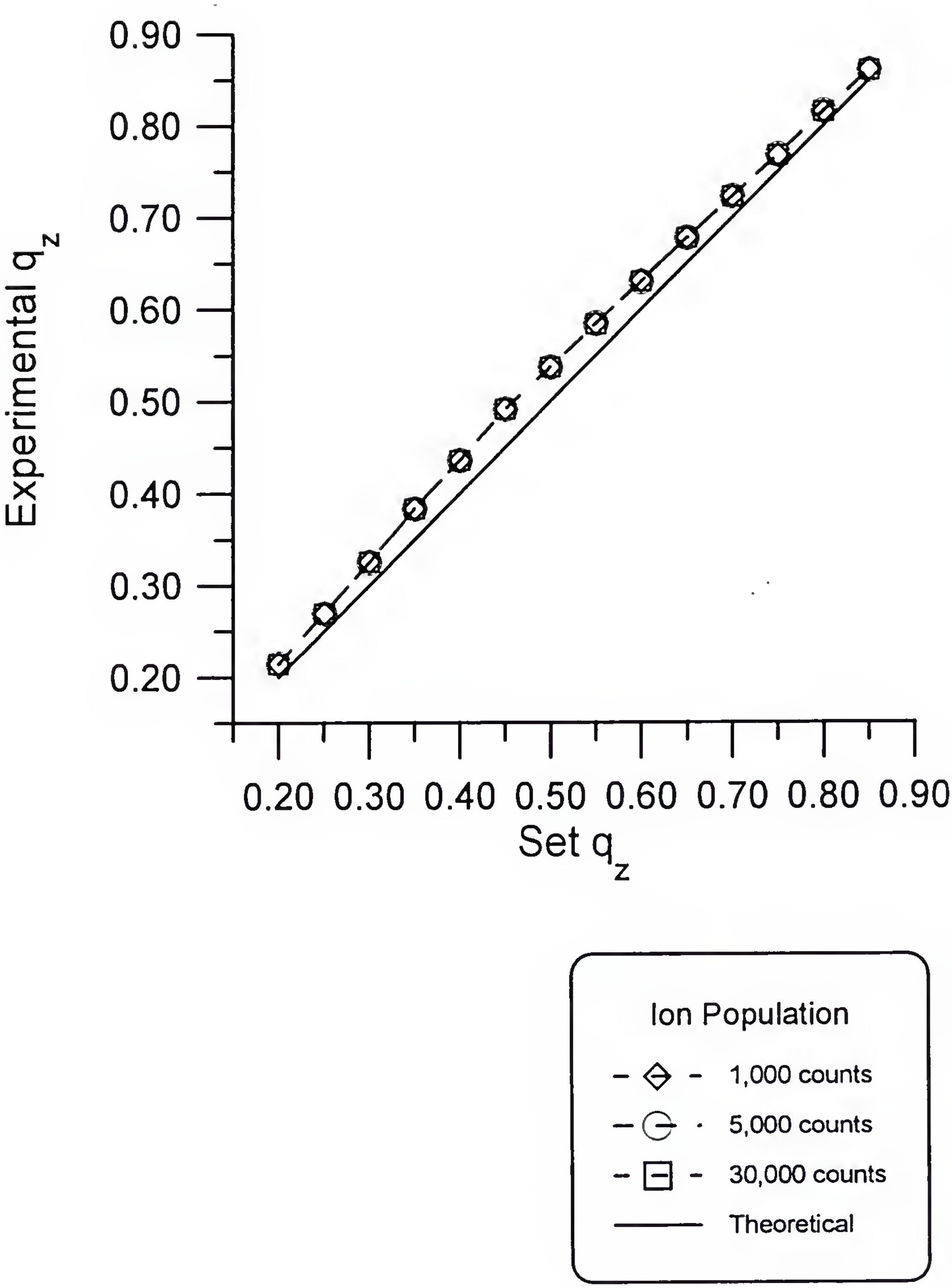
0.90
0.80
0.70
0.60
0.50
0.40
0.30
0.20
Experimental q_z
0.20 0.30 0.40 0.50 0.60 0.70 0.80 0.90
Set q_z
Ion Population
1,000 counts
5,000 counts
30,000 counts
Theoretical

Figure 6-13. The deviation of the experimentally determined q_z value from theory for the furan ion (m/z 68) without helium. The solid line denotes the theoretical response which was calculated using the iterative approach.

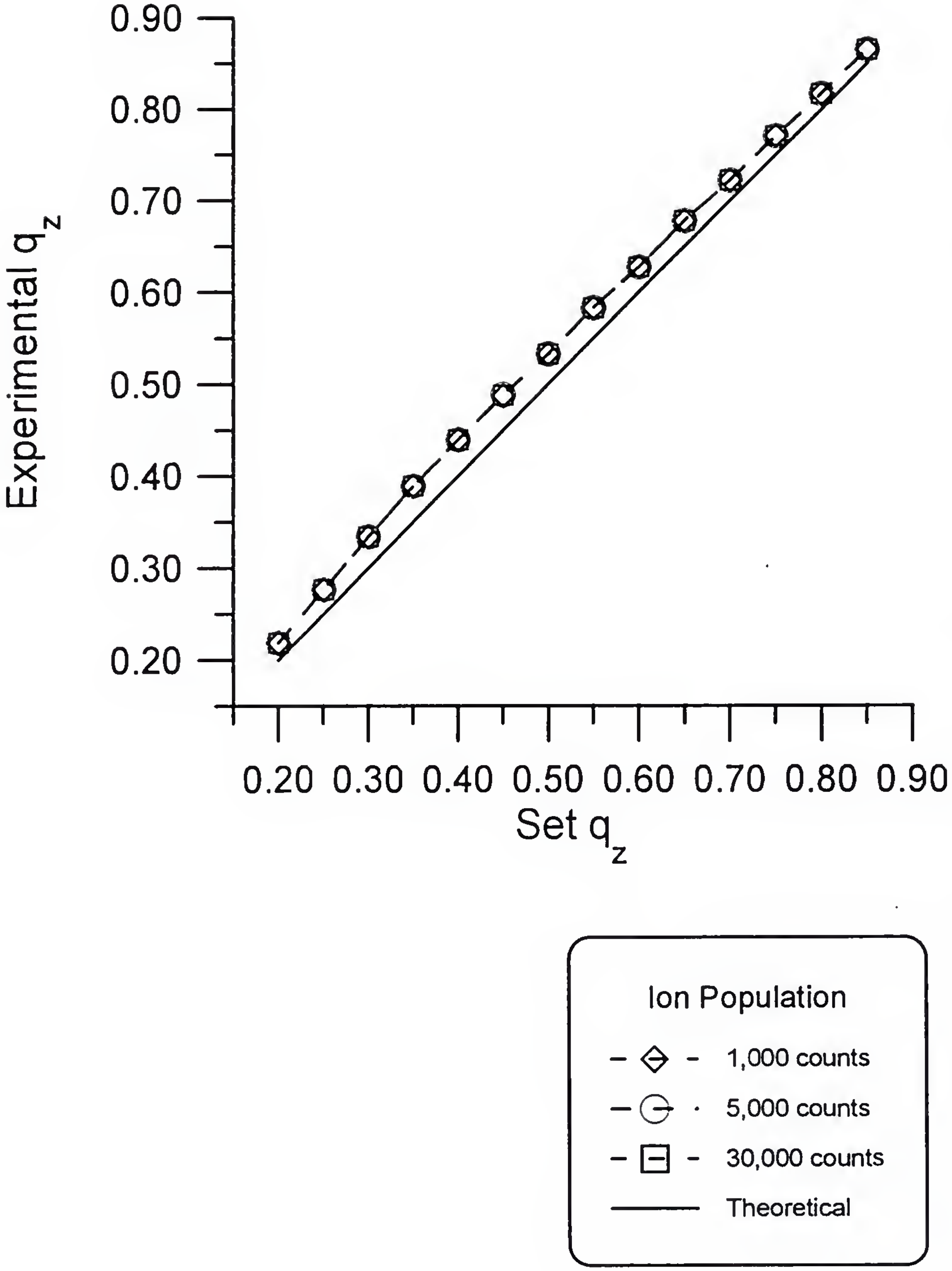
0.90
0.80
0.70
0.60
0.50
0.40
0.30
0.20
Experimental q_z
0.20 0.30 0.40 0.50 0.60 0.70 0.80 0.90
Set q_z
Ion Population
1,000 counts
5,000 counts
30,000 counts
Theoretical

Figure 6-14. The deviation of the experimentally determined q_z value from theory for the thiophene ion (m/z 84) without helium. The solid line denotes the theoretical response which was calculated using the iterative approach.

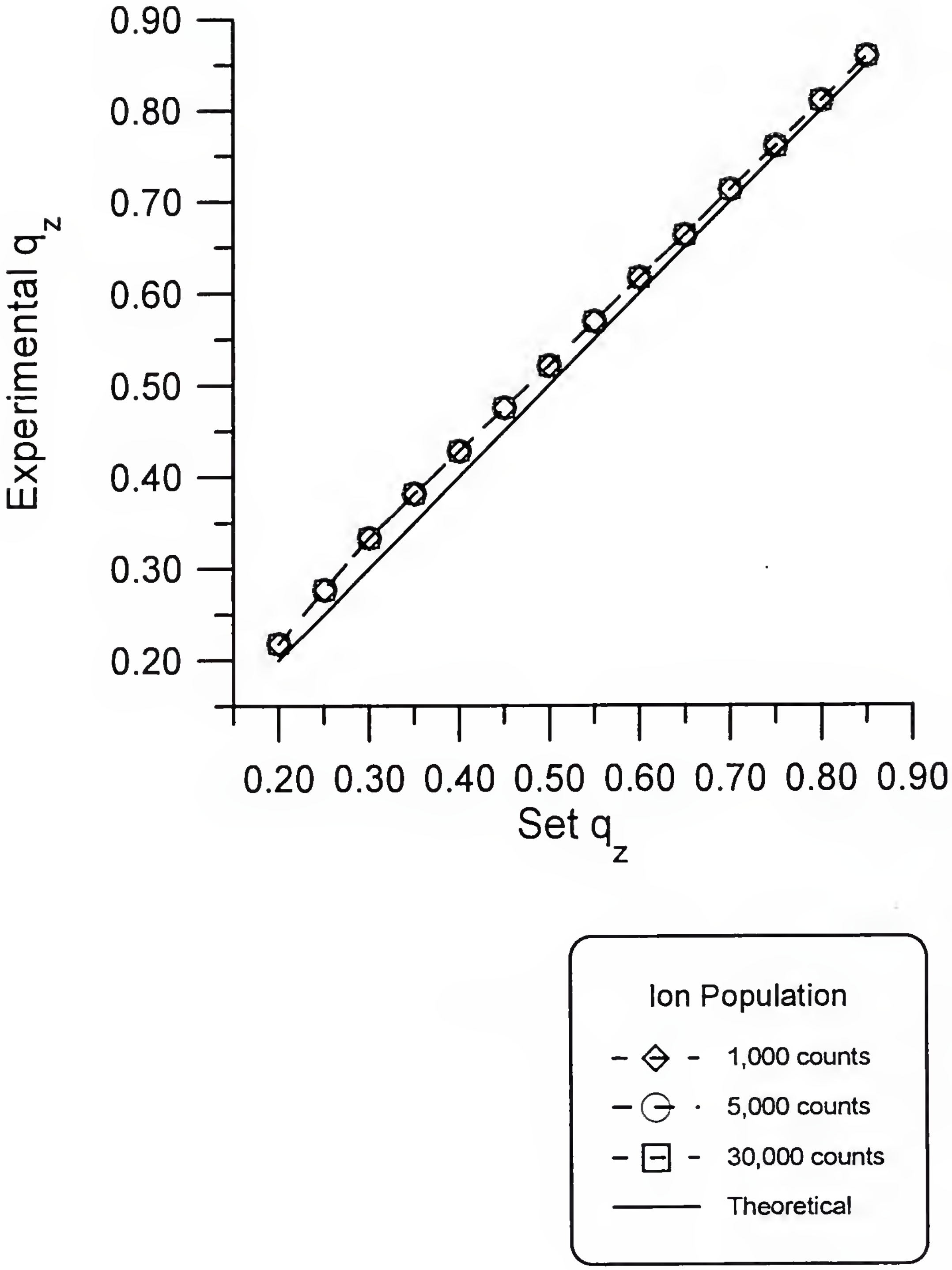
0.90
0.80
0.70
0.60
0.50
0.40
0.30
0.20
Experimental q_z
0.20 0.30 0.40 0.50 0.60 0.70 0.80 0.90
Set q_z
Ion Population
1,000 counts
5,000 counts
30,000 counts
Theoretical

Figure 6-15. The change in q_z versus the set q_z. The ion probes are (a) $C_4H_8^+$, (b) $C_4H_4O^+$, and (c) $C_4H_4S^+$ for ion populations of 30,000 counts.

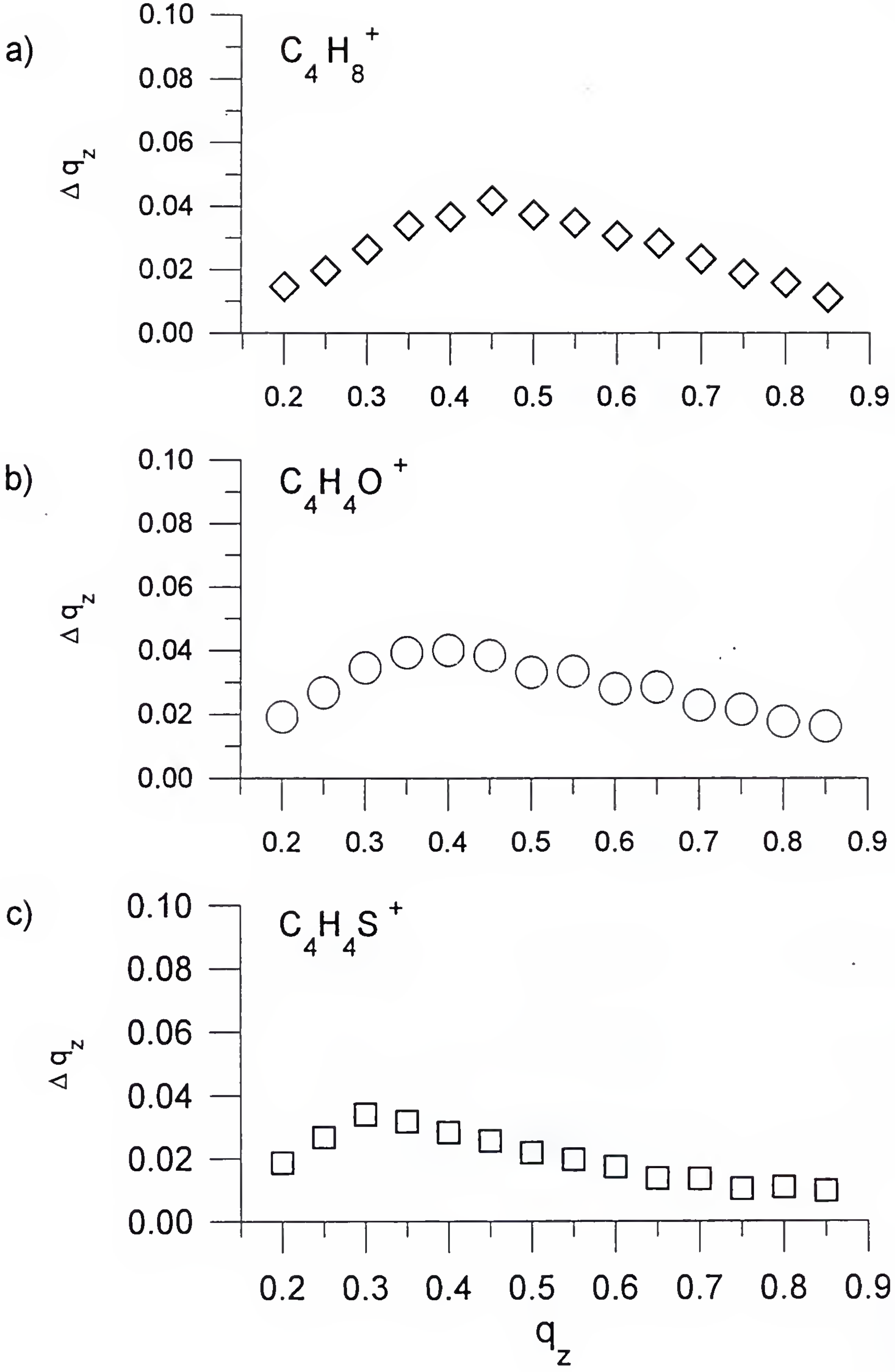
a)
$C_4H_8^+$
b)
$C_4H_4O^+$
c)
$C_4H_4S^+$
Δq_z
0.10
0.08
0.06
0.04
0.02
0.00
0.2
0.3
0.4
0.5
0.6
0.7
0.8
0.9
q_z

were seen for ions of different m/z. No trends could be established based upon the results obtained. The number of ions and m/z of the ions stored in the QITMS may effect both the RF and DC voltages, not just the DC voltage as previously suggested. The results further suggest that the RF voltage calibration may be a factor that influences the experimentally determined secular frequencies. New calibration routines, therefore, need to be developed to accurately predict the secular frequencies of ions, even at low ion populations.

CHAPTER 7
CONCLUSIONS AND FUTURE WORK

Conclusions

The work presented in this dissertation can be seen as being in two sections. They are the development of Gatorware and the examination of fundamental parameters on the QITMS.

Gatorware

The development of a research grade instrument, Gatorware, which included software and hardware modifications was successfully completed. Gatorware was used for all of the experiments discussed in this dissertation. Additionally, Gatorware allowed complete control of the operation of the QITMS while requiring little understanding of the QITMS electronics. This was accomplished by the use of the fundamental parameters of the QITMS. Therefore, knowledge of the theory of the ion trap is necessary to use Gatorware to its fullest potential.

Many new features not available on any other QITMS were included in Gatorware. They include the use of ramped DC voltages to move the ions around the stability diagram, are shown in Chapter 3. The use of ramped DC voltages was shown to enhance the ability of the operator to place the ion of interest at a position that is required for an experiment without significant ion losses. An additional feature is the ability to use and modify AGC. This enabled the development of a method to automatically adjust the ionization time based upon the number of ions at a specific m/z in the QITMS. This method, called MSAGC, was shown to improve the linear dynamic range for co-eluting compounds; in addition, MSAGC has been used for GC/MS/MS.

Fundamental Studies

Fundamental studies which examined the effect that ion population has on the fundamental parameters of the QITMS also were performed. The investigations included the experimental determination of where the boundaries of the stability diagram are located. Additional studies of the secular frequency also were performed.

The positions of the stability diagram boundaries were investigated for different ion populations and m/z. There were not seen any large shifts of the stability boundaries for changes in either ion population or m/z. Indeed, changes were so small that no trend could be established. No correlation with previous work or theory was found. Specifically the reasons why Todd's results were not confirmed are not known. It is believed, however, that instrumental variations might be the underlying reason. Variations based on m/z were also observed but, again, they were extremely small. The variations also were not reproducible and thus no overall trend was determined.

Work investigating the secular frequency showed large deviations from theory. There were not seen any overall trend based on ion population. The trends usually associated with ion population were not observed for these experiments. While the previous theory has modeled space charge as an application of DC voltage to the ring electrode in practice both the RF and DC voltages may be affected effected to some extent.

Future Work

The future work is discussed in two basic sections. The first is the further development of Gatorware. These new modifications include methods to enable Gatorware to be more flexible and easer to operate. Additional experiments that could be performed to further our understanding of the influence of ion population on tandem mass spectrometry within the QITMS also are discussed.

Gatorware

Gatorware has been used for all of the experiments discussed in this dissertation; in addition, many other experiments are being performed by a variety of different users. This has helped to improve the platform. There are very few bugs, or problems, in the software; they have been corrected as they were found. Improvements, however, can be made in some of the routines to help improve the ease of use and versatility of the software.

The major work that could be done to improve the versatility of Gatorware is to improve the RF voltage calibration routines. The routines could be improved to allow the user to input the auxiliary frequency that is used during detection. Additionally, the high mass limit could be entered by the user. These two options would enable the user to calibrate the mass spectrometer for mass range extension. This would greatly enhance the flexibility and ease of use of the instrument. Currently the only calibration methods available for mass range extension are done off-line or require the addition of a DEC station. These methods require extensive data workup, are very time consuming and are not always reproducible.

Further improvements of the software could include the automation of many of its operating routines. Software could be written to adjust and optimize automatically the factors that are used for tandem mass spectrometry such as the selection of the amplitude and frequency of the auxiliary frequency, isolation optimization, and selection of the MSAGC parameters. These automatic routines would enable the software to be used with greater ease. The knowledge base necessary to use Gatorware also would help allow users unfamiliar with MSAGC or MS/MS to use these functions. The automatic routines also would make the experiments more reproducible.

Fundamental Studies

Future studies which investigate the fundamental operation of the QITMS could be performed. The studies include determining the effect that ion population and m/z has on ion frequencies at different q_z, a_z combinations, i.e., off the a_z=0.00 line. Further investigations into the effect that ion structure has on secular frequency also could be performed.

To develop a theoretical model to determine the secular frequency, a detailed look at the effect of ion structure needs to be performed in conjunction with different ion populations. This could allow the complete development of a semi-empirical model for determining the secular frequency. These studies would help to automate the MS/MS procedure on the QITMS and enable real-time control during a GC run. This would help to make GC/MS/MS on the QITMS a routine analytical tool, easily implemented.

REFERENCE LIST

1. Yost, R.A.; Enke, C.G. *J. Amer. Chem. Soc.* 100 (1978) 2274.

2. Johnson, J.V.; Yost, R.A.; Kelly, P.E.; Bradford, D.C. *Anal. Chem.* 62 (1990) 2162.

3. Kaiser Jr., R.E.; Cooks, R.G.; Moss, J.; Hemberger, P.H. *Rapid Comm. Mass. Spec.* 3 (1989) 50.

4. Schwartz, J.C.; Syka, J.E.P.; Jardine, I. *J. Amer. Soc. Mass Spectrom.* 2 (1991) 198.

5. Louris, J.N.; Amy, J.W.; Ridley, T.Y.; Cooks, R.G. *Int. J. Mass Spectrom. Ion Processes* 88 (1989) 97.

6. Yates, N.A. *Methods for Gas Chromatography-Tandem Mass Spectrometry on the Quadrupole Ion Trap* Doctoral Dissertation, University of Florida 1994.

7. Yates, N.A.; Yost, R.A. *Ion Catcher Software* University of Florida, 1994.

8. Stafford, G.C.; Taylor, D.M.; Bradshaw, S.C.; Syka, J.E.p; Ulrich, M. *Proceedings of the 35th ASMS Conference on Mass Spectrometry and Allied Topics*, Denver, CO (1987) 775.

9. March, R.E.; Hughes, R.J. *Quadrupole Storage Mass Spectrometry*, John Wiley & Sons, New York, 1989.

10. Stafford, G.C.; Kelly, P.E.; Stephens, D.R. United States Patent 4,540,884 (1985).

11. Fulford, J.E.; Hoa, D.N.; Hughes, R.J.; March, R.E.; Bonner, R.F.; Wong, G.J. *J. Vac. Sci. Technol.* 17 (1980) 829.

12. Yates, N.A.; Yost, R.A.; Bradshaw, S.C.; Tucker, D.B. *Proceedings of the 39th ASMS Conference on Mass Spectrometry and Allied Topics*, Nashville, TN (1991) 1489.

13. Gronowska, J.; Paradisi, C.; Traldi P.; Vettori, U. *Rapid Comm. Mass Spec.* 4 (1990) 306.

14. McLuckey, S.A.; Goeringer, D.; Glish, G.L. *Anal. Chem.* 64 (1992) 1455.

15. Yates, N.A.; Yost, R.A.; Bradshaw, S.C.; Tucker, D.B. *Proceedings of the 39th ASMS Conference on Mass Spectrometry and Allied Topics*, Nashville, TN (1991) 132.

16. Marshall, A.G.; Wang, T.C.L.; Ricca, T.L. *J. Am. Chem. Soc.* 107 (1985) 1893.

17. Stiller, S.W.; Kelly, P.; Hoekman, D.; Bradshaw, S. *Presented at the Pittsburgh Conference*, Atlanta, GA (1993) 267.

18. Schwartz, J.C.; Jardine, I. *Rapid Comm. Mass Spec.* 6 (1992) 313.

19. *Microsystem Components Handbook--Microprocessors*, Intel Corporation, Santa Clara, CA, 1 (1986).

20. Qualcomm, Inc., *Q2334 Dual Direct Digital Synthesizer Technical Data Sheet*, San Diego, CA, January 1992.

21. Strife, R.J.; Simms, J.R.; Lacey, M.P. *J. Am. Soc. Mass Spectrom.* 1 (1990) 265.

22. Tucker, D.B.; Hameister, C.H.; Bradshaw, S.C.; Hoekman, D.J.; Weber-Grabau, M. *Proceedings of the 36th ASMS Conference on Mass Spectrometry and Allied Topics*, San Francisco, CA (1988) 628.

23. McLuckey, S.A.; Goeringer, D.E.; Glish, G.L. *J. Am. Soc. Mass Spectrom.* 2 (1993) 11.

24. Eades, D.M.; Yates, N.A.; Yost, R.A. *Proceedings of the 39th ASMS Conference on Mass Spectrometry and Allied Topics*, Nashville, TN (1991) 1492.

25. Julian, R.K.; Cooks, R.G. *Anal. Chem.* 65 (1993) 1827.

26. Buttril, S.E.; Shaffer, B.I.; Kamicky, J.; Amold, J.T. *Proceedings of the 40th ASMS Conference on Mass Spectrometry and Allied Topics* Washington D.C., (1992) 1015.

27. *Finnigan MAT -- ITS-40 Operator Manual, Rev. C*, San Jose, CA, June 1990.

28. Basic, C. *Probing Trapped Ion Energies in a Quadrupole Ion Trap Mass Spectrometer* Doctoral Dissertation, University of Florida, 1992.

29. Quarmby, S.T.; Griffin, T.P.; Yost, R.A. *Proceedings of the 42nd ASMS Conference on Mass Spectrometry and Allied Topics*, Chicago, IL (1994) 706.

30. Eades, D.M.; Johnson, J.V.; Yost, R.A. *J. Am. Soc. Mass Spectrom.* 4 (1993) 917.

31. Kleintop, B.L.; Abolin, C.R.; Yost, R.A. *J. Am. Soc. Mass Spectrom.* 3 (1992) 85.

32. Todd, J.F.J.; Waldren, R.M.; Mather, R.E.; Lawson, G. *Int. J. Mass Spectrom. Ion Phys.* 28 (1978) 141.

33. Mather, R.E.; Lawson, G.; Todd, J.F.J. *Int. J. Mass Spectrom. Ion Phys.* 28 (1978) 347.

34. Todd, J.F.J.; Waldren, R.M. *Int. J. Mass Spectrom. Ion Phys.* 29 (1979) 301.

35. Todd, J.F.J.; Waldren, R.M. *Int. J. Mass Spectrom. Ion Phys.* 31 (1979) 15.

36. Mather, R.E.; Waldren, R.M.; Todd, J.F.J. *Int. J. Mass Spectrom. Ion Phys.* 33 (1980) 201.

37. Todd, J.F.J.; Waldren, R.M.; Mather, R.E.; Lawson, G. *Int. J. Mass Spectrom. Ion Phys.* 34 (1980) 325.

38. Todd, J.F.J.; Waldren, R.M.; Freer, D.A.; Turner, R.B. *Int. J. Mass Spectrom. Ion Phys.* 35 (1980) 107.

39. Todd, J.F.J.; Freer, D.A.; Waldren, R.M. *Int. J. Mass Spectrom. Ion Phys.* 36 (1980) 371.

40. Fulford, J.E. Hoa, D.-N.; Hughes, R.J.; March, R.E.; Wong, G.J. *J. Vac Sci. Technol.* 17(4) (1980) 829.

41. Fisher, E. *Z. Phys.* 156 (1959) 1.

42. Schwebel, C.; Moller, P.A.; Manh, P.T. *Rev. Phys. Appl.* 10 (1975) 227.

43. Moller, P.A.; Manh, P.T.; Schwebel, C.; Septier, A. *IEEE Transactions on Nuclear Science*, NS-23 No.2, (1976) 3.

44. Dehmelt, H.G. *Adv. At. Mol. Phys.* 3 (1967) 53.

BIOGRAPHICAL SKETCH

Timothy P. Griffin was born at Portsmouth, VA, on September 22, 1963. His father was in the military so he attended numerous elementary and junior high schools. After a year at Holmes High School, San Antonio, TX, he moved to Knob Noster, MO. He graduated from Knob Noster High School in 1981. He then attended the University of Missouri at Rolla for two years. Afterwards he attended Johnson County Community College where he joined the Phi Theta Kappa national honor fraternity and Who's Who Among Students in American Junior Colleges. He earned an electronics/biomedical equipment technology associates degree in 1985.

After graduation from Johnson County Community College he was employed by Floyd Brown and Associates as the Technical Service Manager. The job required extensive travel throughout Kansas and Missouri repairing and maintaining medical electronics. In 1988, while still working for Floyd Brown and Associates, he started the University of Kansas (KU). While at KU he joined Phi Lambda Epsilon Honorary Chemical Society and the Golden Key National Honor Society. He earned a bachelor of science degree in chemistry in 1991.

He then attended the University of Florida were he earned his Ph.D. in analytical chemistry in 1995. He has accepted an offer to be the Vice President of Research and Development with a company that is developing membrane interfaces for mass spectrometers, MIMS Technology, located in Melbourne, FL.

I certify that I have read this study and that in my opinion it conforms to acceptable standards of scholarly presentation and is fully adequate, in scope and quality, as a dissertation for the degree of Doctor of Philosophy.

Richard A. Yost, Chair
Professor of Chemistry

I certify that I have read this study and that in my opinion it conforms to acceptable standards of scholarly presentation and is fully adequate, in scope and quality, as a dissertation for the degree of Doctor of Philosophy.

James D. Winefordner
Graduate Research Professor of
Chemistry

I certify that I have read this study and that in my opinion it conforms to acceptable standards of scholarly presentation and is fully adequate, in scope and quality, as a dissertation for the degree of Doctor of Philosophy.

Daniel R. Talham
Associate Professor of Chemistry

I certify that I have read this study and that in my opinion it conforms to acceptable standards of scholarly presentation and is fully adequate, in scope and quality, as a dissertation for the degree of Doctor of Philosophy.

Robert T. Kennedy
Assistant Professor of Chemistry

I certify that I have read this study and that in my opinion it conforms to acceptable standards of scholarly presentation and is fully adequate, in scope and quality, as a dissertation for the degree of Doctor of Philosophy.

Roger L. Bertholf
Associate Professor of Pathology
and Laboratory Medicine

This dissertation was submitted to the Graduate Faculty of the Department of Chemistry in the College of Liberal Arts and Sciences and to the Graduate School and was accepted as partial fulfillment of the requirements for the degree of Doctor of Philosophy.

December, 1995

Dean, Graduate School

LD
1780
1995
.G849

UNIVERSITY OF FLORIDA
3 1262 08553 7164